VYSOKÉ UČENÍ TECHNICKÉ V BRNĚ

BRNO UNIVERSITY OF TECHNOLOGY

FAKULTA CHEMICKÁ
ÚSTAV CHEMIE MATERIÁLŮ

FACULTY OF CHEMISTRY
INSTITUTE OF MATERIALS SCIENCE
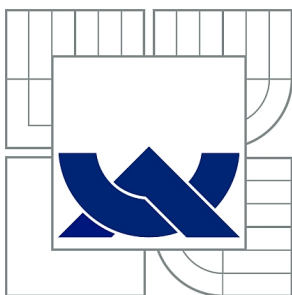
FUNCTIONALIZATION OF POLY(LACTIC ACID)
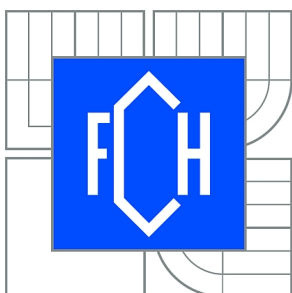
DIZERTAČNÍ PRÁCE
DOCTORAL THESIS

AUTOR PRÁCE   Ing. JOSEF PETRUŠ
AUTHOR

BRNO 2015

VYSOKÉ UČENÍ TECHNICKÉ V BRNĚ

BRNO UNIVERSITY OF TECHNOLOGY

FAKULTA CHEMICKÁ
ÚSTAV CHEMIE MATERIÁLŮ

FACULTY OF CHEMISTRY
INSTITUTE OF MATERIALS SCIENCE

FUNCTIONALIZATION OF POLY(LACTIC ACID)

FUNKCIONALIZACE POLY(MLÉČNÉ KYSELINY)

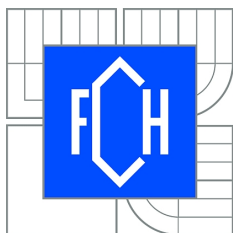## DIZERTAČNÍ PRÁCE
DOCTORAL THESIS

AUTOR PRÁCE   Ing. JOSEF PETRUŠ
AUTHOR

VEDOUCÍ PRÁCE   doc. RNDr. JAROSLAV PETRŮJ, CSc.
SUPERVISOR

BRNO 2015

Zadání dizertační práce

Číslo dizertační práce: **FCH-DIZ0115/2015**   Akademický rok: **2015/2016**
Ústav: Ústav chemie materiálů
Student(ka):   **Ing. Josef Petruš**
Studijní program: Makromolekulární chemie (P1422)
Studijní obor: Chemie makromolekulárních materiálů (1405V003)
Vedoucí práce   **doc. RNDr. Jaroslav Petrůj, CSc.**
Konzultanti:

Název dizertační práce:

Funkcionalizace poly(mléčné kyseliny)

Zadání dizertační práce:

Cílem disertační práce je příprava a charakterizace poly(mléčné kyseliny) PLA roubované pomocí anhydridu kyseliny itakonové IAH na kopolymer (PLA-g-IAH).

Termín odevzdání dizertační práce: 30.10.2015

Dizertační práce se odevzdává v děkanem stanoveném počtu exemplářů na sekretariát ústavu a v elektronické formě vedoucímu dizertační práce. Toto zadání je přílohou dizertační práce.

-          -   -
     Ing. Josef Petruš   doc. RNDr. Jaroslav Petrůj, CSc.   prof. RNDr. Josef Jančář, CSc.
       Student(ka)   Vedoucí práce   Ředitel ústavu

                                                  - -
V Brně, dne 1.9.2015   prof. Ing. Jaromír Havlica, DrSc.
                                                          Děkan fakulty

ABSTRACT

The theoretical part of proposed thesis describes principle of radical grafting as well as the most important controlling factors affecting reaction course. Radical grafting of poly(lactic acid) (PLA) via reactive modification is the most promising technique for the preparation of biodegradable polymeric materials with various properties. Actual knowledge of PLA modification via radical grafting in melt is mentioned in the literature review as well as its potential applications.

Experimental part deals with functionalization of PLA with itaconic anhydride (IAH) via radical grafting in the melt. Grafting reaction was initiated by 2,5-bis(tert-butylperoxy)-2,5-dimethylhexane (L101).

In the first part, radical grafting is investigated "in situ" using differential scanning calorimetry (DSC) and thermogravimetric analysis (TGA). Exothermic peak on DSC thermogram reflects grafting reaction which allows calculation of activation energy of reaction. With regard to "in situ" TGA thermogram, formation of byproducts during radical modification was observed.

In the second part, functionalization of PLA was achieved in discontinuous internal mixer under defined reaction conditions which were tailored to half-life time of chosen initiator and PLA processing parameters. Reaction temperature 190 °C was calculated according to Arrhenius equation and reaction time 6 min. These conditions were considered to be convenient with respect to decomposition kinetics of L101 and suppression of PLA degradation. IAH was succesfully grafted onto PLA backbone which was proved by Fourier transform infrared spectroscopy (FTIR) due to presence of $-CH_2$ vibrations at 2860 and 2920 cm^{-1}. Increase of integral intensity of the absorption band centered at 1750 cm^{-1} proved appearance of anhydride C=O vibrations overlapped by C=O vibrations of PLA backbone. Nuclear magnetic resonance (^{1}H-NMR) did not detect oligomeric IAH grafted onto PLA. Different concentration of reactants (0.5–10 wt % of IAH, 0.1–2 wt % of L101) was applied in order to evaluate its influence on grafting yield and the extent of side reactions such as β-scission, branching and crosslinking. At high concentration of both IAH and L101, IAH homopolymerization occurs although it is neglected in the most of research works. This argument is supported by colorimetric analysis, characterization of samples prepared by polymerization of IAH under grafting conditions and thermal stability of fractions extracted from PLA-g-IAH. Radical modification of PLA improves chain flexibility due to bulky IAH which was detected as a decrease of glass transition temperature (T_g). Increased content of amorphous phase, improved hydrophilicity, branched structure and chain scission enhanced biodegradability of PLA-g-IAH compared to neat PLA.

Non-radical degradation during processing was proved by change of melt behaviour. This undesired effect was suppressed by addition of chain extender with reactive epoxy groups. Reaction between epoxy groups of chain extender and carboxyl groups of PLA was proved by structure analysis and change of rheological behavior of PLA-g-IAH.

KEYWORDS

Radical grafting, poly(lactic acid), itaconic anhydride, homopolymerization.

ABSTRAKT

Teoretická část předložené dizertační práce popisuje princip radikálového roubování a faktory ovlivňující reakční průběh. Radikálové roubování poly(mléčné kyseliny) (PLA) reaktivní modifikací je vhodnou technikou přípravy biodegradabilních polymerních materiálů s rozličnými vlastnostmi. Současný stav problematiky modifikace poly(mléčné kyseliny) radikálovým roubováním v tavenině je obsahem literární rešerše včetně možných aplikací.

Experimentální část se zabývá modifikací PLA anhydridem kyseliny itakonové (IAH) radikálovým roubováním v tavenině. Reakce byla iniciována 2,5-bis(tert-butylperoxy)-2,5-dimethylhexanem (L101).

V první části je průběh radikálového roubování pozorován "in situ" pomocí diferenciální kompenzační kalorimetrie (DSC) a termogravimetrické analýzy (TGA). Exotermní pík na DSC záznamu odpovídá průběhu radikálové reakce, na jehož základě lze definovat aktivační energii reakce. Průběh TGA křivky "in situ" radikálové reakce umožnil detekovat vedlejší produkty vznikající v průběhu radikálové modifikace.

Ve druhé části byla PLA funkcionalizována reakcí v diskontinuálním laboratorním mixéru za reakčních podmínek navržených dle poločasu rozpadu zvoleného iniciátoru a zpracovatelských podmínek PLA. Reakční teplota 190 °C byla stanovena výpočtem z Arrheniovy rovnice pro reakční čas 6 min. Uvedené reakční parametry byly zvoleny s ohledem na kinetiku rozkladu L101 a potlačení degradace PLA. Infračervená spektroskopie (FTIR) potvrdila navázání IAH na PLA řetězec na základě výskytu –CH_2 vibrací s absorpčními pásy při vlnočtu 2860 a 2920 cm^{-1}. Vzrůstající intensita absorpčního pásu 1750 cm^{-1} potvrdila přítomnost minoritních C=O vibrací anhydridového kruhu překrytých dominantními C=O vibracemi PLA řetězce. Nukleární magnetická rezonance (^{1}H-NMR) nepotvrdila roubování oligomerního IAH na PLA. Koncentrace reaktantů ve zvoleném rozsahu (0.5–10 hm % IAH, 0.1–2 hm % L101) byla použita pro posouzení jejího vlivu na obsah naroubovaného IAH a míru vedlejších reakcí, např. β-štěpení, větvení a síťování. Při vysoké koncentraci IAH a L101 byla potvrzena homopolymerace IAH i přes její zanedbávání v tématicky podobných studiích. Tvrzení o IAH homopolymeraci bylo podpořena výsledky kolorimetrické analýzy, charakterizací vzorků připravených polymerací IAH za podmínek radikálového roubování a termickou stabilitou frakcí extrahovaných z PLA-g-IAH. Radikálovou modifikací PLA došlo ke zvýšení flexibility polymerních řetězců díky objemné struktuře IAH navázané na PLA řetězci, což se projevilo poklesem teploty skelného přechodu (T_g). Zvýšený obsah amorfní fáze, hydrofilní chování, rozvětvená struktura a štěpení řetězců má pozitivní vliv na zvýšenou biodegradabilitu PLA-g-IAH v porovnání s nemodifikovanou PLA.

Neradikálová degradace, probíhající v průběhu zpracování PLA, byla prokázána změnou tokových vlastností taveniny. Tento nežádoucí jev byl potlačen přídavkem tzv. "prodlužovače řetězců" obsahujícího reaktivní epoxy skupiny. Reakce mezi epoxy skupinami a karboxylovými skupinami byla potvrzena pomocí FTIR a změnou reologických vlastností PLA-g-IAH.

KLÍČOVÁ SLOVA

Radikálové roubování, poly(mléčná kyselina), anhydrid kyseliny itakonové, homopolymerace.

PETRUŠ, J. Funkctionalization of poly(lactic acid). Brno University of Technology, Faculty of Chemistry, 2015. 118 p., supervisor doc. RNDr. Jaroslav Petrůj, CSc.

Declaration

I declare that the doctoral thesis has been worked out by myself and that all the quotations from the used literary sources are accurate and complete.

....
student's signature

Acknowledgements

TABLE OF CONTENTS

1. INTRODUCTION

Polymer industry in the Czech Republic is focused especially on processing of petroleum-based polymers, such as polyolefins. This situation is given by history of industry in the Czech Republic and relatively low interest in polymer recyclation. Processing of poly(lactic acid) and its modification could lead to higher interest in biodegradable and recyclable polymers with higher applicability in modern applications.

Modification of polymers via reactor and post-polymerization techniques is one of the most promising methods how to prepare new functional materials. Reactor methods are based on the polymer modification via polymerization (e.g. copolymerization). On the other hand, post-polymerization techniques provide new materials via processing of commercially available polymers where no preparation of new monomer is required (e.g. blending, grafting).

Importance of post-polymerization modifications arises from requirement of wider applicability of polymers and for tailoring. For example, post-polymerization modification of PLA promises to improve miscibility with different thermoplastics to enhance poor mechanical properties. Moreover, improved miscibility with certain thermoplastic may lead to substitution of hardly recyclable thermoplastics with biodegradable PLA. Experiences from the modification of commonly used polymers can be applied for modification of PLA. This fact makes PLA more attractive.

Theoretical part of this work is focused on the description of radical grafting as commonly used post-polymerization modification method. One of the first applications of radical grafting was an effort to increase polarity of nonpolar polymers due to grafting of polar monomers onto polymer backbone. Thus modified polymers exhibited enhanced miscibility with polar polymers. For example, polypropylene grafted with maleic anhydride via reactive extrusion allowed to prepare polymer blends with polyamides with improved morphology and mechanical properties compared to unmodified polypropylene used for blending.

Recently, polymer modifications are applied for large scale of polymers including PLA which is interesting for its biodegradability, recyclability and specific properties. PLA can be obtained from renewable resources and has potential to replace traditional polymers in specific applications. PLA biodegradability is desired in applications where life cycle of products is controlled. However, thermal and hydrolytical degradation requires defined condition upon processing cycle and limits processing at elevated temperatures. Reactor modification of PLA with epoxy compounds or unsaturated compounds gives polymers which are coupled via radical reaction with elastomers [1]. PLA grafted with suitable monomer by post-polymerization modification may be used as a compatibilizer in polymer blends and composites which reduce interphase tension leading to enhanced adhesion to polymer matrix or filler [2]. Finally, biodegradability and other properties can be combined in resulting material.

2. THEORETICAL PART

2.1 Principle of polymer modification via radical grafting

Radical grafting is used to modification of polymers via reaction with monomer(or monomers) is bonded onto polymer chain. One monomer is usually grafted within one-step reaction. Two or more monomers can be grafted simultaneously or in sequence reaction steps. Bonding of new functional groups via grafting reaction affects hydrophility, solubility, thermal properties or adhesion. Scheme of radical grafting is illustrated for radical grafting of biomacromolecule with appropriate monomer in Figure 1. It can be noted that proposed scheme can be generalized for any polymeric material. Three general grafting methods can be distinguished: a) Grafting to: A pre-existing polymer with a functional chain end-group reacts with a complementary functional group present on the biomacromolecule; thus prepared grafted or crosslinked polymers prepared using crosslinking agent; b) Grafting from: Polymerization originates from a specific site on the biomacromolecule that is capable of producing radicals (e.g. initiator) and initiates polymerization of monomer; c) Grafting through: Radical polymerization occurs in the presence of a biomacromolecule that contains a polymerizable group, thus acting as a monomer, and can copolymerize with a different type of monomer to yield a polymeric chain bearing biomacromolecules attached to its backbone [3].
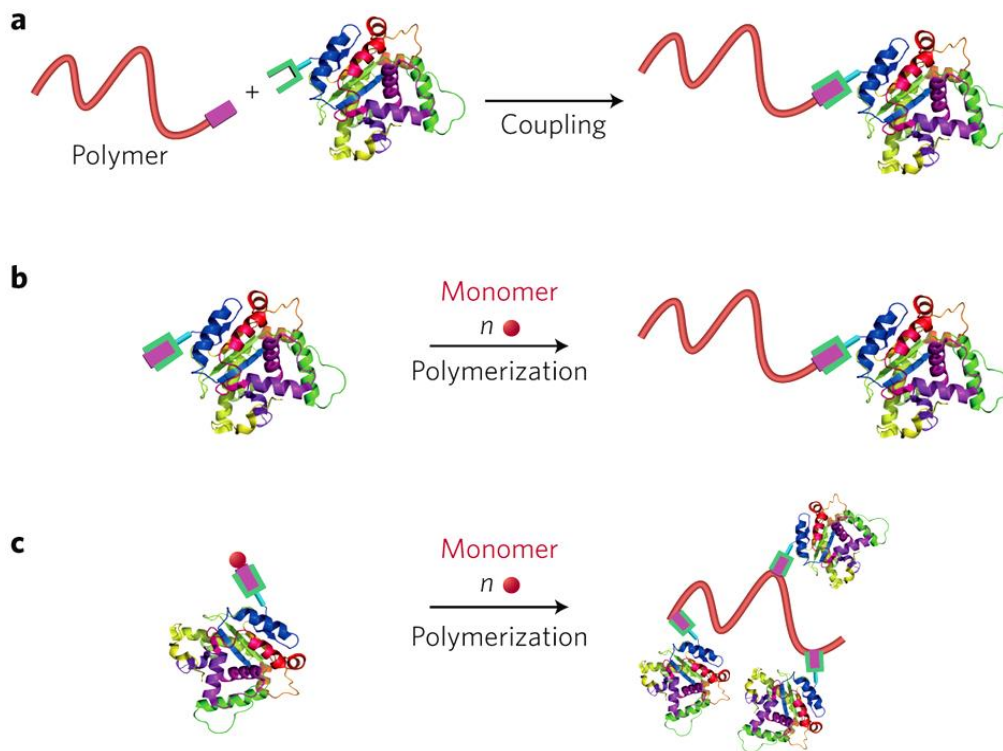
Figure 1. Scheme of radical grafting methods; grafting to (a), grafting from (b) and grafting through (c) [4].

Depending on the reaction conditions, grafting reaction may run according to different mechanisms - direct or indirect, chemical or physical. Based on the initiation process, grafting methods can be sorted on chemical, photochemical, enzymatic, radiation and plasma-induced grafting [3].

In the grafting reaction, formation of reactive species (radicals, ions) is the key step for bonding of monomer onto polymer backbone or covalent bonding of two polymer chains (see Figure 1). Regarding grafting method applied in experimental part of this work, free-radical grafting is the most commented method below. Primary radicals can be generated via chemical reaction (i.e. redox reaction), by application of energy needed for homolytical scission of C–H, O–O or C–C bond or application of radiation for generation of excited species (UV, plasma, photochemical decomposition, etc.). Most cited ways are schemed in Figure 2 [5].
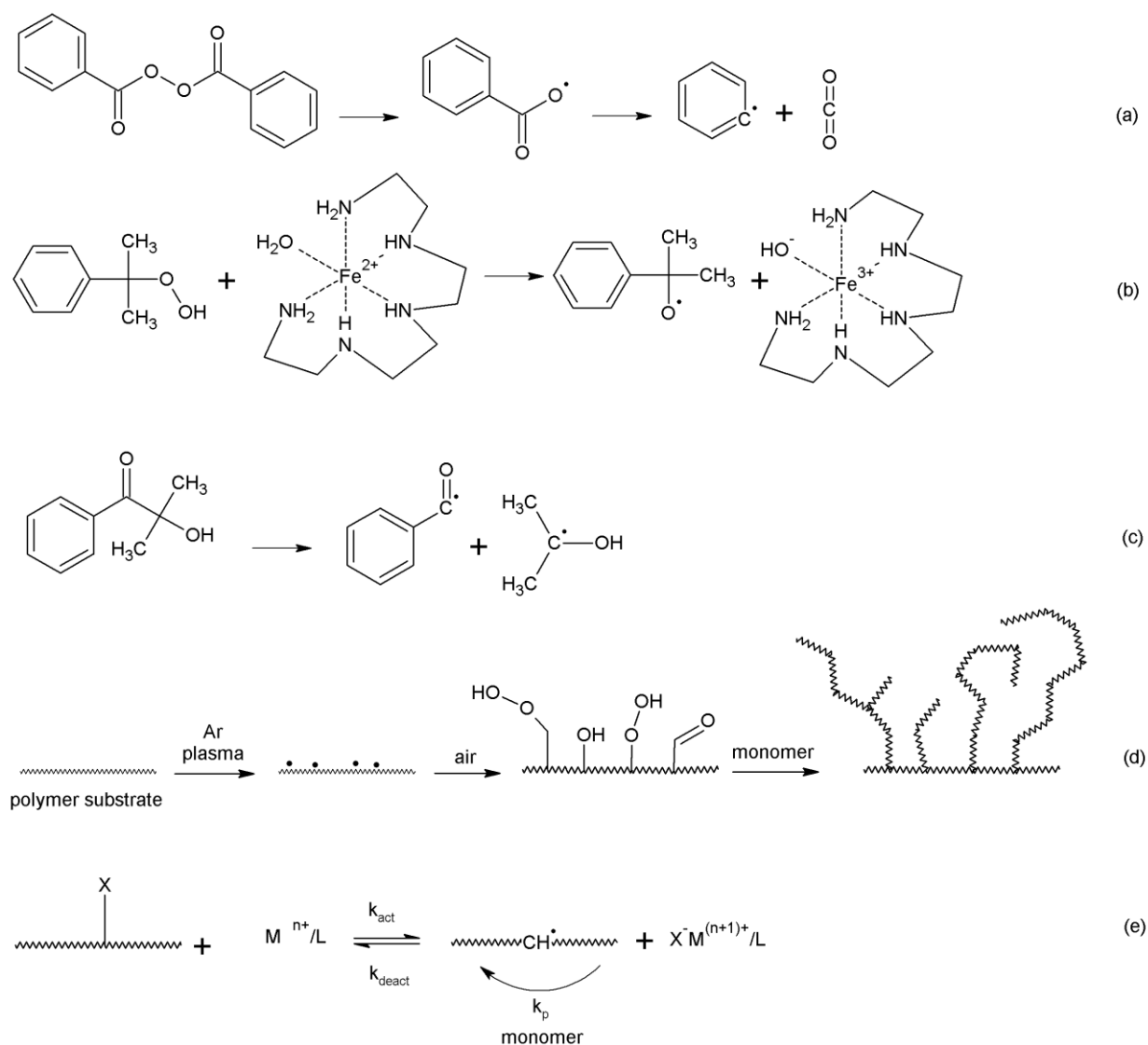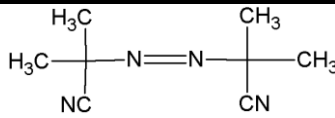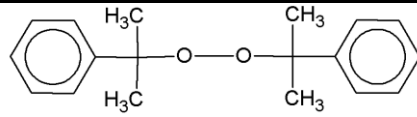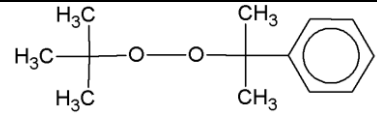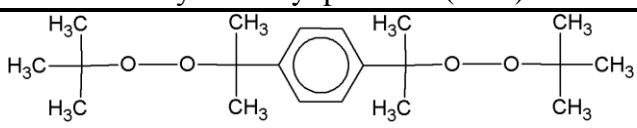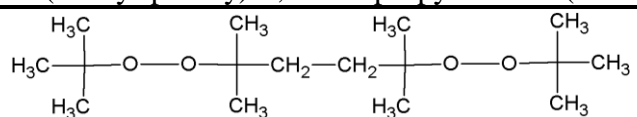
Figure 2. Radical grafting initiated by: DBP decomposition (a); formation of cumyl radicals by redox reaction (b); photochemical decomposition of photoinitiator (2-hydroxy-2-methyl-1-fenylpropan-1-on) (c); plasma (d); living radical formation through atom transfer (e) [5].

2.2   Radical grafting initiated by decomposition of thermolabile compounds

Chemically initiated radical grafting can be realized according to mechanisms depicted in Figure 2. Different types of initiators affect course of reaction as well as mechanism of primary radicals generation. Most common mechanisms include decomposition of thermolabile compounds, redox reactions and other specific reactions, such as enzymatic reactions or atom transfer reaction.

Most of grafting methods are based on the radical reactions in melt. Compared to other grafting methods, reactions in melt can be achieved under different reaction conditions using different industrial devices (i.e. extruders, mixers, kneaders) providing high efficiency of polymer modification. Peroxides, hydroperoxides and azocompounds are commonly used for generation free radicals. Free radicals attack polymer chain and thus formed active center can react with monomer [6]–[8]. Table 1 summarizes compounds with peroxide bond R–O–O–R' which is homolytically decomposed onto highly reactive primary radicals containing unpaired electron in their structure. Initiators can be sorted acording to ability to form active center on polymer chain and half-life time $\tau_{1/2}$ affecting reaction conditions (e.g. temperature, time). An overview of commonly used initiators as well as relating $\tau_{1/2}$ summarized Table 1.

Table 1. Overview of commonly used thermal initiators [9].

Structure, name, abbreviation	T [°C] = $f(\tau_{1/2})$		
	10 h	1 h	0,1 h
2,2′-azodi(isobutyronitril) (AIBN)	64	82	101
Dicumyl peroxide (DCP)	116	136	175
t-butyl α-cumyl peroxide (BCP)	118	138	180
α,α′-di(t-butyl-peroxy)-1,3-diisopropyl benzen (DBPIB)	120	142	190
2,5-di(t-butyl-peroxy)-2,5-dimethyl hexane (DTBPH)	120	142	190

Overall scheme of free-radical grafting onto polymer backbone presentes by Al-Malaika [9] usually contains three types of reactants: polymer, unsaturated monomer and free radical initiator. Primary radicals are generated in the presece of polymer and monomer by specific decomposition mechanism depending on the type of initiator. Regarding scheme in Figure 3, primary radicals can participate on two different reactions with monomer - homopolymerization and grafting. Homopolymerization occurs upon reaction between free radical and monomer whereas further addition of monomer results in formation of oligomers and polymers (reaction b). Grafting starts with hydrogen atom abstraction which was described above. Grafting of oligomeric chain is less probable due to limited hydrogen atom abstraction. After hydrogen atom abstraction (reaction a), three different reactions may be observed. Except of desired reaction between macroradical and monomer (reaction a3), chain scission (reaction a1) or crosslinking (reaction a2) can be observed. Macroradical of grafted monomer can act as a center suitable for bonding new monomer molecules, extending of grafted chain (reaction a3-1) or hydrogen atom transfer (reaction a3-2) [9].
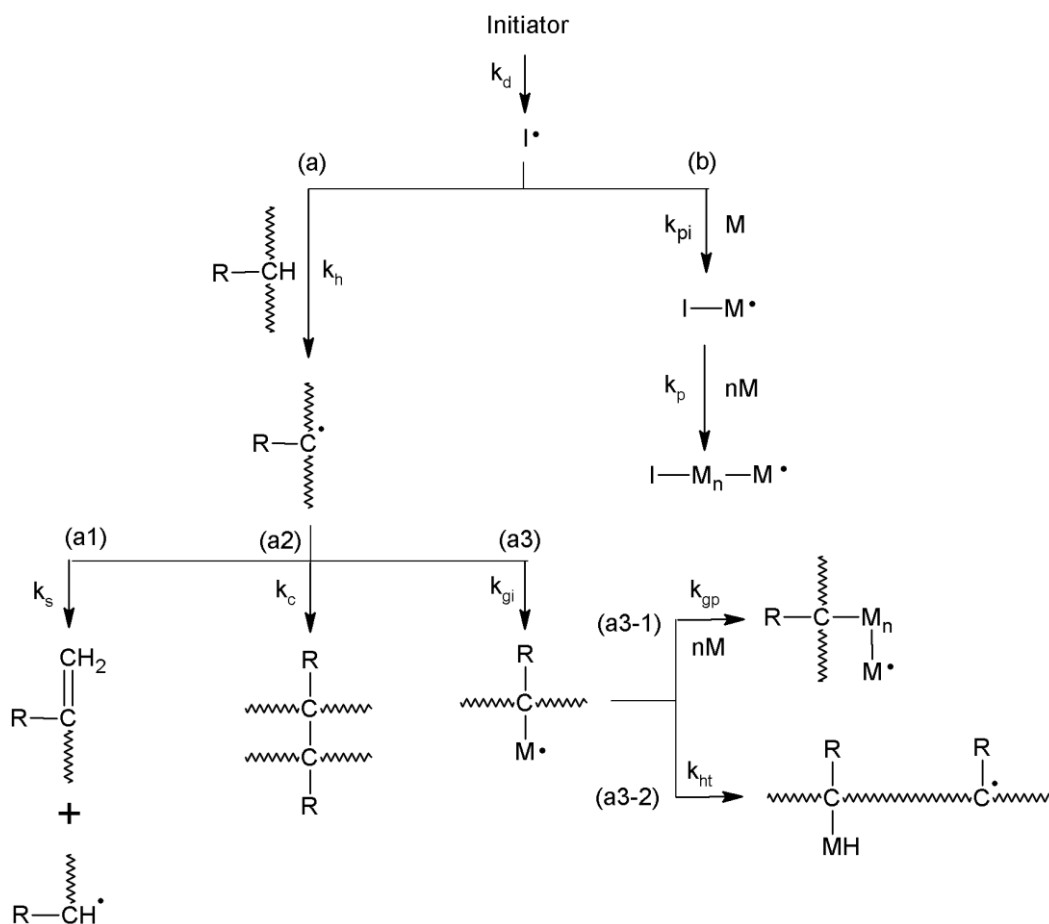
Figure 3. Mechanism of: homopolymerization of monomer (b), hydrogen atom abstraction (a) with subsequent β-scission (a1); crosslinking (a2) and monomer grafting (a3); homopolymerization of grafted monomer (a3-1) and intramolecular transfer of hydrogen atom forming new active center (a3-2) [9].

2.2.1 Mechanism of radical grafting

2.2.1.1 Initiation

Initiation is the particalr reaction controlling the kinetics of grafted polymers prepared by a radical mechanism. Initiation can be divided into three parts:

1) Generation of the initial radical species.
2) Reaction of these species to generate other radicals.
3) Addition of either the initial radical, or its products, to a monomer, to begin the propagation reactions.

Equations 1a–c represent simplified scheme of free radicals generation via thermal decomposition and subsequent steps included in initiating part. Thermal decomposition of initiator is given by Equation 1a. Equation 1b represents homopolymerization of monomer due to reaction between primary radical and monomer unit. Substitution reaction between primary radicals and polymer results in hydrogen atom abstraction where macroradical is formed (Equation 1c) [5].

$$I_2 \longrightarrow 2\,I\cdot \tag{1a}$$

$$I\cdot + M \rightarrow IM\cdot \xrightarrow{+M} IMM\cdot \tag{1b}$$

$$I\cdot + RH \longrightarrow R\cdot + IH \tag{1c}$$
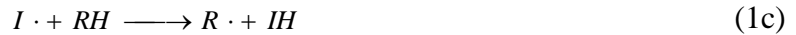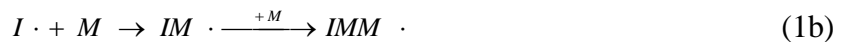
Generation of the initial radicals depends predominately on the nature of the initiator. Radical grafting can be controlled by by choice of sufficient initiator with low volatility of decomposition products, toxicity, susceptible $\tau_{1/2}$ and high initiating efficiency [5], [10], [11]. For a given chemical initiator the dissociation rate can be controlled by varying the temperature and a wide range of radical fluxes can be generally achieved by varying the initiator concentration. The extent of subsequent reactions of radical species depends on other reactants presented in the reaction system such as polymer substrate, monomer, additives, etc.

As mentiond in previous chapter, dialkyl peroxides are commonly used for initiation of radical grafting. In the most cases, an initiator is initially homogeneously distributed which is typical for most single-phase reactions using a peroxy initiators as mentioned above. The rate of gthus generated free radicals I˙ is the same everywhere in the system and can be given by Equation 2:

$$-\frac{d[I^{\cdot}]}{dt} = f \cdot k_d \cdot [I] \tag{2}$$

where [I] is a function of time, k_d is rate coeffecient which can be considered to include the stoichiometry of the decomposition and f represents viscosity-dependent constant which includes "cage effect" where two radicals held in close proximity combine to form an unreactive

product. Constant f determines the effectivity of flux of radicals. Because of high viscosity of reaction system, decrease of $[I^{\bullet}]$ due to recombination reactions will be large and f will be small. It is in contrast with grafting in dilute solution which exhibit much higher effectivity of radical flux compared to grafting in high viscous system.

Generally, peroxide initiators can be distinguished regarding their decomposition products. For example, thermal decomposition of cumylhydroperoxide gives cumyloxy radicals (Figure 4, reaction a) whereas, for example, dibenzoylperoxide provides benzoxy radicals with subsequent scission onto secondary phenyl radicals. The decomposition mechanism of dialkyl peroxides is well established as involving initial O–O bond homolysis to generate the corresponding alkoxy radicals. If not trapped by reaction with substrate, the initially formed alkoxy radicals undergo β-scission with preferential cleavage of the weakest C–C bond. Bonds to sp^3 carbons are broken rather than bonds to sp (acetylenic) or sp^2 (aromatic, olefinic) carbons. Bonds to higher alkyl chains are cleaved in preference to those to methyl radicals.
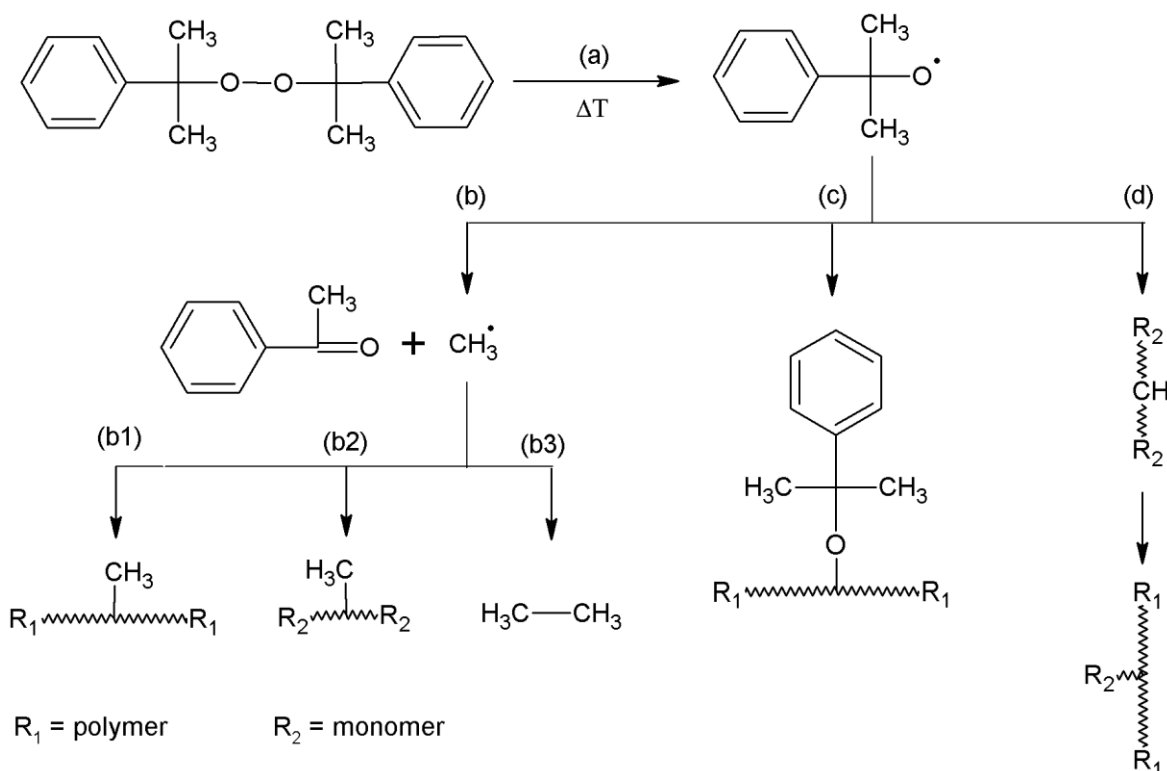
Figure 4. Homolytical decomposition of dicumyl peroxide (a); β-scission of cumyloxy radicals to secondary methyl radicals (b); addition of secondary methyl radicals on polymer (b1), monomer (b2) and recombination (b3); addition of primary cumyloxy radicals on polymer chain (c); hydrogen atom abstraction from molecule of monomer using cumyloxy primary radicals with subsequent addition of monomer onto polymer (d) [12].

Detailed description of dicumylperoxide decomposition within grafting of surface nanotubes with pentadecane was proposed by Akbar et al. [12]. Authors concluded that higher temperatures resulted in higher amount of secondary methyl radicals $CH_3^{\bullet}$ due to thermal decomposition of dicumylperoxide with subsequent β-scission of cumyloxy radicals. In the next step, methyl

14

radicals recombined (Figure 4, reaction b3) or were bonded to either polymer and/or monomer (Figure 4, reaction b1 and b2). Second reaction way occured due to reaction conditions which prefer formation of cumyloxy radicals which abstract hydrogen atom from pentadecane or radical is bonded onto polymer chain (Figure 4, reaction c). Cumyloxy radicals can be also decomposed to phenyl radicals and acetone as a byproduct. Both phenyl and methyl radicals are nonselective against C–H bonds due to high strength of C–H bond included in benzene ring and methane. Different reactivity of primary and secondary radicals allows control of reaction course.

Radicals formed via thermal decomposition of peroxide initiators may undergo two different reaction types leading to formation of initiating species - abstraction and addition. It is well established that the reactivity and specificity shown by initiator-derived radicals in abstraction and addition reactions depend strongly on the nature of the radicals and thus on the particular initiator. Abstraction is an efficient way for O–O bond containing initiators to introduce a reactive center to the backbone or side chain of a polymer [5]. This kind of reactions depends on the hydrogen-abstracting capacity of the radical and susceptibility of the substrate to abstraction. In the case of hydrogen-abstracting capacity, heteroatom-centered radicals are usually considered to be more effective in abstraction on electronic grounds, and a relatively persistent radical will usually be more reactive toward abstraction than addition on steric grounds. Abstraction efficiency is also given by the strenght of R–X in polymer substrate which is needed for removing $X^\bullet$ while $R^\bullet$ is formed. Table 2 summarizes dissociation energies of different C–H bonds including activation energies which are necessary for hydrogen atom abstraction. Typical values of activation energies of abstraction relevant to grafting are of the order 20–30 kJ·mol^{-1} [13].

Table 2. Disociation energies E_d of C–H bond needed for hydrogen abstraction depending on the kind of carbon atom [14].

Bond	E_d (C–H) [kJ/mol]	Bond	E_d (C–H) [kJ/mol]	Bond	E_d (C–H) [kJ/mol]
$(R_3)C–H$	404	$C_2H_5O–H$	435	$C_2H_5–H$	410
$(R_2)CH–H$	413	$CH_3–H$	435	$C_3H_7–H$	395
$RCH_2–H$	423	Phenyl–H	463	$C_4H_9–H$	384

Addition mechanism is based on replacement of high energy π-bond by σ-bond. Weak C–H bond of tertiary carbon (E_d = 404 kJ·mol^{-1}) is replaced by stronger O–H bond formed via reaction between hydrogen atom and peroxide radical R–O$^\bullet$ (E_d = 463 kJ·mol^{-1}) [8]. Addition mechanism is typical for radicals with C–C bond [5]. The addition to a double bond in the polymer is a common means for a small radical to generate a reactive center [15]. Common polymers based on a diene monomer, such as polyisoprene and polybutadiene, have both double bonds in the backbone and pendant double bonds to which addition may take place.

In radical grafting, the final step of initiation will be when the radical center R$^\bullet$ adds to a molecule of a monomer. If R$^\bullet$ is localized on the polymer backbone, this will give the "grafting from" process; if R$^\bullet$ is a small molecule, this will give a potential "grafting to" process. This step

is unlikely to be rate-controlling unless the previous steps of initiation give rise to persistent radicals.

2.2.1.2 Propagation

Propagation is the next step subsequent to initiation. It consists of a large number of reactions which occur once initiation is complete and all events occurring before termination form part of the "kinetic chain". These reactions may include addition to the monomer and functionalities on the polymer, or chain transfer, typically to polymer or an additive. Propagation is the key reaction determining overall kinetics of radical grafting. It can be simplified that total polymerization enthalpy equals to enthalpy of propagation. As consumption of monomer is the primary reaction, propagation ratre can be defined by Equation 3:

$$-\frac{d[M]}{dt} = k_p \cdot [\Sigma R^\bullet] \cdot [M] \tag{3}$$

where $\Sigma R^\bullet$ is the sum of all radical species that can interact withmonomer. As [M] is initially fixed and can only decrease in the course of the reaction, $[\Sigma R^\bullet]$ will be the main parameter controlling the kinetics. This assumes all $R^\bullet$ have the same reactivity, an assumption valid at degrees of polymerization greater than 10 in circumstances where there are few side reactions generating persistent radicals. If one or more comonomers are present, the rate coefficients for each of the possible propagation reactions and the possible change of the relative amounts of the comonomers over time must be considered. Monomers that are reluctant to homopolymerization, such as maleic acid or crotonic acid, generate very short grafts. As discussed in the chapter 2.2.1.1, high viscosity limits effect of chemical control of propagation whereas physical constraints predominate.In that case propagation is controlled by the reactive diffusion of monomer to polymer radicals, giving a greatly reduced k_p value. It can be simplified that total polymerization enthalpy equals to enthalpy of propagation.

2.2.1.3 Termination

Active center can be perished in several ways which are generally based on the pairing of two radicals to form nonradical species. As this reaction is essentially barrier-less, termination is rapid and effectively diffusion controlled under all conditions. One of the most common way is reaction with relatively labile hydrogen atom with subsequent radical transfer to another polymer chain (Figure 5a). Grafting reaction can be terminated either by reaction with radical located on low-molecular oligomer (Figure 5b). Termination can occur as a result of reaction with macroradical which leads to grafting or crosslinking between two polymer chains (Figure 5c).
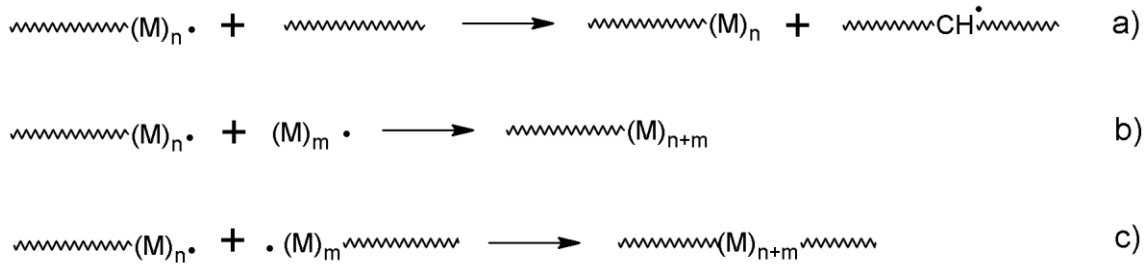
Figure 5. Termination of growing active center by a) radical transfer, b) addition of oligomeric radcial, c) interaction between two active centers.

Since the polymer radicals are much larger than the monomer, with increasing viscosity k_t decreases before k_p begins to decrease. This is the physical basis for the rapid increase in the rate of radical polymerization with viscosity over the course of a reaction [13]. An important consequence of the diffusion dependence of k_t for grafting reactions is that termination will most frequently occur not by the meeting of two large radical species but by the addition of a small mobile radical to a polymer - centered radical. "Grafting to" mechanisms will thus be unlikely except for reactions carried out in dilute solution.

Depending on chain lenght, semiempirical expressions for the chain-length dependence of k_t have been determined and these expressions are given in Table 3.

Table 3. Semiempirical expressions for the chain-length dependence of k_t.

Termination between	Lenght dependence of k_t	Parameters	Reference
equal and relatively short chains	$k_t^{i,i} = k_t^{1,1} \cdot i^{-es}$	$s = 1/2$	[16]
equal and relatively long chains	$k_t^{i,i} = k_t^{1,1} \cdot (i_{crit})^{-(es-eL)} \cdot i^{-eL}$	$s = 1/2$ $L = 1/6$	[17]
relatively short chains and polymer radicals	$k_t^{i,long} = 4 \cdot \pi \cdot D_i \cdot p_i \cdot \sigma \cdot N_A$ $D_i = c_2 \cdot D_1(x) \cdot i^{c_0 + c_1(x)}$	D_i...relative diffusion coefficient p_i...probability of radical termination σ...distance of the order of an atomic diameter x...mass fraction of polymer $D_1(x)$...diffusion coefficient of the monomer	[18]

When polymer chain with functional groups is bonded onto another polymer chain with functional groups, crosslinking occurs due to elimination or addition of low bulky radical species. In this case, crosslinking predominates over the formation of graft copolymers. Since termination is controlled by diffusion, rate coefficient of termination k_t is not a constant because of inverse relationship between k_t and lenght of the polymer chain [9].

Reactions between radicals and nonradical species require some amount of activation energy. On the other hand, radical-radical interactions are characterized by low activation energy which may complicate initiation due to radical recombination and decreases concentration of primary radicals. Due to low activation energy, the extent of radical-radical reaction is controlled by diffusion and dimension of radicals. Low-bulky radicals interact with higher probability which decreases grafting efficiency. On the other hand, bulky radicals prefer interactions with polymer chain due to slower diffusion.

2.3   Controlling factors of radical grafting

2.3.1   Nature of the polymer

Radical grafting can be controlled by many variables that affect grafting way such as the nature of the backbone, monomer, solvent, initiator, additives, temperature, etc. As grafting involves covalent attachment of a monomer to a polymeric backbone, the nature of polymer backbone defines grafting process due to its structure and chemical composition. Characteristic of polymer backbone can affect the grafting course from two directions. First, it determines how readily can be reactive centers generated on the backbone by reaction with the initiator. Second, polymer backbone nature defines how readily generated reactive centers react with the monomer or with other reactive centers. Position of radical centers on polymer backbone can be changed depending on polymer structure which can be changed via β-scission. For the most of grafting mechanisms, reaction rate relates to concentration of functional groups on polymer chain [5].

Influence of polymer structure on grafting process was evaluated by several authors. For example, Ng et al. [19] reported the influence of cellulose structure on grafting with charge transfer complex including maleic anhydride, maleates and vinyl acetate. Even though the backbone of cellulose is highly structured and bulky, enhanced diffusion of generated radicals to the active sites located on the substrate backbone. This effect was influenced by an appropriate solvent which caused swelling of the backbone. An enhancement in the initiation of the grafting reaction could therefore occur.

Similar conclusion was reported by Cardona et al. [20] who grafted poly(tetrafluorethylene-co-perfluoropropylvinyl ether) (PFA) with styrene initiated by γ-radiation in solution. It was proved that grafting degree increased with decrease of crystallinity of PFA. Therefore, it was presumed that grafting is is favoured in amorphous phase due to more complicated diffusion of styrene through crystalline PFA domains. Sakurai, Shiotani, Yahiro [21] studied the same problematique as mentioned above for grafting of poly(tetrafluoroethylene) (PTFE) with methylmethacrylate (MMA).

Polymer structure can be affected by substituents on the polymer backbone as discussed by Ibrahem and Nada [22] evaluated that crystallinity of polymer decreases with increasing degree of substitution, affecting the grafting of acrylamide on acetylated wood pulp. As the crystallinity decreased, less ordered polymer matrix facilitated the grafting reaction

Okieimen and Idehen [23] studied different initiation techniques used for grafting of vinyl monomers onto cellulose. Depending on the functional group, authors focused on hydrogen atom abstraction from carbon with OH group, oxidation of glycolic bonds resulting in C–C bond scission, oxidation of the end of cellulose chains or interactions between Ce^{4+} ions with –C=O group included in cellulose structure. As –OH group was replaced by –SH group, increase of grafting degree was observed for hydrogen atom abstraction from carbon with –OH group initiated by Ce^{4+} ions.

The influence of p-nitrobenzoyl groups bonded on polymer chain on grafting yield was discussed by Nakanuta, Yoshikawa and Matsuzaki [24]. Presence of aromatic nitro group resulted in higher grafting yield of copolymerization between cellulose ester derivate and styrene compared to grafting of polymer with incorporated double bonds.

Several studies describe the influence of microstructure of PE on radical grafting and crosslinking [25]–[29]. In these studies, increase of grafting yield and extent of crosslinking is generally supported by high concentration of unsaturated ends of chains in the presence of initiator or monomer.

Effect of the microstructural characteristics of the backbone on the grafting was reported by Clark, Baker and Whitney [30]. In this study, three polyethylenes with different levels of terminal unsaturation were used to investigate the effect of their microstructure on the course of grafting. Enhanced crosslinking was observed for polyethylenes containing high levels of terminal unsaturation in the presence of peroxide or peroxide–maleic anhydride. Although styrene was added as comonomer to to eliminate undesirable crosslinking, low reactivity between styrene and the allylic radical generated on the polyethylene backbone was responsible for the increased crosslinking.

Except of polymer structure, some reports evaluate the influence of chemical composition of modified polymers on grafting. For example, the presence of lignin in straw affected the grafting of 2-methyl vinyl pyridine, since lignin is a good scavenger of radicals [31]. This phenomenon has also been observed in ethyl acrylate grafted to a sisal fiber system with 8 % of lignin. The grafting rate was higher when NaOH was used as a lignin remover, but the reverse has also been reported, i.e. the presence of lignin increases the grafting yield if the backbone is ozonized and grafted using Fe^{2+}-H_2O_2 as the initiator.

2.3.2   Reactivity of monomer

A number of monomer related factors need to be considered in designing experiments. These include: the monomer concentration, the solubility of the monomer in the polyolefin melt, the volatility of the monomer, the method of introducing the monomer, the reactivity of the monomer

towards initiator and substrate derived radicals, and the susceptibility of the monomer to homopolymerisation. Radical modifications in melt are ussualy achieved by adsorbtion of monomer onto polymer matrix (pellets or powder). This procedure allows appropriate homogenity of reaction mixture commonly applied within reaction extrusion. Monomer can be also added to the molten polymer directly, adsorbed on further polymer, or be dissolved in an appropriate solvent. The method of introduction depends on the solubility of the monomer in the polymer melt and the stability and volatility of the monomer [2].

Except of the nature of plymer backbone, the reactivity of grafted monomer is also important in grafting. The reactivity of monomers depends on several factors, i.e. concentration of monomers, polarity, steric nature, swellability of backbone in the presence of the monomers and. Larg scale of monomers has been already studied, i.e. maleic anhydride [32]–[35], methacrylic acid [36]–[37] and its derivates, oxazoline [38]–[40] and conjugated aliphatic monomers (e.g. oleic acid) [9]. The relative reactivity of a monomer towards polymer and other radicals generated in the system is the most critical factor affecting grafting and crosslinking reactions. Monomers that readily homopolymerize encourage grafting over crosslinking and thus generate significant amount of homopolymer (e.g., butyl acrylate). On the other hand, monomers that are exhibit reluctant to homopropagate will give short grafts and may enhance crosslinking (e.g. ethyl maleate) [41]–[42].

Reactivity of chosen monomer towards polymer and radical species is the key factor determining reaction course. Reactivity of monomer relates to its polarity, concentration or steric arrangement. Monomers with copolymerization parameter $r_i \gg 1$ prefer homopolymerization and related grafting of long chains. On the other hand, monomers with low probability of homopolymerization form short grafted chains and the extent of crosslinking increases.

Naguib et al. [43] presented study illustrating modification of PP through its grafting with two comonomers namely vinylimidazole and acrylic acid. Authors calculated the reactivity ratio of vinyl imidazole (r = 0.121) and acrylic acid (r = 1.126) by different models. It was found that maximum grafting on polypropylene films initiated by γ-irradiation was achieved for a monomer composition with 60% vinyl imidazole and 40% acrylic acid. For this reaction composition, grafting yield reached maximum at concentration 3 mole/L. Further decrease of grafting yield was assigned to the increase in the viscosity of the reaction mixture at the later stages of polymerization which may inhibit the diffusion of monomer towards the polymeric matrix.

Misra, Sharma, Mehta [44] determined percentage of grafting as functions of the concentration of chelate, nitric acid, monomer, time, and temperature in order to estimate optimal grafting conditions for different monomers (methylmethacrylate MMA, ethyl acrylate EA, butyl acrylate BA, methacrylate MA, vinylacetate VAc). The difference in grafting of VAc (2.6%) and EA (60.8%) on wool was explained regarding reactivity of these monomers. Since VAc acts as electron donating monomer, it is extremely susceptible to monomer concentration, whereas EA is highly reactive to free radicals.

Influence of acrylamide structure on grafting of cellulose was described by Bhattacharya, Das, De [45]. Authors have compared grafting for substituted acrylamides, showing that the grafting order on cellulose acetate is acrylamide > methylacrylamide > N,N dimethylacrylamide. Low

grafting yield for methylacrylamide was assigned to reduced mobility of methylacrylamide due to methyl group suppressed grafting and stability of the polymer radical, which is tertiary (a) whereas polymer radical from acrylamide is secondary (b). The secondary radicals are more reactive than the tertiary (Figure 6).

Figure 6. Tertiary (a) and secondary (b) acrylamide radical formed during grafting of cellulose acetate [45].

In the case of grafting with N,N dimethyl acrylamide, two methyl groups strongly influenced grafting yield. Due to the steric effect of the two-methyl groups, the easy approach of the monomer to the backbone is maximally hindered, and thus the extent of grafting is the least. Earlier workers also observed this phenomenon in the case of substituted acrylates [46]. It was also proposed that grafting depends upon the stability of the radical. The polymer radical that is formed in case of methyl methacrylate is relatively stable, whereas in case of methyl methacrylate, which is the most reactive, the corresponding polymer radical is probably stable.

Study presented by Huang, Sundberg [47] was focused on grafting of poly(butadiene) and unsaturated resin with butylacrylate (BA) and methylmethacrylate (MMA). Higher grafting efficiency was reached for grafting with BA due to more preferable addition of BA onto macroradical and enhanced mobility of growing active center $R–(BA)_n^{\bullet}$. Tsavalas, Luo, Schork [48] found more efficient grafting of butyl acrylate (BA) than methyl methacrylate (MMA) via miniemiulsion polymerization. The improved grafting with BA instead of MMA may be explained by improved addition of a polymer radicals to BA instead of MMA, better abstraction by the poly(BA)$^{\bullet}$ radical from the backbone to generate polymer radicals, better addition of poly(BA) across double bonds in the alkyd, or a higher mobility of $R(BA)_x^{\bullet}$ than $R(MMA)_x^{\bullet}$ within the alkyd matrix because of the lower x value for the more hydrophobic BA.

Monomers that are reactive towards the backbone macroradical, but that generate radicals, which are unreactive towards propagation, have been used to enhance crosslinking. Spencer et al. [49] who investigated the grafting of vinyltrime-thoxysilane (VTMS) onto PE. It was found that the monomer was not grafted homogeneously, but was concentrated in "clusters" generated by chain transfer from a VTMS radical to a nearby site liable to H-abstraction, which was then able to add additional VTMS. Similar issue was discussed by Rätzsch et al. [42] who focused on grafting of PE and PP with different monomers. Authors found that many non-homopolymerizable monomers giving short chains onto polypropylene also gave these "clusters" of grafting sites (vinyltri-ethylsiloxane, monovinyl ester of ethylene glycol, vinyl butyl ether, vinyl iso-butyl ether). In this work, non-homopolymerizable monomers that did not form clusters of grafted units were either allylic (generated radicals with little propensity to abstract from the backbone) or were unable to swell the polypropylene substrate (e.g., dibutyl maleinate).

The overall result of maintaining an unreactive polymer radical in these zones, instead of reactivity being transferred to a more reactive polymer radical, is to enhance crosslinking over grafting [50]. Addition of non-homopolymerizable monomers can also inhibit degradation mechanisms in polymers such as PP where the backbone is vulnerable to β-scission reactions.

As mentioned previously, the grafting efficiency also depends on the monomer concentration. For example, higher grafting efficiency of PE modification with MA compared to 4-vinylpyridine was observed ny Kaur et al. [51]. Observed phenomenon was explained in terms of the monomer solubility and the polymerizability defined by ($k_p/k_t^{1/2}$) values 213×10^{-3} and 7×10^{-3} for MA and 4-vinyl pyridine, respectively. The higher $k_p/k_t^{1/2}$ for MA relates to higher content of MA homopolymer than for grafting with 4-vinylpyridine. In addition, 4-vinyl pyridine, being more soluble than MA in an aqueous medium, produces higher grafting in an aqueous environment owing to its greater accessibility to the active sites.

It is often reported that the grafting efficiency increases with monomer concentration up to a certain limit and then decreases with further increase of monomer concentration [52]. This behavior may reflect an initial increase of the monomer concentration in close proximity to the backbone. After a certain limit, the increase in monomer concentration accelerates the homopolymerization reaction rather than grafting.

Macromonomers are represented by oligo- or polymeric compounds with a reactive double bond including styrene, (meth)acrylate ester or maleimide derivatives. The inherent reactivity of the macromonomer double bond towards radicals in solution is usually similar to that of the analogous monomers. Instead of their monomeric form, macromonomers exhibit lesser tendency to undergo homopolymerization due to steric factors. Because of the non-volatility of macromonomers, it is difficult to removed unreacted species from reaction product.

The inherent susceptibility of a monomer to undergo homopolymerization under grafting conditions is an important factor in determining the extent of homopolymer formed as a byproduct during polymer modification and the length of the grafted chain. The susceptibility to homopolymerization depends both on the propagation rate constant (k_p) and the propagation/depropagation equilibrium constant. As schemed in Figure 7, the ceiling temperature is that temperature at which the rates of depropagation and propagation are equal. Ceiling temperatures of the most common grafted monomers are summarized in Table 4.
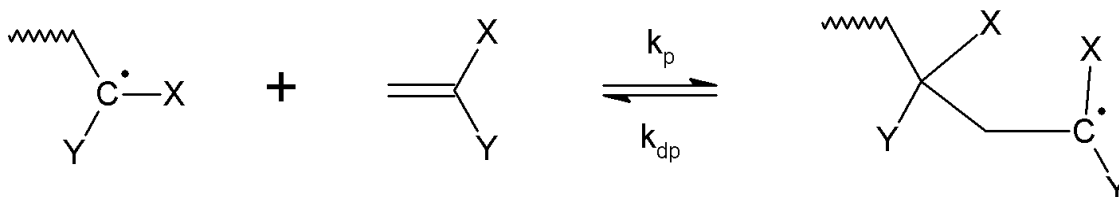

Figure 7. Illustration of propagation/depropagation equilibrium for radical polymerization.

Table 4. Thermodynamic parameters for polymerization of selected monomers [53].

Monomer	ΔH_p [kJ·mol^{-1}]	ΔS_p [J·mol^{-1}·K^{-1}]	T_c [°C]
Methyl methacrylate	55–58	118	202
Ethyl methacrylate	58–60	124	211
Acrylonitrile	75	109	415
Methyl acrylonitrile	57–64	142	177
Styrene	69–73	104	428

However, it should be noted that these values were determined at one atmosphere pressure and for a specific monomer concentration (usually 1 M). Ceiling temperatures increase with increasing pressure or monomer concentration. This may explain why MAH homopolymerisation has been observed under extrusion conditions at 170 °C even though higher operating temperature [33].

The monomer acts to trap radicals that would otherwise undergo chain scission or crosslinking. Thus, use of a higher monomer concentration may result in less degradation of the polyolefin substrate. However, it is often found that the dependence of grafting yield with monomer concentration passes through a maximum. If the monomer concentration becomes too high, phase separation can occur resulting in reduced grafting yields and an increased likelihood for homopolymerisation. In these circumstances, higher graft levels can better be achieved by multipoint/multipass addition of monomer and initiator [54].

2.3.3 Type of the initiator

Chapter 2.2.1.1 described formation of different radical species via thermal decomposition of various initiators regarding their structure. Except of this, other parameters are necessary to be considered when selecting an initiator:

(a) The solubility of the initiator in the polymer melt and its partition coefficient between the various phases in the case of multiphase melts,
(b) concentration of the initiator,
(c) volatility of the initiator - this is a concern both in choosing the method of introduction and for safety,
(d) physical form of the initiator,
(e) the method of introducing the initiator - the initiator may be i) introduced with the feedstock, ii) added with the monomer, iii) added as a separate feed, iv) added directly or adsorbed onto the polymer, v) added as a solution in the monomer or a solvent, vi) added all at once or by multipoint addition,
(f) the extent of cage reaction and the formation of initiator derived byproducts – it depends on the nature of the initiator and increases in importance with the viscosity of the medium,
(g) susceptibility of the initiator to induced decomposition and other side reactions - diacyl peroxides and hydroperoxides are particularly prone to induced decomposition,

(h) reactivity and specificity of initiator-derived radicals towards the polymer substrate.

Commonly used peroxides are introduced in Table 1, chapter 2.2 whereas their structure and radical species created via thermal decomposition can be distinguished by different reactivity and preferable abstraction/addition reaction. Bisperoxy-compounds (e.g. DTBPH, DBPIB; see Table 1) are preferred for initiation of reactive modifications because of lower volatility and easy handling. Two peroxy groups breakdown independently to yield a variety of alkoxy and alkyl radicals whereas both types of radicals may initiate grafting reaction. The decomposition of DTBPH is rendered more complex because the alkoxy radical intermediate cleaves to give the higher alkyl radical preferentially (rather than a methyl radical) [55].

Diacyl peroxides are sources of primary acyloxy radicals which may subsequently undergo β-scission to give the corresponding secondary alkyl/aryl radicals and carbon dioxide. Aliphatic acyloxy radicals have insufficient $\tau_{1/2}$ to react with substrates and aliphatic diacyl peroxides should therefore be considered sources of alkyl rather than acyloxy radicals. Diacyl peroxides are more prone to induced decomposition than most dialkyl peroxides.
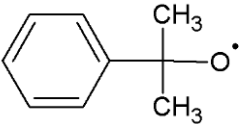
Peresters (e.g. TBPB) are sources of acyloxy and alkoxy radicals. While peroxides are the generally preferred initiators in monomer grafting experiments, azo-compounds have been also investigated by many authors. For example, AIBN was studied by Misra, Jassal and Pande [56] which is in general unsuitable because of both short $\tau_{1/2}$ and low tendency of cyanoalkyl radicals to hydrogen abstraction. In this study, influence of AIBN and DBP on grafting efficiency was examined. Grafting degree increased with increasing reaction time for both initiators. Higher grafting degree was reached for reaction initiated by AIBN due to relatively low reactivity of primary radicals which resulted in lower extent of undesired side reactions such as homopolymerization and termination reactions. High reactivity of phenyl and benzyloxy radicals arising from DBP decomposition resulted in higher rate of macroradical formation. On the other hand, high reactivity of DBP caused higher rate of consumption of primary radicals via reaction with highly reactive vinylacetate. Prasoetsopha, Chumsamrong, Suppakarn [57] studied radical grafting of natural rubber with acrylate monomers (glycidylmethacrylate, methylmethacrylate). Authors examined the influence of AIBN and DBP on grafting degree. Reaction temperature was 80 °C and reaction time 2 h. Higher grafting degree was determined for reaction initiated by DBP.

It has been noted in literature [9] that based purely on a consideration of bond dissociation energies (included in Table 2), methyl and alkoxy radicals should be equally proficient at hydrogen abstraction because both reactions are similarly exothermic. However, C–CH$_3$ bonds are significantly stronger than C–OR bonds. With regard to this fact alkoxy radicals can be considered to have a propensity for hydrogen abstraction while methyl radicals prefer addition to double bonds. This tendency is greater for higher alkyl radicals (see Table 2).

Table 5 constants rate constants of abstraction/addition reactions of primary and secondary radicals formed as a consequence of dicumyl peroxide (DCP) thermal decomposition. Values are based on Arrhenius parameters determined in solution at low temperatures and extrapolated to temperatures applied for grafting in melt. With regard to data in Table 5, primary cumyloxy radicals have a propensity for hydrogen abstraction which is enhanced at higher temperatures. Thus, the selection of an initiator which generates alkoxy radicals might be one way to minimise

homopolymerisation as a side reaction. In the contrast, methyl radicals show a lesser propensity for hydrogen abstraction which is approximately three orders of magnitude lower than that for cumyloxy radicals. In iaddition, the rate constant for addition reaction of methyl radicals is much greater than that for abstraction [58]. As shown in Table 5, higher reaction temperatures favoures β-scission of cumyloxy radicals.

Table 5. Rate constants for primary cumyloxy and secondary methyl radicals created via thermal decomposition of DCP.

Radical	Parameter	Temperature		
		140	180	220
cumyloxy radical	k_{sec}/k_{prim}	5.2	4.5	4.0
	k_{tert}/k_{prim}	7.4	6.1	5.2
	$k_{abstraction}$ (M$^{-1}\cdot$s$^{-1}\cdot\times10^{-6}$) [a]	6.8	8.7	10.8
	$k_{addition}$ (M$^{-1}\cdot$s$^{-1}\cdot\times10^{-6}$) [b]	64.4	162.4	352.5
	$k_{\beta\text{-scission}}$ (M$^{-1}\cdot$s$^{-1}\cdot\times10^{-6}$)	11.3	12.1	12.8
$CH_3^\bullet$	k_{sec}/k_{prim}	2.7	2.5	2.2
	k_{tert}/k_{prim}	12.6	9.9	7.4
	$k_{abstraction}$ (M$^{-1}\cdot$s^{-1}) [c]	7400	17000	36000
	$k_{addition}$ (M$^{-1}\cdot$s$^{-1}\cdot\times10^{-6}$) [b]	2.4	4.0	6.2

[a] hydrogen abstraction from cumene
[b] addition to styrene
[c] hydrogen abstraction from isooctane

As mentioned in chapter 2.2.1.1, the most important thing about the initiator is the effective flux of radicals which are generated. Morevoer, the miscibility of the initiator and radicals generated from it with the polymer phase is of key importance. Pesetskii et al. [41] observed the influence of initiator structure on grafting degree of low-density polyethylene (LDPE) with itaconic acid (IA) via reactive extrusion. Reaction was initiated by different monoperoxides and diperoxides. LDPE was impregnated by acetone solution of IAH and initiator. It was found that effect of solubility parameters δ of initiators is more important than k_d values. For example, solubility parameters of 2,2-di(tert-butyl peroxy)-5,5,6-trimethyl bicyclo [2.2.1] heptane (D-1), 2,2-di(3-methyl-1-butine-3-ylperoxy)-5,5,6-trimethyl bicyclo [2.2.1] heptane (D-2) and 2,5-dimethyl-2,5-di(terc-butyl peroxy)-hexane (L101) are similar to that of LDPE. The highest grafting efficiency was reached for reaction initiated by L101 due to similar δ of L101 and LDPE. Reaction conversion was in the range 50–90 % for L101 concentration between 0.05 and 3 wt %. Moreover, low extent of monomer homopolymerization was expected for different δ of monomer and initiator. Different grafting efficiency of two initiators was explained by different thermal stability although δ was similar. For example, lower thermal stability of D-2 compared to D-1 resulted in lower initiation activity. Reaction between LDPE and primary radicals of TBP resulted in higher amount of LDPE macroradicals with enhanced recombination and crosslinking.

The initiator $\tau_{1/2}$ should be in consistence with the concentration of generated radical species and with the residence time of reactants in the reaction zone.

In general, the initiator should be completely converted into corresponding radicals within the grafting reaction. High $\tau_{1/2}$ is unattractive from an economic view. In that case, residual initiator may have negatively affect product stability. Therefore, $\tau_{1/2}$ of the initiator should be short compared to the reaction time. It can be expected that no grafting occurs after consumption of the initiator [59]. It means that the use of long reaction times in conjunction with low $\tau_{1/2}$ has no beneficial effect and, moreover, may lead to shear induced degradation On the other hand, relatively low $\tau_{1/2}$ initially gives a higher concentration of radical species which may enhance the extent of side reactions such as crosslinking or radical-radical coupling. It is generally postulated, that the residence time corresponding to five half-lives equals to 97% consumption of the initiator.

2.3.4 Additives

In general, additives employed in radical grafting reactions can act in two ways: as radical traps or as chain-transfer agents. Various coagents have been described which improve grafting yields and/or reduce side reactions during melt phase processing. Grafting yield can be improved by addition of second monomer - comonomer. Various electron-rich comonomers have been shown to be effective as coagents for improving grafting yields and reducing side reactions of electron deficient monomers, such as styrene, MAH and methacrylic monomers [9], [60].

Comonomer limits extent of undesired side reaction (i.e. β-scission, crosslinking) by trapping radicals formed on polymer chain and reaction with macroradical at high reaction selectivity against grafted monomer. Function of comonomer is schemed in Figure 8. Many studies demonstrate the effect of styrene as comonomer during grafting of PP with maleic anhydride or glycidylmethacrylate [60]–[63]. This strategy involves choosing a monomer combination such that the coagent monomer is both effective in trapping the radicals formed on the polyolefin backbone and such that the propagating radical formed is highly reactive towards the desired monomer (Figure 8).
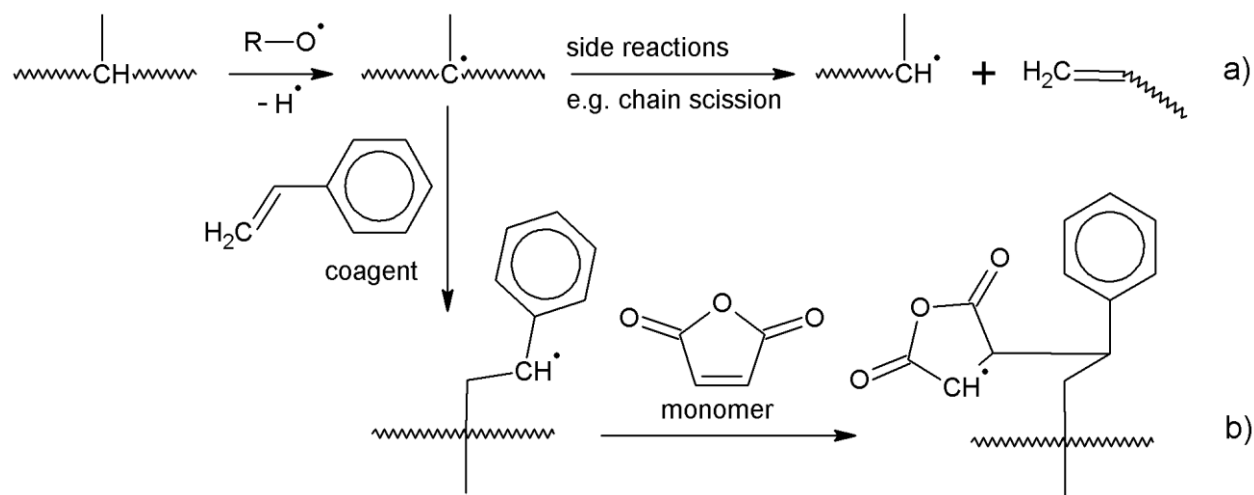

Figure 8. Limitation of β-scission of polymer chain (a) by addition of comonomer into the polymer system (b) [60].

In the peroxide crosslinking of PE, addition of organic nitroxides can retard the rate of cure by reducing the radical flux, but monofunctional nitroxides also impair the final properties by reducing the crosslink density. Bifunctional nitroxides, however, can enhance formation of intermolecular crosslinks [64]. For the same system (PE crosslinking with peroxide), Anbarasan et al. found the degree of crosslinking achieved in the presence of ester additives was inversely correlated with the degree to which the additives were incorporated into the polymer [65]. It is probable that these additives form radicals by abstraction and terminate radicals on the polymer backbone.

Gaylord observed that the signifi cant enhancement in crosslinking achieved with molten PE in the presence of maleic anhydride vanishes upon addition of any of a large number of sulfur-, nitrogen-, or phosphorus-containing compounds that also inhibit maleic anhydride homopolymerization [66]. This inhibition of grafting was observed even when dimethyl sulfoxide, dimethylacetamide, or nonylphenyl phosphite were added at an additive to maleic anhydride ratio of 1:10, where insufficient amounts will be present to react with maleic anhydride in some fashion before it attaches to grafting sites [67].

2.3.5   Reaction temperature

The reaction temperature strongly affects the kinetics of graft polymerization. General postulate says that grafting yield increases with increasing temperature, until some limit is reached. As in the case of radical species, faster monomeric diffusion occurs as temperature increases. This is in consistence with conclusions reported by Dilli et al. [68] who studied grafting of MMA on silk. The graft yield increased significantly with increasing temperature due to greater swelling of silk, and a corresponding enhanced rate of diffusion of the monomers in the vicinity of silk [69]. Different explanation given by Sun et al. [70] was based on increased thermal decomposition rate of initiator and the initiator efficiency in producing polymer macroradicals. Increased concentration of polymer macroradicals thus enhanced the graft polymerization.

Sacak and Pulat [71] and Sanli and Pulat [72] studied graft copolymerization of acrylamide on poly(ethylene terephthalate)films initiated by DBP. Both reseracher groups observed that the maximum graft yield occurs for a temperature near the glass transition temperature T_g. For temperatures below the T_g, the radicals formed in the polymer chains cannot react, owing to the reduced diffusion of the monomer, whereas for T above T_g, the number of radicals available for grafting will decrease with increasing temperature due to enhanced coupling of monomer radicals resulting in lower graft yield [73].

2.4   State of the art of PLA functionalization

PLA relates to the class of biodegradable, thermoplastic and aliphatic polyesters which are derived from renewable resources such as corn starch or sugar cane [74]. PLA has been used in many applications such as medical implants, sutures or drug delivery systems. Introducing new

functional groups onto PLA backbone paves the way to prepare composites, laminates, coated items and blend with improved properties and cost effectiveness. Functionalizing matrix polymer and the fiber/filler with highly reactive groups is perhaps the most successful strategy leading to a variety of commercial composites and alloys made by reactive processing. Possibility of chemical degradation makes PLA interesting alternative to petroleum-based polymers with tough recyclation.

Many grafting techniques can be used for production of variety functional groups onto the surface of natural polymers. Commonly used methods are melt grafting, solid state grafting, solution grafting and suspension grafting in aqueous or organic solvents. The post-polymerization free-radical functionalization process, generally performed in the melt by using extruders or melt mixers, is considered to be one of the most practical, cost effective and also green approach, since it is a solvent-free method. Regarding mentioned advantages, it can be applied for large-scale production. Functional groups such as isocyanata, amine, anhydride, carboxylic acid, epoxide and oxazoline are often introduced during reactive extrusion with a short residence time. Coupling reactions between mentioned functional groups provide interfacial bondings in composites, laminates, coated items and in immiscible polymer blends with improved control of the phase size and strong interfacial adhesion.

MAH was first monomer used for grafting onto biodegradable polymers such as poly(caprolactone), poly(butylene succinate-co-adipate) and PLA [75]–[79]. Maleation reaction mechanism has been already proposed by many authors as a complex process consisting of three steps (Figure 9). In first step, free radicals are formed via thermal decomposition of convenient initiator. In the second step, free radicals attack most labile C–H bond on backbone while PLA macroradical are generated. Finally, PLA macroradicals may react with the MAH. Radical functionalization with MAH initiated by peroxide is a complex process affected by polymer nature and by the feed ratio between the reagents. Moreover, many concurrent side reactions can limit the grafting yield and change the polymer structure.

Many studies deal with relationship between reaction parameters and grafting degree. For example, Ramkumar, Bhattacharya and Vaidya [77] mentioned increase of grafting degree with increase of concentration of initiator. Same results were presented by Carlson et al. [76] who performed free-radical-initiated grafting of MAH onto a PLA backbone at 180–200 °C initiated by 2,5-dimethyl-2,5-di-(tert-butylperoxy) hexane (Lupersol 101) concentration ranging from 0 to 0.5 wt % and 2 wt % of MAH using twin-screw reactive extruder. Under these conditions, between 0.066 and 0.672 wt % MAH was grafted onto the PLA chains.

Radical grafting of PLA with reactive monomers affects properties of modified PLA. Enhanced reactivity of PLA-g-MAH was discussed by Pan et al. [80] as a result of highly reactive carboxylic group. Carlson et al. [81] investigated the influence of concentration of initiator on the amount of grafted MAH and molecular weight of PLA-g-MAH. Increasing concentration of initiator resulted in increasing grafting degree while molecular weight decreased due to chain scission. Thus modified PLA improved miscibility in PLA/starch blend. Hwang et al. [82] investigated the influence of concentration of initiator on physical (T_g, T_m, X_c) and mechanical (tensile strenght, Young modulus, tensile elongation) properties. Grafting with MAH resulted in decrease of glass transition temperature and crystallinity due to branching. On the other hand, mechanical properties were unchanged.
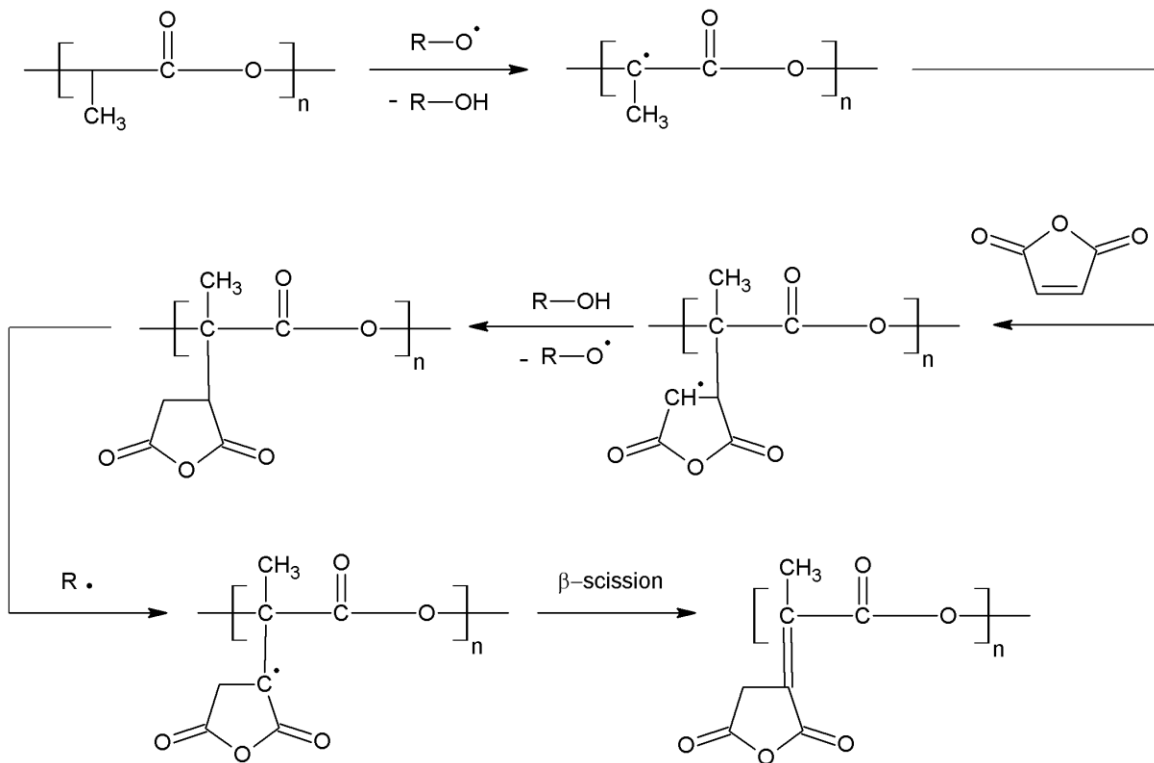
Figure 9. Scheme of maleation of PLA adapted from study Pan et al.[80].

Modified PLA can be used in composites reinforced by filler which exhibit improved biodegradability, adhesion towards filler particals and inhibited flammability.The effect of PLA-g-MAH in biocomposites was studied by Plackett [83]. Thus prepared biocomposites exhibited enhanced adhesion towards filler in wood fibers and nanoclay. Zhang and Sun [84] focused on testing mechanic properties of PLA/starch blends which were prepared by "in situ" compounding of PLA, starch and MAH in the presence of organic peroxide initiator. To compare, composites were also prepared by compounding of PLA, starch and PLA-g-MAH. In both cases, enhanced interfacial adhesion between PLA and starch resulted in increased tensile strenght and elongation

An effort to substitute petroleum-based polymers, leads to preparation of polymer blends with high content of polymers derived from renewable resources with improved biodegradability of prepared materials [85]. On the other hand, study proposed by Reddy, Nama and Yang [86] describes preparation of PP/PLA blend in order to avoid degradation and hydrolytic scission of PLA. Authors expect possible applicability of PP/PLA fibers with respect to lower price compare to PLA fibers. Possitive effect of compatibilizer on mechanical and thermal properties of polymer blends with PLA is mentioned in several works [86]–[87].

3. AIMS OF THE WORK

The main goal of proposed thesis is preparation and characterization of PLA grafted with IAH (signed as PLA-g-IAH). Reaction compounds (PLA and IAH) derived from renewable resources in combination with reaction method without using solvent make PLA-g-IAH to be a promising material with large scale of applications.

First part of experimental section is focused on investigation of grafting reaction "in situ" using thermal analysis. The aim of this section is to describe the influence of reaction parameters on reaction course. Formation of byproducts and their decomposition will be detected "in situ" during grafting reaction which is not able to observe within conventional procedure in internal mixer.

In the second part, PLA is functionalized via radical grafting with IAH in internal mixer at different concentration of reactants. Aims of this part are as follows:

1) Successful grafting of IAH onto PLA backbone, structure analysis and qualitative analysis of grafted IAH.
2) Proposition of reaction conditions and their optimization with respect to processing parameters of PLA and $\tau_{1/2}$ of chosen initiator.
3) Investigation of the influence of reaction conditions on grafting yield and extent of side reactions, possibility of IAH polymerization and structure of PLA-g-IAH.
4) Determination of kinetic parameters for selected reaction system.
5) Study of non-radical degradation of PLA during processing and its suppression by addition of chain extender.
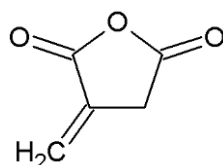
4. EXPERIMENTAL PART

This chapter provides detail description of materials, methods and characterization used in this thesis.
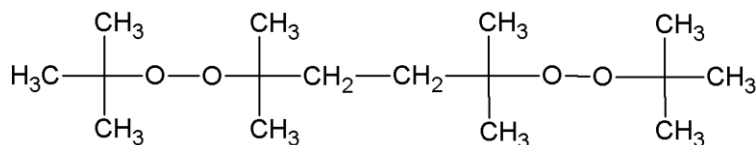
4.1 Reactants

- POLYMER: Poly(lactic acid) (PLA) Ingeo 2003D grade - NatureWorks Ltd; m. p. 150 °C; 1.24 $g \cdot cm^{-3}$; MFR (210/2.16) = 6 g/10 min.
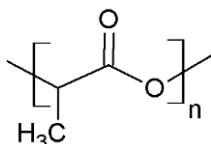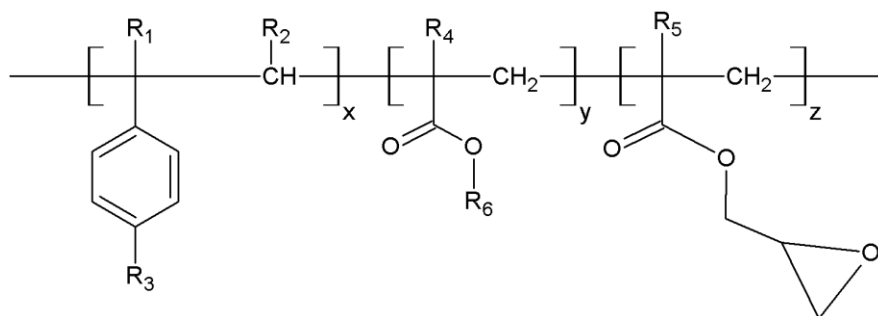
- MONOMER: Itaconic anhydride (IAH) - Fluka; M_w = 112.09 $g \cdot mol^{-1}$; m. p. 66–70 °C.

- INITIATOR: 2,5-bis(tert-butylperoxy)-2,5-dimethylhexane (L101) - Sigma-Aldrich; M_w = 290.44 $g \cdot mol^{-1}$; b. p. 55–57 °C; $\tau_{1/2}$ = 10 h (108 °C).

- CHAIN EXTENDER: Joncryl ADR-4368 C – BASF; M_w = 6800 $g.mol^{-1}$; T_g = 54 °C; epoxy equivalent weight 285 $g \cdot mol^{-1}$.

R_{1-5}: H, CH_3, C_{2-10} alkyl group, R_6: alkyl group

4.2 Experiments overview

4.2.1 Melt radical grafting of PLA in internal mixer

The PLA-g-IAH was prepared via grafting reaction between PLA and IAH initiated by L101 in laboratory kneader Brabender (Brabender, Germany) with 50 mL volume of reaction chamber. The reaction parameters used for reaction are summarized in Table 6. Defined amount of PLA was loaded into reaction chamber and plasticized for 2 min. After that, monomer was added and homogenized continuously for 1 min. Finally, initiator L101 was added and the reaction continued during mixing for next 6 min except of the experiments focused on reaction kinetics (see chapter 4.2.1.2).

In order to limit evaporation of initiator at processing temperature, a mixture of L101 and mineral oil was prepared at four different concentrations shown in Table 6. Desired amount of initiator was dissolved in 0.5 ml of mineral oil and stirred with magnetic stirrer for 10 min for completely dissolving of initiator. For each reaction the volume of mineral oil was the same in order to minimize its influence on rheology of the reaction system within reaction.

Table 6. Overview of reaction conditions applied for radical grafting of PLA.

[IAH]$_0$ [wt %]	signification (IAH/L101 molar ratio) [L101]$_0$ [wt %]			
	0.1	0.5	1	2
0.5	0.5-0.1 (12.96)	0.5-0.5 (2.59)	0.5-1 (1.30)	0.5-2 (0.65)
1	1-0.1 (25.91)	1-0.5 (5.18)	1-1 (2.59)	1-2 (1.30)
5	5-0.1 (129.56)	5-0.5 (25.91)	5-1 (12.96)	5-2 (6.48)
10	10-0.1 (259.11)	10-0.5 (51.82)	10-1 (25.91)	10-2 (12.96)

Reaction temperature 190 °C (T_m of PLA equals to 150 °C) was calculated using Arrhenius equation:

$$k = A \cdot \exp\left(\frac{-E_a}{R \cdot T}\right)$$
(4)

where activation energy parameter ($E_a = 155.7$ kJ·mol^{-1}) and pre-exponential parameter ($A = 8.731 \times 10^{15}$·s^{-1}) of L101 were applied. Reaction time 6 min equaled to $10 \times \tau_{1/2}$ of peroxide where $\tau_{1/2}$ equals to 36 s. After 6 min of reaction period, L101 is completely decomposed.

Following Equation 5, calculated L101 percent remaining decreases exponentially with increase of reaction time:

$$L101 \quad percent \quad remaining \quad = \exp\ (-\ k \cdot t) \qquad\qquad (5)$$

where k represents rate constant of L101decomposition given by the Equation 4. Time dependence is illustrated in Figure 10.
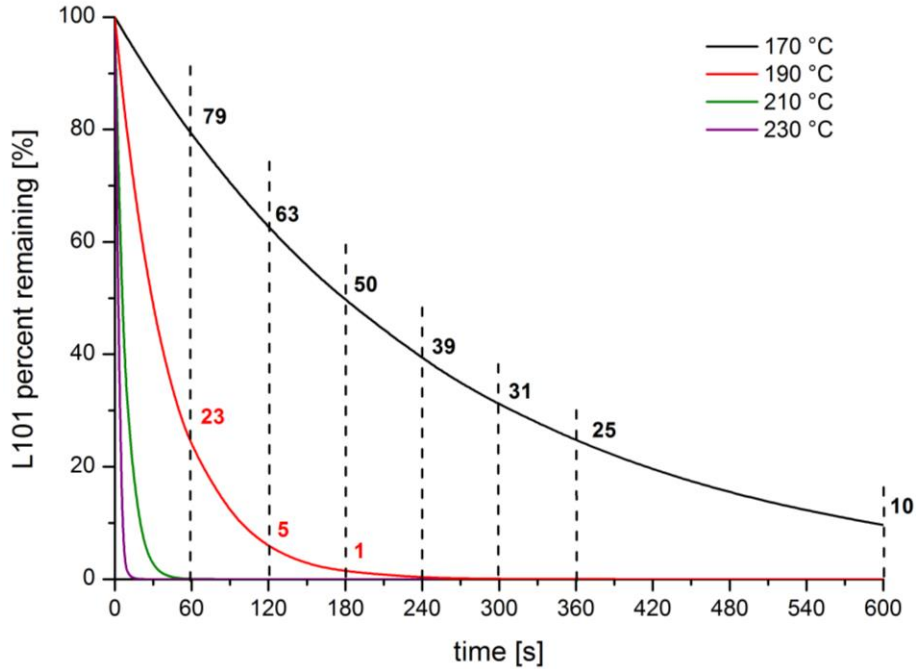

Figure 10. Calculated L101 percent remaining as a function of time determined for different reaction temperatures.

Calculated temperature 190 °C also minimizes the effect of trans-esterification as a dominant degradation mechanism at temperatures above 200 °C [88]. Moreover, degradation products of trans-esterification can enhance the thermal degradation of PLA [89].

Prepared PLA-g-IAH was pressed between two metal plates and approximately 15 g of sample were chopped onto small pieces and pressed using hydraulic laboratory press machine Fontijne (Netherlands) to prepare films with the thickness of 100 µm.

Unreacted monomer was removed by dissolving 5 g of grafted polymer in 50 ml of 1,2-dichlorbenzene at boiling temperature using reflux condenser. After complete dissolving, polymer solution was precipitated into ethanol, filtered and white powdered product was dried in vacuum oven at 60 °C for 12 h.

4.2.1.1 Radical reaction of PLA with IAH in the presence of chain extender

Chain extender Joncryl ADR-4368 C was chosen in order to avoid PLA hydrolytic degradation during processing. The effect of chain extender was detected by change of PLA-g-IAH rheological properties of PLA-g-IAH. In consistence with parameters given in Table 7, PLA-g-IAH samples were prepared via radical reaction according procedure which is described in chapter 4.2.1. 0.5 wt % of the chain extender was loaded into the polymer melt just before loading of initiator.

Table 7. Reaction parameters applied for radical grafting of PLA in the presence of 0.5 wt % chain extender.

	signification			
	(IAH/L101 molar ratio)			
	$[L101]_0$ [wt %]			
$[IAH]_0$ [wt %]	0.1	0.5	1	2
0.5	0.5-0.1-0.5 *(12.96)*	0.5-0.5-0.5 *(2.59)*	0.5-1-0.5 *(1.30)*	0.5-2-0.5 *(0.65)*
5	5-0.1-0.5 *(129.56)*	5-0.5-0.5 *(25.91)*	5-1-0.5 *(12.96)*	5-2-0.5 *(6.48)*

4.2.1.2 Kinetics of grafting

Influence of reaction time, reaction temperature and concentration of initiator was studied in kinetic experiments regarding reaction conditions summarized in Table 8. Reaction procedure consisted of five main steps: 1) reactants loaded into the reaction chamber; 2) radical reaction proceeded for desired reaction period; 3) screw drive stopped, cetrain amount of polymer removed from reaction chamber; 4) reaction product cooled down to stop the reaction; 5) screw drive turned on, continuation of radical grafting. Reaction products were purified according previous procedure by dissolving in dichloromethane and precipitation in methanol. Purified PLA-g-IAH was dried in vacuum oven for 12 h at 60 °C.

Thus prepared samples were characterized via acid-base titration in order to determine amount of grafted monomer and reaction conversion. Quantitative analysis was achieved according to procedure described in chapter 4.3.2.

Table 8.   Reaction parameters applied for kinetic study of PLA radical grafting.

[IAH]$_0$ [wt %]	[L101]$_0$ [wt %]	T$_r$ [°C]	t$_r$ [min]
	0.1	170	1, 3, 6, 10
0.5	0.5	170	1, 3, 6, 10
	1	170	1, 3, 6, 10
	0.1	190	1, 3, 6, 10
0.5	0.5	190	1, 3, 6, 10
	1	190	1, 3, 6, 10
	0.1	210	1, 3, 6, 10
0.5	0.5	210	1, 3, 6, 10
	1	210	1, 3, 6, 10

4.2.1.3   *Extraction of low molecular weight fractions*

Low molecular weight fractions were extracted from raw PLA-g-IAH by extraction in aceton at room temperature for 48 h. Solvent was evaporated under atmospheric pressure and thus prepared powdered samples were overdried in vacuum oven at room temperature. Thus obtained samples were used for further characterization.

4.2.2   **Investigation of radical grafting "in situ"**

Radical grafting was also studied "in situ" using differential scanning calorimetry (DSC) and thermogravimetric analysis (TGA). Concentrations of monomer and initiator were used according to Table 6, chapter 4.2.1. Granules of PLA were milled and thus prepared powder was impregnated with mixture of IAH and L101 in acetone. First, mixture of IAH and L101 in aceton was homogenized in closed flask for 10 minutes using magnetic stirrer to obtain homogenous mixture. Subsequently, aceton solution was mixed with PLA powder and solvent was evaporated at room temperature. Prepared samples were overdried in vacuum oven at laboratory temperature for 12 h. Thus prepared PLA/IAH/L101 mixtures were used for analysis.

DSC was used for determination of reaction parameters, such as activation energy or reaction enthalpy. Approximately 20–30 mg of reaction mixtures PLA/IAH/L101 was loaded into the hermetically closed aluminum crucible. Grafting reaction was studied via DSC run (TA Instruments 2920) achieved in temperature range from 30 to 210 °C at heating rate of 5 °C/min under nitrogen atmosphere. Raw data were processed by TA Universal Analysis software.

TGA was used for qualitative analysis of decomposition products released during grafting reaction. Desired amount of powdered sample was loaded into the platinum pan and reaction was achieved in the temperature range from room temperature to 240 °C and a heating rate 5 °C/min, consequently from 240 °C to 500 °C and a heating rate 10 °C/min.

4.2.3 Simulation of side reactions

4.2.3.1 Homopolymerization of IAH

In the system monomer-initiator several side reactions may occur simultaneously with the main grafting reaction. One of the most discussed side reaction in described reaction system is reaction monomer-monomer (homopolymerization).

Radical IAH homopolymerization was simulated via reaction in glass tubes at conditions similar to those applied to grafting reactions in chapter 4.2.1. Glass tube was heated in oil bath at 190 °C. Once the desire reaction temperature was reached, IAH/L101 mixture was placed into the glass tube in given IAH/L101 ratio which is shown in Table 9 as well as other reaction parameters.

Solution polymerization of IAH was achieved in the presence of AIBN initiator in order to prepare p(IAH) according to method giving sufficient polymerization yield [90]–[92]. Polymerization of IAH was accomplished by modified method published by Otsu and Yang [93]. Itaconic anhydride was polymerized in ethyl acetate at 80 °C for 12 h in the presence of AIBN radical initiator (4 mole % with respect to monomer). Thus prepared p(IAH) was precipitated in toluene and dried at 80 °C for 10 h.

Table 9.   Reaction parameters applied for side reaction between IAH and L101.

Signification	IAH/L101 [mol/mol]	T_r [°C]	t_r [min]
2.59	2.59		
5.18	5.18		
25.91	25.91		
51.28	51.28	190	6
129.56	129.56		
259.11	259.11		

4.2.3.2 Reactions between PLA and primary radicals

Reaction between PLA and L101 was studied via reaction without IAH in internal mixer at 190 °C and 6 min residence time. Concentrations of L101 were in agreement with those given in Table 6, chapter 4.2.1 (0.1–2 wt %).

4.2.3.3 IAH isomerization

Possible IAH isomerization onto citraconic anhydride (CAH) was studied via reaction achieved in glass tube at 80, 100, 120, 140, 160 and 180 °C for 6 min residence time.

4.3 Characterization methods

4.3.1 Structure analysis

Characteristic functional groups of PLA-g-IAH were observed by Fourier transform infrared spectroscopy (FTIR) and compared to FTIR spectrum of neat PLA. PLA-g-IAH films with thickness of 100 µm were analyzed using FTIR spectrometer (Bruker) in attenuated total reflection (ATR) mode (32 scans, resolution 4 cm^{-1}).

Proton nuclear magnetic resonance (^{1}H-NMR) was used to estimate the structure of modified PLA to prove the presence of grafted monomer. Approximately 10 mg of purified PLA-g-IAH was dissolved in 0.7 ml of deuterated chloroform CDCl$_3$. Thus prepared polymer solution was put into the test tubes and measured using Varian 500 MHz spectrometer.

4.3.2 Grafting yield determination

Approximately 0.2 g of purified PLA-g-IAH was dissolved under stirring in 20 ml of THF using reflux condenser. After complete dissolving, the solution was cooled down at room temperature and 6–8 drops of 1% thymol blue in ethanol were added. The acid-base titration was carried out with 0.005M potassium hydroxide (KOH) in ethanol. The equivalence point was recognized due to yellow-blue change of colour. The grafting degree [IAH]$_{PLA}$ was calculated according to Equation 6:

$$[IAH]_{PLA} = \frac{c_{KOH} \cdot (V_{KOH} - V_{blank}) \cdot M_{IAH} \cdot \frac{1}{2}}{m_v} \cdot 100 \quad [wt \ \%] \tag{6}$$

where c_{KOH} is concentration of KOH solution (mol·L^{-1}); V_{KOH} and V_{blank} (mL) is the volume of KOH solution at equivalence point for the PLA-g-IAH and neat PLA, respectively; M_{IAH} is molecular weight of IAH (g·mol^{-1}); m_v is the weight of the sample used for analysis (g). Since different –COOH groups can be presented in PLA-g-IAH solution, neat PLA was titrated in order to minimize innacurancy of quantification of grafted IAH [94]. Accordingly, except of –COOH groups of IAH, appearance of end groups of PLA can be presumed as a result of hydrolysis of PLA backbone appeared during processing [95].

4.3.3 Rheological properties

The melt flow rate (MFR) of PLA-g-IAH and neat PLA was measured by Melt Flow Tester Ceast (Ceast MMF 70-24.000, Italy). Approximately 6 g of sample were loaded into the heated barrel equipped with capillary and the MFR was performed according to ISO 1133D standard method (190 °C/2.16 kg).

Flow curves for chosen PLA-g-IAH samples prepared with/without addition of chain extender were measured by the same device as for regular melt flow index measurement. Four different loadings were applied depending on viscosity of polymer melt: 1.2, 2.16 and 3.8 kg for samples without chain extender, 2.16, 3.8 and 5 kg for samples prepared in the presence of chain extender. MFR was always measured at 190 °C.

The viscometric measurements of PLA-g-IAH solutions were carried out using Ubbelohdeho viscometer. The concentration of PLA-g-IAH solutions covered 1–20 g/L where the maximum concentration was limited by the thickness of viscometer capillary. All measurements were carried out at 30 ± 0.1 °C where all measured solutions were tempered at least for 30 minutes before measuring. Each sample was measured three times for satisfactory reproducibility. Thus obtained concentration-viscosity was extrapolated to zero concentration to obtain intrinsic viscosity and deduce molecular weight of tested PLA-g-IAH samples.

4.3.4 Molecular weight determination

Size exclusion chromatography SEC was used to determine changes of molecular weight due to grafting reaction. Approximately 1 mg of purified PLA-g-IAH was dissolved in 1 ml of THF and ca 0.8 mL of each sample solution was injected into the SEC chromatograph (Waters, USA) through the 0.45 µm filter to remove insoluble fragments which may block the system. Flow rate 0.5 mL.min^{-1}, run time 30 min and temperature 35 °C was applied.

4.3.5 Thermal properties

Thermal properties of prepared samples such as glass transition temperature T_g, melting temperature T_m, cold crystallization temperature T_c and percent crystallinity X_c were determined using differential scanning calorimeter DSC (Netzsch, Germany). Analysis was achieved in temperature range from 20 to 220 °C at heating rate of 20 °C/min and 10 °C/min during first and second heating cycle, respectively. All measurements were carried under nitrogen atmosphere. Mentioned phase transitions were determined using Netzch software (Netzsch Proteus thermal analysis) and the X_c was calculated using the following Equation 7:

$$X_c = \frac{\Delta H_m - \Delta H_c}{\Delta H_m^o} \cdot 100 \quad [\%]$$ (7)

where ΔH_m, ΔH_c and ΔH_m^o (J·g^{-1}) are enthalpies of fusion, enthalpy of cold crystallization and enthalpy of fusion of 100% crystalline PLA (93.1 J·g^{-1}), respectively [96].

4.3.6 Thermal stability

Thermal stability was carried out using TA instruments Q500 device. Thermogravimetric analysis (TGA) was carried out under nitrogen atmosphere from room temperature to 500 °C and a heating rate of 10 °C/min. Raw and purified PLA-g-IAH samples were analyzed.

Differential thermal analysis (DTA) of IAH was achieved in order to detect exothermic and endothermic processes simultaneously with degradation processes. DTA analysis was carried out under argon atmosphere from room temperature to 250 °C and a heating rate of 5 °C/min.

4.3.7 Biodegradation test

Purified PLA-g-IAH foils used for biodegradation test were prepared by evaporation of solvent (THF). Thus prepared samples were placed into glass vials and 4 ml H_2O was added. The pH values of suspension liquor were measured once a week for 12 weeks using pH meter S2K712 (ISFETCOM, Japan).

4.3.8 Colorimetric analysis

Color change of unpurified PLA-g-IAH was measured using X-rite i1 spectrophotometer in visible spectrum 380–760 nm. Polymer foils with the thicknes of 450±20 µm were used for measurement while each sample was measured five times for satisfactory reproducibility.

4.3.9 Contact angle measurement

Contact angle tester (rame-hart Model 250) was used to predict the influence of grafted IAH on hydrophilic properties and surface tension of PLA-g-IAH. Polymer films of non-purified samples were prepared by evaporation of THF from polymer solution and thus prepared PLA-g-IAH films were used for analysis.

5. RESULTS AND DISCUSSION

5.1 Prediction of grafting mechanism

As mentioned in the theoretical background, radical grafting is a complex of reactions which occur simultaneously with the main grafting reaction. Generally, these reactions can be split on desired main grafting reaction and undesired side reactions which complicate grafting process. The main grafting reaction is schemed vertically in the Scheme 1 and contains following reaction steps: a) thermal decomposition of initiator (L101) according to reaction 1 and generation of primary radicals which may be decomposed on secondary radicals (reaction a1) - both types of radicals signed as L101$^\bullet$; b) PLA macroradicals formation (PLA$^\bullet$) by hydrogen abstraction mainly from tertiary carbon of PLA backbone (reaction 2); c) covalent bonding of monomer (IAH) onto PLA$^\bullet$ (reaction 3); d) termination of grafting by hydrogen donors (reaction 4). Proposed reaction sequence leads to preparation of PLA modified with IAH, in this thesis signed as PLA-g-IAH.

Main grafting reaction is limited by several side reactions which may occur during functionalization depending on reaction conditions (e.g. initiator and monomer concentration, reaction temperature, reactivity of generated radicals, etc.). Most important side reactions are expected and horizontally schemed in the Scheme 1.

Except of hydrogen atom abstraction, L101$^\bullet$ (formed in reaction 1 and 1a) can either recombine (reaction 1b) or interact with IAH forming inactive species and IAH radicals (IAH$^\bullet$), respectively. Both reactions decrease grafting yield. Moreover, it is expected that secondary methyl radicals are more favoured to participate on IAH homopolymerization via addition to IAH double bond (reaction 1a) compared to bulky t-butoxy radicals.

PLA$^\bullet$ generated according to reaction 2 can undergo several reactions which may affect flow properties and mechanical properties. Due to reaction between PLA$^\bullet$ and L101$^\bullet$, active centers become inactive for grafting (reaction 2a). Coupling reactions between PLA$^\bullet$ cause crosslinking (reaction 2b) which influences solubility and gel content. Degradation reaction 2c represents β-scission with subsequent radical branching (reaction 2ca).

When IAH is bonded on PLA backbone, reactive center located in the structure of bonded IAH can be deactivated in several ways. PLA-g-IAH radicals (PLA-g-IAH$^\bullet$) are perished by interactions with other radical species (reaction 3a), coupling with another PLA-g-IAH$^\bullet$ (reaction 3b) or homopolymerization on PLA chain (reaction 3c).

Molecular weight of PLA-g-IAH can decrease although grafting degree increases. This may occur due to presence of labile hydrogen atom on tertiary carbon of grafted IAH which can be abstracted by radical species. Thus formed PLA-g-IAH may undergo β-scission according to Scheme 1.

Except of radical reactions, non-radical reactions participate on the grafting process and affect properties of functionalized PLA. These reactions are based on the nature of PLA and will be discussed below.
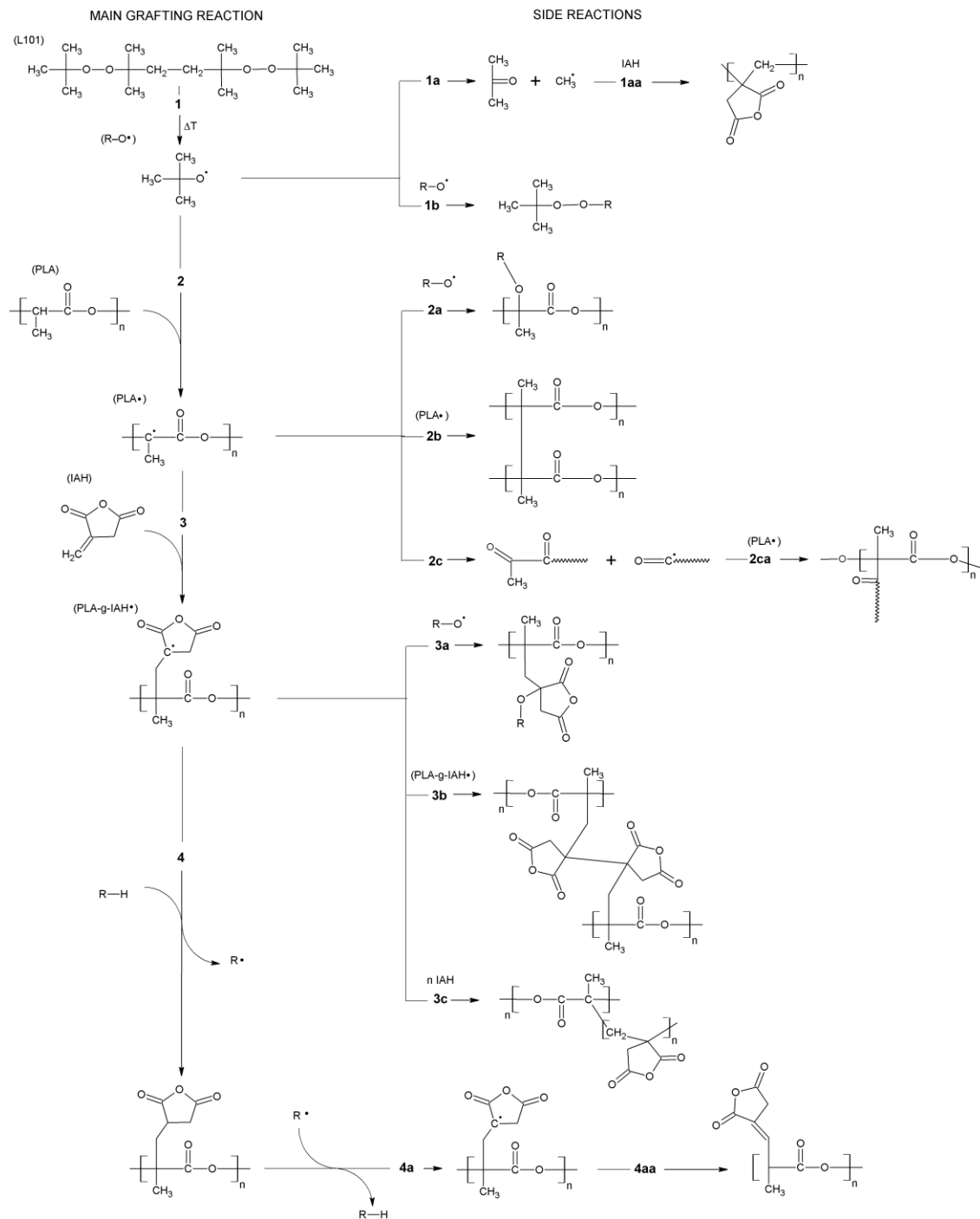
Scheme 1. Expected main grafting reaction including: generation of primary radicals via thermal decomposition of L101 (1); hydrogen abstraction from PLA backbone (2); addition of IAH onto PLA (3); termination of grafting (4). Possible side reactions: formation of secondary methyl radicals (1a) and possible IAH homopolymerization (1aa); primary radicals recombination (1b); extinction of active center on PLA backbone (2a); crosslinking (2b); β-scission (2c) with subsequent radical branching (2ca); addition of radicals on PLA-g-IAH• (3a); coupling of PLA-g-IAH• (3b); homopolymerization of grafted IAH (3c); hydrogen abstraction from PLA-g-IAH (4a) with subsequent β-scission (4aa).

41

5.2 Investigation of PLA grafting "in situ"

Radical grafting of PLA with IAH was investigated "in situ" using DSC in the temperature range 30–220 °C at heating rate 5 °C/min. Different $[IAH]_0$ and $[L101]_0$ were applied according to concentrations of reactants used for grafting reaction achieved in internal mixer (Table 6, chapter 4.2.1). DSC thermogram typical for "in situ" grafting reaction is shown in Figure 11a. DSC curve of each sample consists of three phenomena: a) glass transition of PLA at ~50 °C; b) melting of PLA reflected by endothermic peak at ~150 °C; c) broad exothermic peak attributed to grafting reaction in melt. Dashed curve in Figure 11 represents decreasing content of L101 which was calculated regarding heating rate. L101 is completely consumed at ~180 °C which corresponds with maximum of exothermic peak reflecting grafting reaction. Below this temperature, reaction conversion increases as both reaction time and concentration of L101$^\bullet$ increase. Above 180 °C, decrease of reaction rate is expected due to absence of L101$^\bullet$ while termination reactions are prefered.

Although many authors do not expect simultaneous IAH homopolymerization due to high processing temperature, configuration of DSC experiments allows predicting IAH homopolymerization occuring simultaneously with main grafting reaction. DSC curves in Figure 11a–d represent reaction system with 0.5–10 wt % of IAH and 0.1–2 wt % of L101. As mentioned above, each DSC curve exhibits exothermic peak in the range 160–210 °C which reflects overall grafting reaction. Reaction system with 0.1 and 0.5 wt % of L101 contains exothermic peak which is signifficantly separated from the endothermic peak reflecting PLA melting. On the other hand, DSC curves of reaction system containing 1 and 2 wt % L101 does not exhibit sharp boundary between endothermic melting and exothermic grafting. This phenomenon may suggest hypothesis that homopolymerization of IAH occurs at lower temperature compared to main grafting reaction.

Hypothesis described above is based on the fact that melting of PLA occurs in the temperature range 110–160 °C depending on the molecular weight of melted polymer and polydisperzity of system. Concentration of primary radicals is expected to be low in this temperature range with respect to high $\tau_{1/2}$ of L101 in this temperature range. Consequently, IAH homopolymerization can be expected and p(IAH) could be formed. At relatively lower temperature (around PLA melting), low mobility of polymer chains retards grafting reaction. Low bulky IAH molecules with high mobility can thus interact with L101$^\bullet$ whereas their relatively high mobility allows formation of p(IAH). Although high mobility of low molecules could support their interactions, high concentration of polymer chains and tertiary carbons prefers reaction between PLA and L101$^\bullet$. Consequently, high $[IAH]_0$ and $[L101]_0$ could enhance the extent of interactions between IAH and L101$^\bullet$ which would raise yield of IAH homopolymerization.
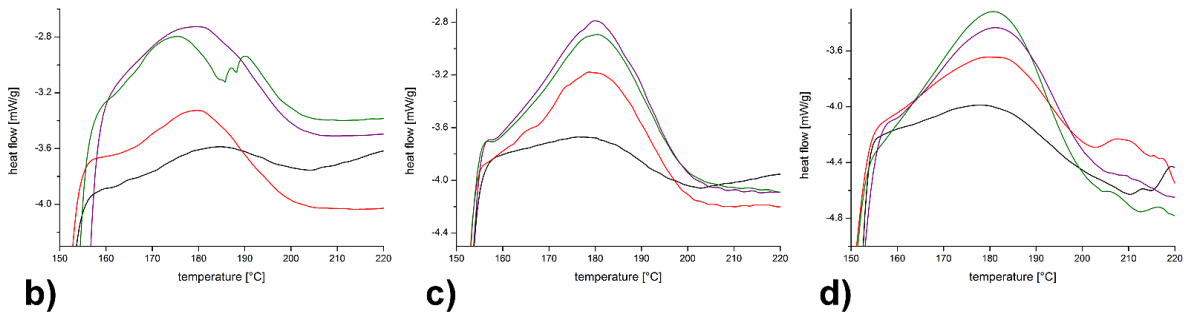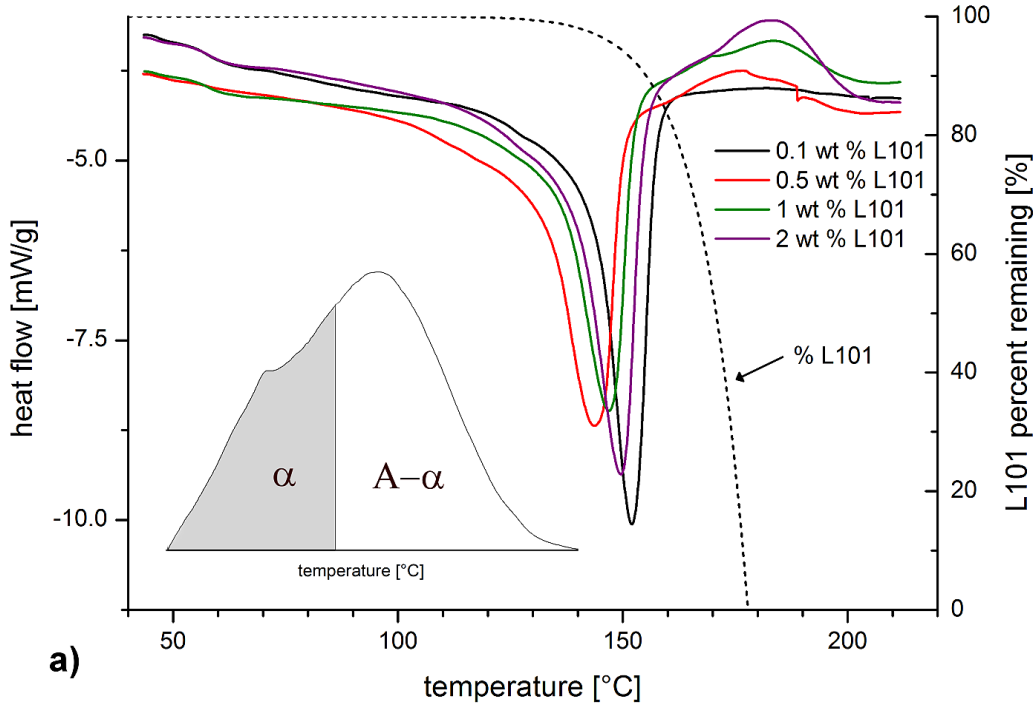
Figure 11. "In situ" investigation of PLA grafting with IAH: DSC thermogram representing thermal response of grafting reaction of samples 0.5-x (a), 1-x (b), 5-x (c) and 10-x (d) where x = [L101]$_0$ = 0.1–2 wt %; part (a) includes schematic illustration of observed exothermic peak attributed to heat of reaction vs. temperature for grafting reaction.

Depending on the [IAH]$_0$ and [L101]$_0$, heat of reaction ΔH_r changes. 3D plot in Figure 12 illustrates the influence of concentration of reaction compounds on heat evolving during reaction. It can be assumed that heat of reaction relates to reaction composition and increases with increasing [IAH]$_0$ and [L101]$_0$. As [IAH]$_0$ is constant, heat of reaction increases rapidly with increase of [L101]$_0$. Observed relationship is in good agreement with previous assumption that higher [L101]$_0$ supports formation of PLA$^•$ with subsequent bonding IAH. When [L101]$_0$ is low (i.e. 0.1 wt %), ΔH_r slightly increases (1.7–4.9 J.g^{-1}) with increasing [IAH]$_0$. At these reaction conditions, grafting degree reached 0.18–0.88 wt % (see Figure 17, chapter 5.4.1). It can be concluded that total heat of reaction can be evolved mainly from grafting reaction. On the other hand, two main differences should be mentioned. First, efficiency of radical grafting achieved in internal mixer was supported by intensive homogenization during processing. Instead of this,

calorimetric study of PLA grafting is strongly dependent on diffusion of reaction compounds as well as on their mobility. From this reason, reactions of bulky radicals are more disadvantaged. Second, total heat of reaction represents sum of heats of individual side reactions which were mentioned in previous text. Especially at high $[IAH]_0$, homopolymerization may affect total heat of reaction althogh it is not usually expected due to high operating temperature.
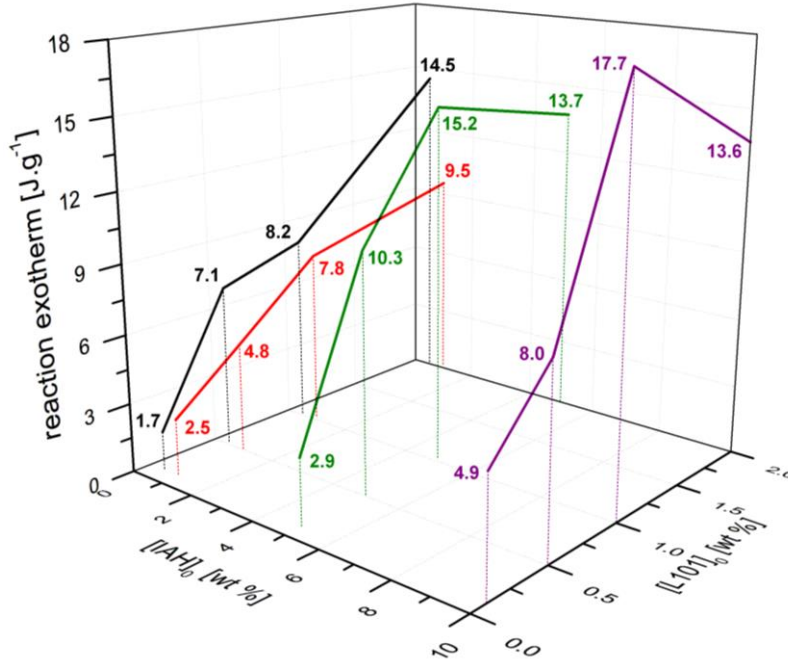
Figure 12. Relationship $[IAH]_0$-$[L101]_0$-ΔH_r derived from DSC thermogram obtained during „in situ" calorimetry grafting.

The heat of grafting reaction determined for reaction system with constant $[L101]_0$ does not increase so rapidly with increasing $[IAH]_0$. It can be concluded that at low $[IAH]_0$, secondary reactions occur, i.e. crosslinking and chain branching. Based on the heat evolved during reaction, these undesired reactions exhibit higher reaction enthalpy compared to reactions that predominate at high $[IAH]_0$.

Grafting reaction can be expressed by the universal Equation 8 which was applied in study Passaglia et al. [97]:

$$\frac{d\alpha}{dt} = k \cdot (1 - \alpha)^n \tag{8}$$

where α is the degree of reaction conversion, n is the order of the reaction and k is the specific rate constant defined as follows:

$$k = k_0 \cdot \exp\left(-\frac{E_a}{R \cdot T}\right) \tag{9}$$

Combination of Equation 8 and 9 gives:

$$\frac{d\alpha}{dt} = \beta \cdot k_0 \cdot \exp\left(-\frac{E_a}{R \cdot T}\right) \cdot (1 - \alpha)^n \tag{10}$$

Figure 11a describes exothemic peak characteristic for radical reaction. Heat of reaction can be used for calculation overall kinetic parameters of the grafting reaction main reaction as well as other secondary reactions. Integral area of exothermic peak A gives total heat ΔH evolved during the overall reaction. In this case, $\Delta H = A$ and the heat of polymerization per mole is given by A/n_0, where n_0 is initial number of IAH molecules.

Change of enthalpy dH over a gradient of time dt equals to number of IAH molecules that have reacted during a certain reaction period:

$$dH = -\left(\frac{A}{n_0}\right) dn \tag{11}$$

where A/n_0 determines heat of reaction per mole of IAH used for reaction. Equation 11 is converted to Equation 12 which describes consumption of IAH during grafting reaction by:

$$-\frac{dn}{dt} = \left(\frac{n_0}{A}\right)\frac{dH}{dt} \tag{12}$$

With respect to first-order kinetics, IAH consumption can be expressed by Equation 13:

$$\frac{dH}{dt} = k \cdot [IAH] \cdot \left(\frac{A \cdot V}{n_0}\right) \tag{13}$$

According to Equation 13, IAH concentration at any instant of time can be expressed as:

$$[IAH] = \frac{n_0}{V} - \frac{n_0}{V} \cdot \left(\frac{\alpha}{A}\right) = \frac{n_0}{V} \cdot \left(\frac{A - \alpha}{A}\right) \tag{14}$$

where α is the partial area of exothermic peak (shaded) indicating change of enthalpy at time t. Substituting the value of [IAH] in Equation 14 it can be written:

$$\frac{dH}{dt} = k \cdot \left(\frac{n_0}{V}\right) \cdot \left(\frac{A - \alpha}{A}\right) \cdot \left(\frac{A \cdot V}{n_0}\right) = k \cdot (A - \alpha) \tag{15}$$

where k is rate constant expressed from the Arrhenius form in Equation 9.

Theoretical background given by Equations 8–15 was used to calculate pre-exponential factor k_0 and activation energy E_a. Relationship between logarithmic form of rate constant $\ln k$ and 1/RT was linearly fitted giving linear approximation $y = a \cdot x + b$ where constant a equals to activation energy and constant b relates to pre-exponential factor. Thus obtained data are summarized in Table 10.

Table 10. Reaction enthalpies ΔH_r, activation energy E_a and pre-exponential factor k_0 for different composition of PLA/IAH/L101 reaction system derived from DSC experiments.

Sample	[IAH]/[L101] [mol/mol]	ΔH_r [J.g^{-1}]	E_a [kJ.mol^{-1}]	$\ln k_0$ [-]
0.5-0.1	12.96	1.73	152.6	39.1
0.5-0.5	2.59	7.13	177.3	47.4
0.5-1	1.30	8.24	167.7	44.4
0.5-2	0.65	14.52	158.8	42.8
1-0.1	25.91	2.50	179.2	44.8
1-0.5	5.18	4.81	111.0	29.9
1-1	2.59	7.76	152.2	40.5
1-2	1.30	9.52	159.1	42.8
5-0.1	129.56	2.88	149.0	37.2
5-0.5	25.91	10.28	152.1	41.4
5-1	12.96	15.21	157.1	42.6
5-2	6.48	13.72	147.4	40.1
10-0.1	259.11	4.97	111.3	27.9
10-0.5	51.82	8.02	178.1	47.9
10-1	25.91	17.70	141.7	38.7
10-2	12.96	13.63	155.5	42.1

Grafting reaction was studied by TGA analysis in order to detect reaction products formed "in situ" during reaction depending on their thermal stability. TGA curves of reaction were recorded in the temperature range 20–240 °C at heating rate 5 °C/min whereas L101 was completely decomposed under these conditions. In the temperature range 240–500 °C (heating rate 10 °C/min) all reaction products were completely decomposed. Figure 13 represents plot between weight loss and temperature reflecting decomposition of both PLA-g-IAH and byproducts formed during temperature ramp for all tested samples. Obtained TGA curves were converted into derivative curves with higher resolution of individual decomposition steps.
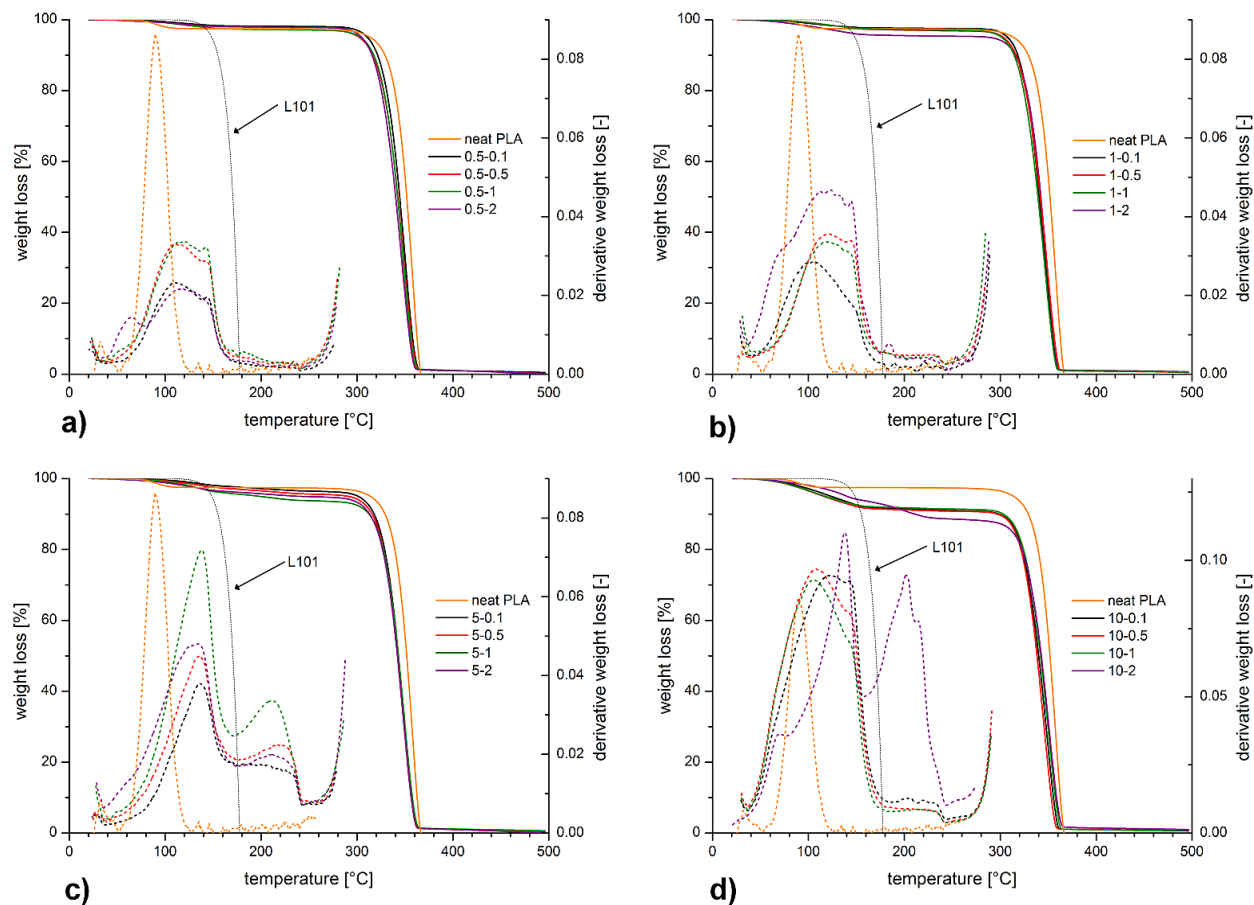
Figure 13. TGA curves recorded "in situ" for reaction system PLA/IAH/L101 with different $[IAH]_0$ and $[L101]_0$; dashed line represents L101 percent remaining during temperature ramp.

Neat PLA is decomposed in two major degradation steps. Decomposition step #1 with maximum decomposition rate (T_{max}) at ~90 °C is probably attributed to the released moisture. Decomposition step #5 reflects decomposition of PLA matrix with T_{max} at around 357 °C.

TGA plots of all „in situ" grafted samples contain negligible decomposition step #1 in the range 50–60 °C which can be assigned to partial evaporation of adsorbed initiator (boiling point 55–57 °C) or residual amount of solvent (boiling point 56 °C). This assumption is supported by increasing weight loss with increasing $[L101]_0$.

TGA curves of "in situ" modified PLA contain decomposition steps #2 reflecting reaction products of IAH-L101˙ interactions with lower thermal stability compared to IAH. Therefore, decomposition step #3 can be assigned to decomposition of IAH whereas thermal stability of untreated IAH is discussed more extensively in chapter 5.5.1.

Decomposition step #4 was observed only for samples with high $[IAH]_0$ (5 and 10 wt %). High $[IAH]_0$ and T_{max} at around 210 °C could indicate decomposition of p(IAH) with various polymerization degree. This it is in good agreement with conclusions of Shang, Huang and Weiss [91]. In this study, p(IAH) began to degrade at 170 °C. Regarding derivative TGA plot, increase of $[L101]_0$ leads to slight increase of p(IAH) content (see Table 11).

All measured samples exhibit intensive decomposition step which reflects decomposition of PLA backbone. T_{max} is in the range 346–350 °C slightly depending on the extent of side reactions (Table 11). Highest T_{max} was detected for sample 0.5-0.1 due to low extent of interactions between PLA and L101$^{\bullet}$ which are responsible for subsequent β-scission. On the other hand, high concentration of generated L101$^{\bullet}$ resulted in decrease of thermal stability observed for sample 0.5-2.

It was mentioned above that interactions between reactants are supported by intensive homogenization when the radical reaction is achieved in internal mixer. On the other hand, grafting investigated "in situ" is completely controlled by diffusion of reactive species. This assumption can be demonstrated on samples 0.5-x where x = $[L101]_0$ = 0.1–2 wt %. When $[IAH]_0$ is low (i.e. 0.5 wt %), radical branching and crosslinking would predominate at high $[L101]_0$. However, results of "in situ" experiments show decrease of T_{max} (decomposition step #5) with increasing $[L101]_0$ which indicates predomination of chain scission over branching or crosslinking. This phenomenon can be explained by limited mobility and diffusion of PLA$^{\bullet}$ which leads to relatively lower extent of their interactions.

Table 11. Detailed values of decomposition steps derived from TGA curves.

Sample	decomp step #1		decomp step #2		decomp step #3		decomp step #4		decomp step #5	
	T_{max} [°C]	Δw [%]	T_{max} [°C]	Δw [%]	T_{max} [°C]	Δw [%]	T_{max} [°C]	Δw [%]	T_{max} [°C]	Δw [%]
neat	-	-	90	3.0	-	-	-	-	357.4	96.4
0.5-0.1	-	-	110.3	1.2	139.5	1.0	-	-	349.7	97.3
0.5-0.5	-	-	113.1	2.9	-	-	-	-	348.3	96.8
0.5-1	56.4	0.2	122.7	3.0			-	-	347.7	96.9
0.5-2	65.1	0.5	118.3	1.1	139.3	0.5	-	-	346.2	97.5
1-0.1	-	-	106	1.8	147	0.7	-	-	347.4	96.9
1-0.5	-	-	121	1.9	144	1.3	-	-	348.5	96.3
1-1	-	-	119	1.9	141	1.0	-	-	346.7	96.4
1-2	68.8	0.7	123.4	2.8	145.1	1.2	-	-	348.6	94.5
5-0.1	-	-	-	-	135.8	2.4	208.3	1.5	348.8	95.8
5-0.5	-	-	-	-	135.5	2.9	223.9	1.8	348.3	95.0
5-1	-	-	-	-	134.8	4.1	226.0	2.3	347.7	94.4
5-2	60.2	0.4	-	-	134.8	3.8	210.1	1.7	347.7	94.4
10-0.1	-	-	121.1	6.2	142.5	2.0	219.9	0.6	347.9	90.4
10-0.5	-	-	108.8	6.2	143.6	2.1	216.3	0.7	345.2	90.3
10-1	59.9	0.4	105.0	5.1	144.0	2.4	214.2	0.5	349.8	90.7
10-2	69.0	1.0	-	-	138.0	5.3	202.0	5.1	350.8	87.7

5.3 Evidence of IAH grafted onto PLA backbone

Structure of modified PLA was examined by Fourier transform infrared spectroscopy (FTIR). Expected structure of prepared grafted PLA is illustrated according to reaction mechanism illustrated in Scheme 1.

FTIR spectrum of neat PLA and PLA-g-IAH is shown in Figure 14a. Detail of PLA-g-IAH's FTIR spectrum contains absorption bands at around 2860 and 2920 cm^{-1} which can be assigned to $-CH_2$ groups (Figure 14b). Appearance of $-CH_2$ groups can be considered as a proof of grafted IAH (Scheme 1, reaction 3) whereas $-CH_2$ groups are included in molecule of IAH.
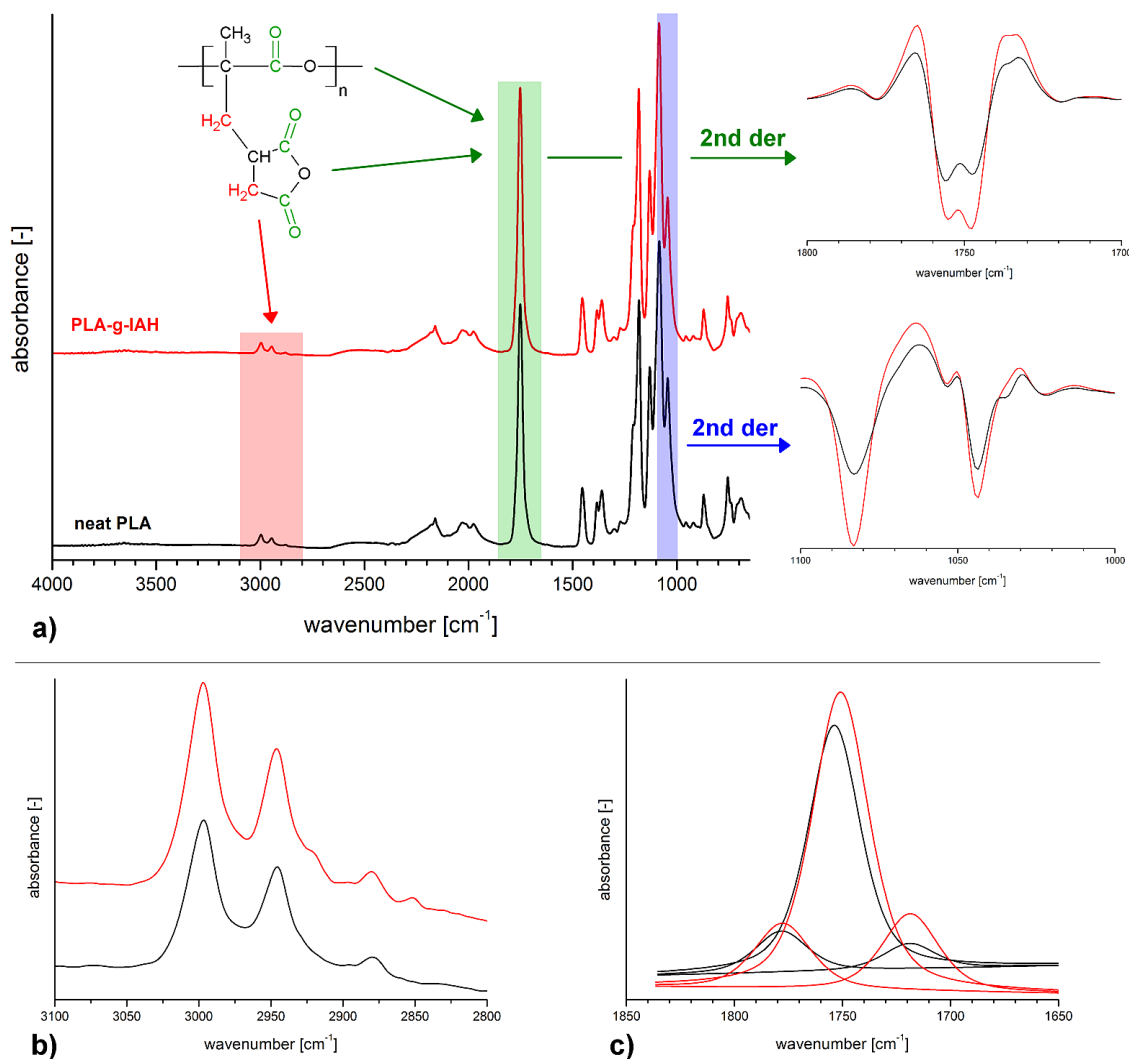
Figure 14. FTIR spectrum of neat PLA and PLA-g-IAH in the wavenumber range 4000–650cm^{-1} with 2nd derivative spectra in the wavenumber range 1800–1700 and 1100–1000 cm^{-1} (a); detail of absorption bands in the wavenumber range 3100–2800 cm^{-1} (b) and 1850–1650 cm^{-1} (c).

FTIR spectrum of PLA-g-IAH does not exhibit any different absorption band in the region typical for C=O vibrations (1600–1800 cm^{-1}) compared to neat PLA. Strong absorption band

49

centered at 1750 cm^{-1} is composed of several types of C=O vibrations which may represent both PLA and grafted IAH. It can be predicted that C=O absorption bands of IAH are overlapped due to low concentration of grafted IAH. Therefore, 2nd derivave FTIR spectra were obtained in order to enhance resolution of overlapped peaks which were not observed in native spectra. This method was applied in study Mani, Bhattacharya, Tang [75] dealing with preparation and characterization of polyesters modified with MAH. Accordingly, authors splitted FTIR signal using 2nd derivation which improved resolution of FTIR spectra. New absorption bands at 1785 cm^{-1} were observed due to presence of bonded MAH on polyester backbone.

The example of 2nd derivative FTIR spectrum is depicted in Figure 14a and contains characteristic peaks in wavenumber range of 1700–1800 cm^{-1} for both PLA and PLA-g-IAH: peak at 1780 cm^{-1} belongs to C=O stretching vibration of ester bond; strong peak at 1760 cm^{-1} is characteristic for C=O stretching vibration; peak at 1740 cm^{-1} assigned to C=O stretching vibrations of carboxylic group; peak at 1730 cm^{-1} characteristic for C=O stretching vibration of ester bond. The difference between 2nd derivative spectra of PLA and PLA-g-IAH was observed in the wavenumbers range 1000–1100 cm^{-1}. FTIR spectrum of neat PLA exhibits peak at 1035 cm^{-1} which is characteristic for C–O stretching of C–OH bond appeared as a result of PLA thermohydrolysis [81]. As will be discussed in next section, chain scission of neat PLA can occur via non-radical degradation such as hydrolysis and thermal degradation whereas β-scission can be promoted by reaction between PLA and L101$^\bullet$. Consequently, it can be assumed that β-scission predominates over the non-radical degradation during reactive modification of PLA.

As discussed above, absorption band centered at around 1760 cm^{-1} includes C=O vibrations of cyclic anhydride group. Due to low concentration of grafted IAH, single peak reflecting C=O stretching vibration of anhydride ring was not observed. Therefore, FTIR spectra of neat PLA and PLA-g-IAH were normalized to the peak at 1167 cm^{-1} which represents C–C stretching vibration between –CH$_3$ group and tertiary carbon of PLA backbone. Constant content of CH$_3$ groups was expected due to lower reactivity of primary –CH$_3$ compared to tertiary –CH defined by strength of C–H bond. Increasing integral intensity of absorption band relating to C=O stretching vibration at 1780 cm^{-1} was observed for PLA-g-IAH compared to neat PLA. Figure 15 contains $A_{PLA-g-IAH}/A_{neat\ PLA}$ values obtained for PLA-g-IAH samples prepared at constant $[IAH]_0$ (1 and 5 wt %) and different $[L101]_0$ (0.1–2 wt %). An increase of $A_{PLA-g-IAH}/A_{neat\ PLA}$ for C=O absorption band at 1760 cm^{-1} is assigned to effect of IAH bonded on the PLA backbone. This can be considered as a proof of bonded IAH in purified PLA-g-IAH.

In order to prove method of peak normalization, PLA/IAH blends were prepared by blending with defined amount of IAH (0.5, 1, 5 and 10 wt %) in THF. Obtained FTIR spectra were normalized to absorption band at 1167 cm^{-1} according to method used for PLA-g-IAH samples. FTIR spectra of PLA/IAH blends are shown in Figure 15 as well as derived values of $A_{PLA-g-IAH}/A_{neat\ PLA}$ for C=O absorption band at 1760 cm^{-1}. It was observed that $A_{PLA-g-IAH}/A_{neat\ PLA}$ increases with increasing concentration of IAH in PLA/IAH blend. Moreover, FTIR spectra of PLA/IAH blends with 5 and 10 wt % IAH contain weak absorption band at 1850 cm^{-1} relating to C=O stretching vibrations of IAH. Described absorption band was not observed for PLA/IAH blends with IAH concentration below 5 wt %. As discussed in chapter 5.4.1, maximum grafting degree 1.1 wt % was reached. It means that FTIR spectra contain C=O stretching vibrations of IAH at 1780 cm^{-1} overlapped in the wavenumber range

50

1700–1800 cm^{-1} while C=O stretching vibrations at 1850 cm^{-1} cannot be observed due to low concentration of grafted IAH.
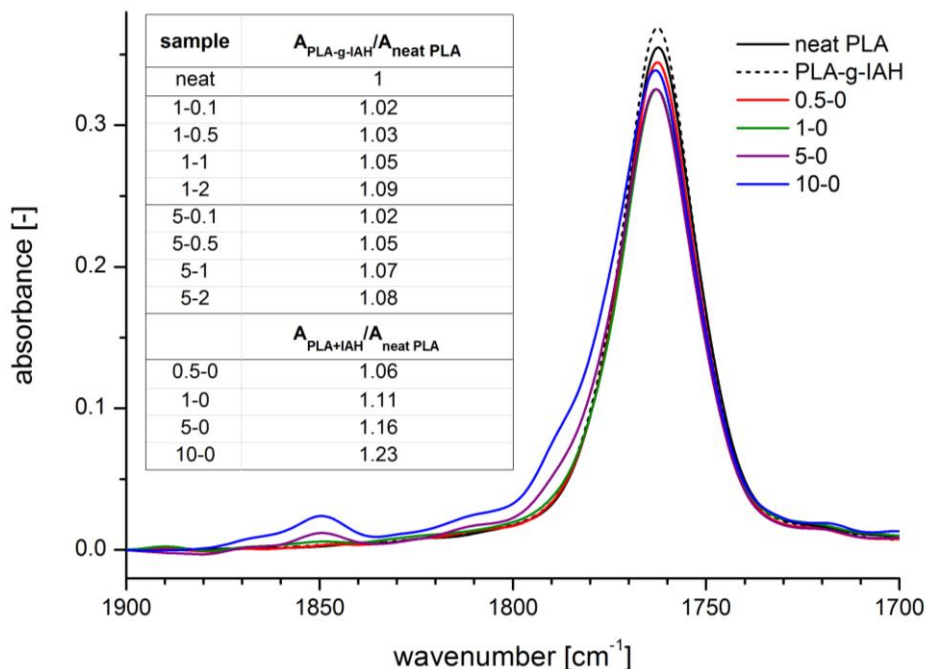

Figure 15. Detail of FTIR spectrum of neat PLA, PLA-g-IAH and PLA/IAH blends with different [IAH]$_0$ − peak at 1760 cm^{-1} (stretching vibrations of C=O) normalized to peak at 1167 cm^{-1} (stretching vibrations of CH$_3$).

Structure of modified PLA was observed by ^{1}H-NMR spectroscopy. The IAH grafted onto PLA backbone was detected in ^{1}H-NMR spectrum in Figure 16 comparing neat PLA and PLA-g-IAH. Strong peak at chemical shift at around 1.5 ppm is assigned to the –CH$_3$ methyl proton which is bonded onto –CH of PLA backbone at chemical shift at 5.2 ppm. At 1.7 ppm a weak peak was observed which can be assigned to –CH$_3$ methyl proton bonded to quaternary carbon atom which is the most sufficient for grafting reaction [80]. The resonances at 7.2–7.5 ppm are attributed to hydrogen atom of –OH group, carboxyl group and CDCl$_3$ solvent. The main difference between PLA-g-IAH and neat PLA spectrum is the peak centered at 3.5 ppm assigned to –CH$_2$ methylene proton of IAH. Homopolymerization of IAH was not expected due to absence of peak at 2.70 ppm which belongs to backbone of p(IAH) [92].
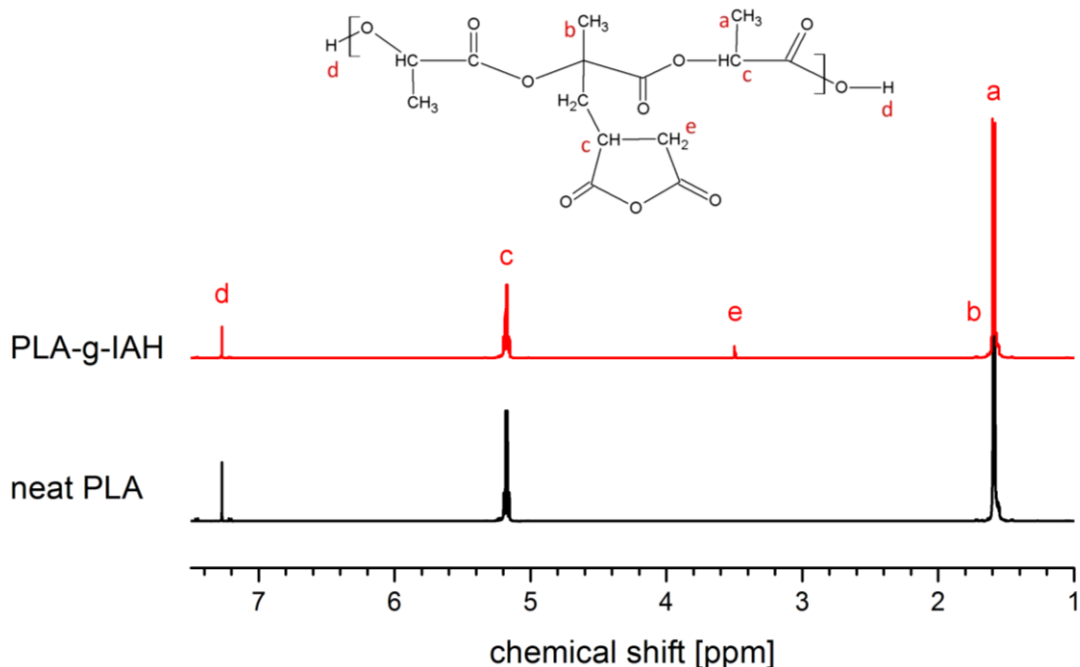
Figure 16. ^{1}*H-NMR spectrum of PLA-g-IAH and neat PLA.*

5.4 Reaction parameters affecting grafting yield

Mechanism of radical grafting was described in chapter 5.1. Main grafting reaction starts with formation of primary radical via thermal decomposition of L101. In the next step, L101$^\bullet$ abstract hydrogen atom from tertiary carbon of PLA backbone while PLA$^\bullet$ represent active center forcovalent bonding of IAH. However, radical grafting of IAH onto PLA may consist of several reactions occuring simultaneously. Extent of these side reactions depends on reaction conditions (especially concentration of reaction compounds and reaction temperature) and strongly influences grafting yield and course of the reaction.

5.4.1 Concentration of reaction compounds affecting grafting yield

Figure 17 represents 3D plot giving relationship between concentration of grafted IAH ($[IAH]_{PLA}$) and concentration of reactants ($[IAH]_0$ and $[L101]_0$) which was determined for PLA-g-IAH samples prepared according to reaction conditions summarized in Table 6, chapter 4.2.1. Grafting yield is represented by conversion-$[IAH]_0$-$[L101]_0$ relationship in Figure 18. With regard to obtained data, it can be assumed that increase of $[IAH]_{PLA}$ can be assigned to increase of $[L101]_0$ in the whole range 0.5–10 wt % IAH. This is in good agreement with assumption that generation of PLA$^\bullet$ is favoured at high $[L101]_0$. Thus formed PLA$^\bullet$ allow covalent bonding of IAH (Scheme 1, reaction 3). Generally, $[IAH]_{PLA}$ increases with increasing $[IAH]_0$ while conversion degree decreases which suggests higher content of low molecular fractions including unreacted monomer or its homopolymer with respect to ceiling temperature for IAH

polymerization. The highest $[IAH]_{PLA}$ was obtained for samples with 10 wt % IAH and 0.5 wt % $[L101]_0$ while highest conversion was reached for reaction with 1 wt % IAH and 2 wt % L101.
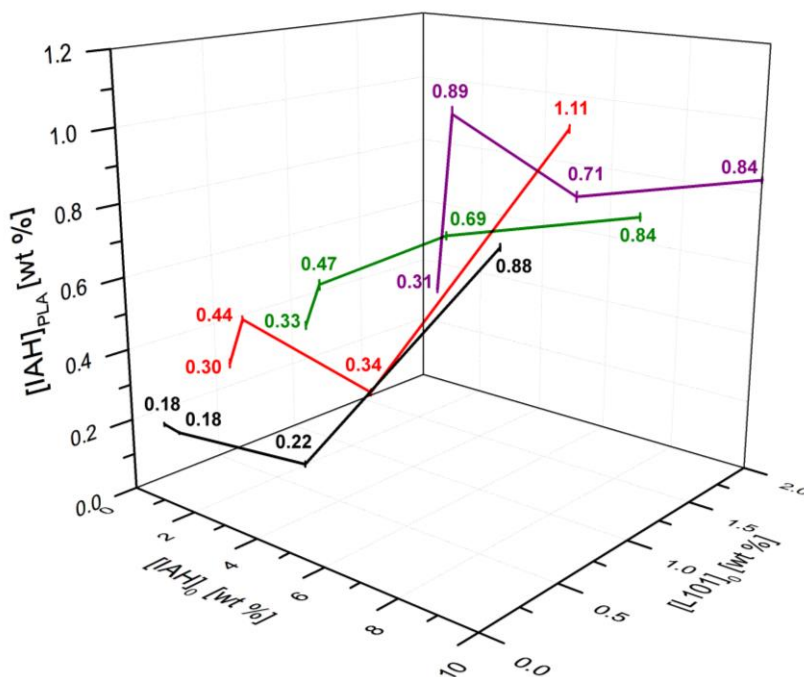
Figure 17. 3D plot representing $[IAH]_{PLA}$-$[IAH]_0$-$[L101]_0$ relationship; 0.5–10 wt % IAH; 0.1–2 wt % L101.
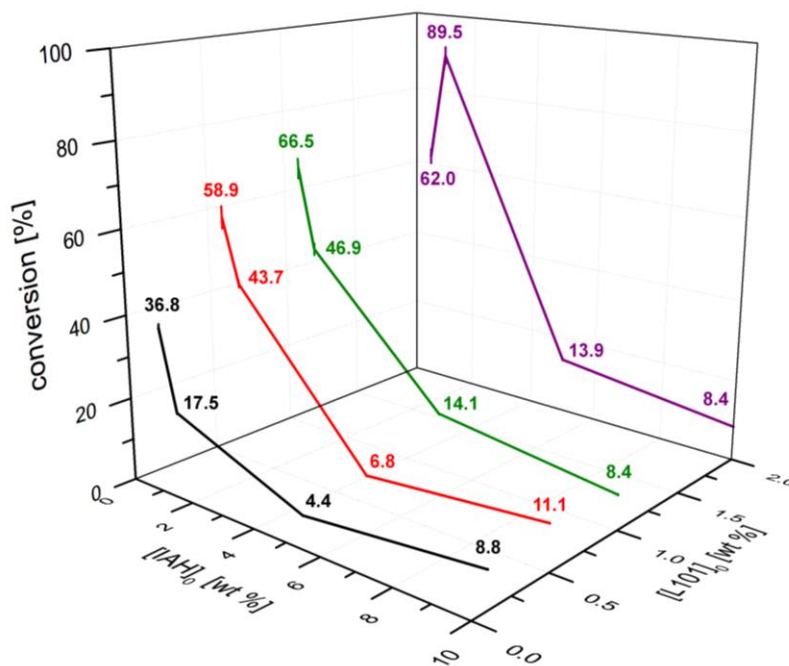
Figure 18. 3D plot representing conversion-$[IAH]_0$-$[L101]_0$ relationship; 0.5–10 wt % IAH; 0.1–2 wt % L101.

Low $[IAH]_0$ (0.5–1 wt %) and low $[L101]_0$ (0.1–0.5 wt %)

At [IAH]$_0$ equals to 0.5 wt %, [IAH]$_{PLA}$ reached plateau at 0.5 wt % of [L101]$_0$. This fact can be explained by the hypothesis that monomer was consumed mainly for grafting reaction (conversion up to ~60 %). At low [IAH]$_0$ and [L101]$_0$, probability of IAH-L101$^\bullet$ interactions is low even though relatively high mobility of both IAH and L101$^\bullet$. IAH-L101$^\bullet$ interactions are limited because of high concentration of tertiary carbons of PLA backbone. Consequently, formation of PLA$^\bullet$ is favoured and IAH homopolymerization can be neglected under these conditions. Relatively high grafting yield was determined at low [IAH]$_0$ and [L101]$_0$, therefore low extent of side reactions can be predicted.

Low [IAH]$_0$ (0.5–1 wt %) and high [L101]$_0$ (1–2 wt %)

At low [IAH]$_0$ and high [L101]$_0$, desired reaction between PLA and L101$^\bullet$ predominates over IAH-L101$^\bullet$ interactions due to several factors. First, high concentration of reactive species and –CH carbons is available for reaction with primary radicals leading to formation of PLA$^\bullet$ (Scheme 1, reaction 2). Second, high melt viscosity of PLA reduces extent of reactions between IAH and L101$^\bullet$ due to physical barrier. Third, higher amount of PLA macroradicals allows further increase of [IAH]$_{PLA}$ which was observed for PLA-g-IAH prepared by reaction with 1 wt % IAH. In this case [IAH]$_{PLA}$ increased in the whole [L101]$_0$ range. As [L101]$_0$ increases, concentration of PLA$^\bullet$ increases which enhances the extent of *β*-scission, branching or crosslinking (reactions 2c, 2ca and 2b in Scheme 1) affecting grafting degree as well as rheological and thermal properties. We just have to note that kind of interactions between radical species and their probability is strongly affected by characteristic parameters such as reactivity, solubility parameter and melt viscosity.

As [L101]$_0$ is high, L101$^\bullet$ can also undergo coupling while inactive species are formed according to Scheme 1, reaction 1b. Moreover, grafting yield is also limited by interactions between PLA• and L101$^\bullet$ (Scheme 1, reaction 2a). L101$^\bullet$ formed via thermal decomposition of L101 can participate on termination of grafting reaction via interactions with PLA-g-IAH$^\bullet$ (Scheme 1, reaction 3a). However, reactions between L101$^\bullet$ and PLA-g-IAH$^\bullet$ do not affect grafting yield so intensive compared to other mentioned side reactions.

High [IAH]$_0$ (1–10 wt %) and low [L101]$_0$ (0.5–1 wt %)

When [IAH]$_0$ is above 1 wt % and [L101]$_0$ is up to 0.5 wt %, [IAH]$_{PLA}$ increases significantly. Under these conditions, recombination of L101$^\bullet$ is not so probable and high [IAH]$_0$ supports main grafting reaction. However, reaction conversion is low due to high amount of unreacted monomer. Low grafting degree can be attributed to "cage effect" where L101$^\bullet$ are surrounded by IAH molecules. In that case, formation of low reactive IAH$^\bullet$ is preferable to grafting according to Scheme 1 (reaction 1b). Consequently, formation of p(IAH) could be possible with respect to the thermodynamic criteria.

Although low concentration PLA$^\bullet$ is expected due to low concentration of L101$^\bullet$, PLA$^\bullet$ can be regenerated according to reaction 4 in Scheme 1. In this scheme, RH can represent PLA which

may supply hydrogen atom for regeneration of PLA$^\bullet$. This reaction can be responsible for enhanced grafting degree.

High [IAH]$_0$ (1–10 wt %) and high [L101]$_0$ (1–2 wt %)

At high [IAH]$_0$ and [L101]$_0$, reaction between IAH and L101$^\bullet$ (Scheme 1, reaction 1aa) affects reactive process more extensively. These reactions generate low reactive IAH$^\bullet$ which are able to polymerize or recombine with other radical species.

Similar value of solubility parameter δ of both IAH and L101 supports IAH-L101$^\bullet$ interactions leading to formation of IAH$^\bullet$ which have potential to polymerize depending on the reaction temperature. Solubility behavior of L101 is characterized by δ equals to 15.5 $J^{1/2} \cdot cm^{-3/2}$ [98] which is close to δ of IAH (14.6 $J^{1/2} \cdot cm^{-3/2}$). Compared to this, δ of PLA (20.2 $J^{1/2} \cdot cm^{-3/2}$) [95] makes IAH-L101$^\bullet$ interactions more favoured compared to PLA-L101$^\bullet$ and PLA$^\bullet$-IAH interactions. This theoretical prediction corresponds with results illustrated in Figure 17 where [IAH]$_{PLA}$ decreases with increasing [L101]$_0$ when high [IAH]$_0$ is applied. Although highest [IAH]$_{PLA}$ was reached at high [IAH]$_0$, highest reaction conversion was observed for samples with low [IAH]$_0$ (Figure 18). As mentioned previously, increase of [IAH]$_{PLA}$ with increasing [L101]$_0$ can be assigned to preferable formation of PLA$^\bullet$ according to reaction 2 in Scheme 1. In ideal case, high [IAH]$_0$ would enhance extent of PLA$^\bullet$-IAH interactions leading to high reaction conversion. Though, high [L101]$_0$ does not result in significant increase of reaction conversion when [IAH]$_0$ is above 1 wt %. This situation occurs due to high [IAH]$_0$ remaining for side reactions. As discussed in previous text, high mobility of IAH and L101$^\bullet$ allows their interactions.

Under reaction conditions supporting β-scission, IAH can participate on reaction with PLA$^\bullet$ containing radical site at the end of chain. As [IAH]$_0$ increases and [L101]$_0$ is constant, end-chain grafting is responsible for increase of [IAH]$_{PLA}$ though molecular weight of PLA-g-IAH decreases (see chapter 5.5.2).

It can be concluded that at different [IAH]$_0$ and [L101]$_0$ different reactions predominate which has strong effect on grafting yield. Influence of different reaction parameters is summarized:

- low [IAH]$_0$ and low [L101]$_0$ – low grafting degree and low extent of side reactions; termination mainly via recombination of L101$^\bullet$ (Scheme 1, reaction 1a),
- low [IAH]$_0$ and high [L101]$_0$ – high concentration of PLA$^\bullet$, increase of grafting degree, termination mainly via recombination of L101$^\bullet$, PLA$^\bullet$-L101$^\bullet$ and PLA$^\bullet$-PLA$^\bullet$ interactions (Scheme 1, reactions 1a, 2a and 2b),
- high [IAH]$_0$ and low [L101] – high grafting degree and high amount of byproducts (low conversion); termination via L101$^\bullet$ recombination and PLA-g-IAH$^\bullet$-L101$^\bullet$ interactions (Scheme 1, reaction 1a and 3a),
- high [IAH]$_0$ and high [L101] – reaction between IAH and L101$^\bullet$ is favoured which limits grafting degree; termination via formation of low reactive IAH$^\bullet$ (Scheme 1, reaction 1b).

5.4.2 Influence of reaction temperature on grafting yield

Influence of $[L101]_0$ on $[IAH]_{PLA}$ was evaluated with respect to reaction temperature for experimental series contained 0.5 wt % IAH and 0.1–1 wt % L101. Reaction temperatures 170, 190 and 210 °C were applied for reaction. Experimental data are presented in Figure 19 and show the influence of $[L101]_0$ on $[IAH]_{PLA}$ at different reaction temperature. At 170 °C lowest $[IAH]_{PLA}$ was reached for reaction with 0.1 wt % L101 due to presence of low amount of reactive L101$^{\bullet}$. This prediction explains negligible increase of grafting degree when the temperature rises to 190 °C. At 210 °C most of L101$^{\bullet}$ are consumed via their recombination following reaction 1b in Scheme 1. Increase of $[L101]_0$ leads to increase of grafting degree where the maximum values of $[IAH]_{PLA}$ were observed for PLA-g-IAH prepared at 190 °C for all $[L101]_0$. It is in good agreement with presumed reaction conditions which were calculated and considered as the most effective for grafting reaction.
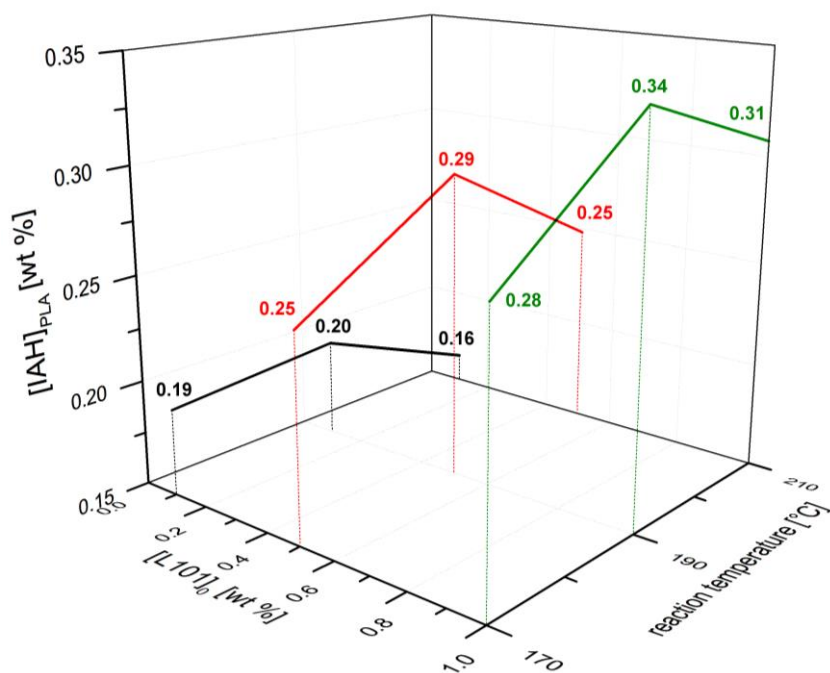
Figure 19. 3D diagram representing $[L101]_0$ - reaction temperature - $[IAH]_{PLA}$ relationship for PLA-g-IAH samples 0.5-x where x = $[L101]_0$ = 0.1–1 wt %.

Both different reaction temperature and $[L101]_0$ lead to different predominating kind of termination. Temperature 210 °C and 1 wt % of L101 enhances termination between PLA$^{\bullet}$ and L101$^{\bullet}$ due to combination of high concentration of L101$^{\bullet}$, their mobility and lower viscosity of polymer matrix compared to lower temperature. Compared to this, when the temperature 210 °C and 0.1 wt % L101 is applied, recombination of L101$^{\bullet}$ has the most significant influence on decrease of $[IAH]_{PLA}$.

It is important to note that β-scission of t-butoxy radicals onto secondary methyl radicals is favoured at higher temperature. According reaction 2 in Scheme 1, t-butoxy radicals have a propensity for hydrogen abstraction while methyl radicals prefer addition to double bonds which

is demonstrated by reaction 1aa, Scheme 1 [2], [55]. Finally, it can be concluded that high reaction temperature, hydrogen absraction propensity and concentration of radical species are key factors resulting in decreases of [IAH]$_{PLA}$ as shown in Figure 19.

5.4.3   Reaction conditions affecting kinetics of grafting

5.4.3.1   Kinetics parameters normalized from conversion curve

As mentioned previously, radical reaction between PLA and IAH is a complex of reactions which proceed simultaneously. Fukuoka [99] described radical grafting of vinylsilane onto polyethylene as a complex of reactions which can be expressed for reaction between PLA and IAH by following equations:

$$L101 \xrightarrow{\ k_d\ } 2R^{\bullet} \tag{16a}$$

$$R^{\bullet} + PLA \xrightarrow{\ k_i\ } PLA^{\bullet} + RH \tag{16b}$$

$$PLA^{\bullet} + IAH \xrightarrow{\ k_g\ } PLA - g - IAH^{\bullet} \tag{16c}$$

$$PLA - g - IAH^{\bullet} + PLA \xrightarrow{\ k_{tr}\ } PLA - g - IAH + PLA^{\bullet} \tag{16d}$$

$$PLA^{\bullet} + PLA^{\bullet} \xrightarrow{\ k_t\ } PLA - PLA \tag{16e}$$
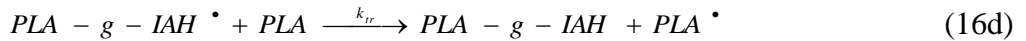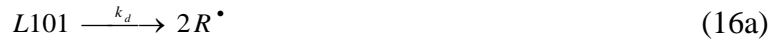
Proposed reaction complex includes decomposition of initiator generating L101$^{\bullet}$ (16a), formation of PLA$^{\bullet}$ by hydrogen abstraction from PLA backbone (16b), addition of IAH monomer onto active center formed on PLA chain (16c), radical transfer between PLA-g-IAH$^{\bullet}$ and PLA by hydrogen abstraction (16d) and coupling of PLA$^{\bullet}$ forming crosslinked chains (16e).

Elementary reaction expressed by Equation 16a–e can be written by kinetic equations as follow:

$$-\frac{d[L101]}{dt} = k_d \cdot [L101] \tag{17a}$$

$$\frac{d[R^{\bullet}]}{dt} = 2 \cdot f \cdot k_d \cdot [L101] - k_i \cdot [R^{\bullet}] \cdot [PLA] \tag{17b}$$

$$-\frac{d[IAH]}{dt} = k_g \cdot [PLA^{\bullet}] \cdot [IAH] \tag{17c}$$

$$\frac{d[PLA - IAH^{\bullet}]}{dt} = k_g \cdot [PLA^{\bullet}] \cdot [IAH] - k_{tr} \cdot [PLA - IAH^{\bullet}] \cdot [PLA] \tag{17d}$$

$$\frac{d[PLA^\bullet]}{dt} = k_i \cdot [R^\bullet] \cdot [PLA] - k_g \cdot [PLA^\bullet] \cdot [IAH] + k_{tr} \cdot [PLA - IAH^\bullet] \cdot [PLA] - k_t \cdot [PLA^\bullet]^2 \quad (17e)$$

In this reaction complex [L101] represents concentration of initiator, [R$^\bullet$] is concentration of primary radicals as a result of L101 thermal decomposition, f is the initiator efficiency, [IAH] is assigned to the concentration of monomer IAH, [PLA-IAH$^\bullet$] is concentration of lactic unit with grafted IAH, [PLA] and [PLA$^\bullet$] represent concentrations of lactic units in the polymer chain and its radicals, respectively.

Quasi-steady-state approximation can be used for study of kinetics of chemical reaction where free radicals and other unstable molecules have very short time of existence. Quasi-steady-state can be derived from Equations 17b, d, e and expressed using Equations 18 and 19, whereas their incorporation into the Equation 26c provides a rate Equation 20:

$$k_i \cdot [R^\bullet] = 2 \cdot f \cdot k_d \cdot \frac{[L101]}{[PLA]} \quad (18)$$

$$2 \cdot f \cdot k_d \cdot [L101] = k_t \cdot [PLA^\bullet]^2 \quad (19)$$

$$\frac{d\alpha}{dt} = K \cdot (1 - \alpha) \cdot [L101]^{1/2} \quad (20)$$

where α represents reaction conversion defined by Equation 21 and K is apparent rate constant given by Equation 22:

$$\alpha = \frac{[IAH]_0 - [IAH]}{[IAH]_0} \quad (21)$$

$$K = \sqrt{\frac{2 \cdot f \cdot k_d \cdot k_g^2}{k_t}} \quad (22)$$

Reaction conditions applied for kinetic experiments are summarized in Table 8. Regarding previous results, reaction between PLA and low amount of both IAH and L101 exhibit limited extent of side reactions and provide sufficient grafting yield. Therefore, PLA-g-IAH was prepared at constant $[IAH]_0$ (0.5 wt %) and different $[L101]_0$ (0.1, 0.5 and 1 wt %). Influence of various reaction temperature (170, 190 and 210 °C) on kinetic parameters was evaluated.

Plot in Figure 20a shows the relationship between reaction conversion and reaction time determined for reaction between PLA and IAH initiated by various $[L101]_0$. After 10 minutes the lowest conversion was reached for reaction between PLA and IAH at 170 °C except of the reaction system with the lowest $[L101]_0$ (0.1 wt %). This reaction system exhibited lowest conversion at 210 °C where the highest concentration of L101$^\bullet$ is presented in reaction system in gradient of time. At these conditions, low concentration of initiator is available for grafting

reaction and L101• are preferably consumed via theire recombination and interactions with PLA•. On the other hand, at higher $[L101]_0$ (0.5 and 1 wt %) the lowest conversion was reached at reaction temperature of 170 °C. This is due to shape of exponential plot between $[L101]/[L101]_0$ and reaction time. After 10 minutes of reaction period, certain amount of unreacted initiator (~10 %) still remains in reaction system (black curve in Figure 10, chapter 4.2.1). This fact leads to slight increase of conversion with increase of reaction time and incomplete grafting reaction with unreacted IAH.
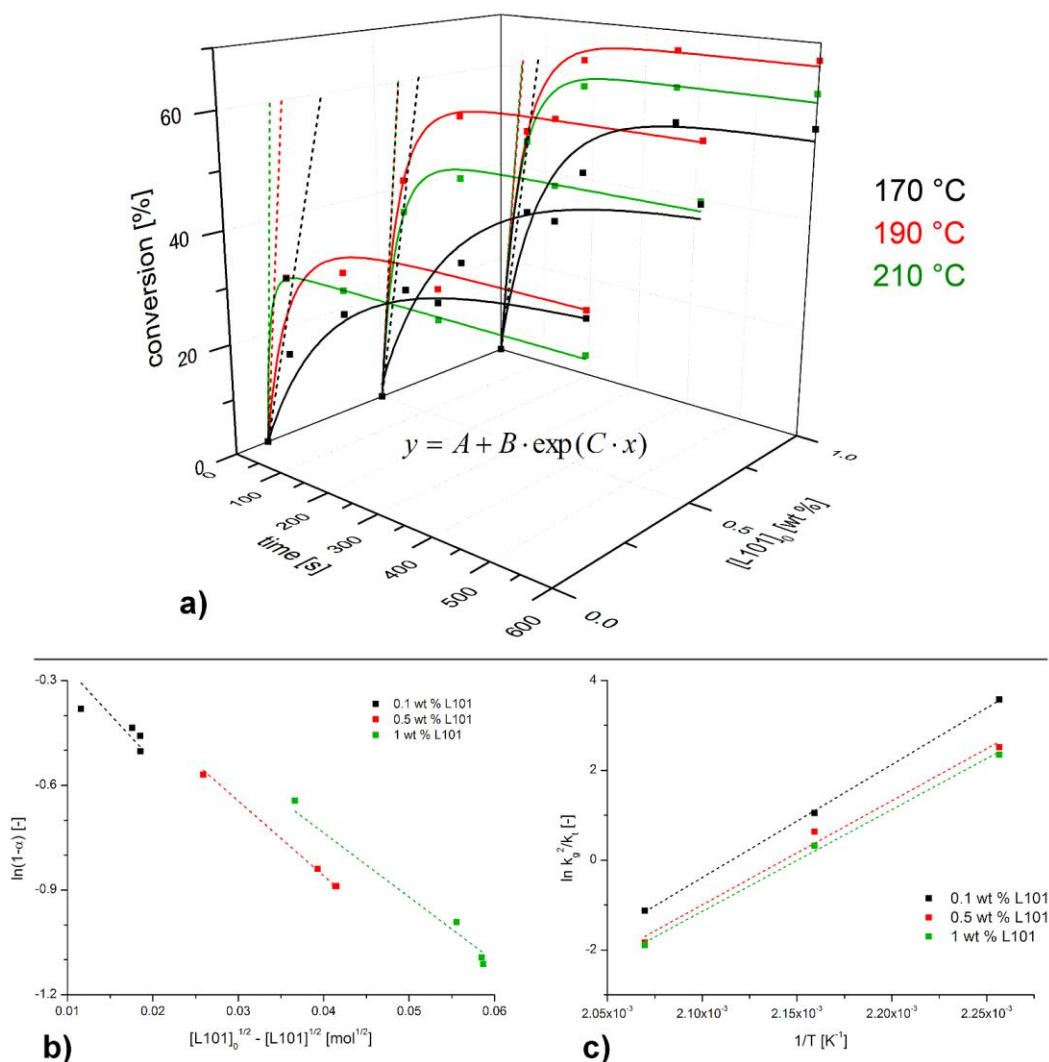
Figure 20. Kinetic data - relationship between reaction conversion and reaction time fitted by simple exponential function $y = A + B·exp(C·x)$ (solid curves), initial grafting rate R_{gi} (dashed curves) derived from linear part of exponential function; kinetic data for samples 0.5-x where $x = [L101]_0 = 0.1–1$ wt %; $T_r = 170$, 190 and 210 °C; b) plot between ln $(1-α)$ and $([L101]_0^{1/2} – [L101]^{1/2})$ with linear regression (dashed lines) for each reaction system (0.5 wt % of IAH, $T_r = 190$ °C); c) plot between ln (k_g^2/k_t) and $1/T$ with linear regression (dashed lines) for each reaction system.

Apparent rate constant K expressed by Equation 22 was determined as a slope of semi-logarithmic plot between (1-α) and ([L101]$_0^{1/2}$ - [L101]$^{1/2}$) giving Equation 23:

$$\ln (1 - \alpha) = -\frac{2 \cdot K}{k_d} \cdot \left([L101]_0^{1/2} - [L101]^{1/2} \right) \tag{23}$$

where $[L101]_0^{1/2}$ represents square root of initial concentration of L101, k_d equals to decomposition rate constant of L101 and $[L101]^{1/2}$ is square root of actual concentration of L101 calculated by Equation 24.

$$[L101] = [L101]_0 \cdot \exp (- k_d \cdot t) \tag{24}$$

Thus formed plot is depicted in Figure 20b and derived rate constants K are shown in Table 12.

Table 12. Kinetic parameters obtained from experimental data; PLA-g-IAH samples 0.5-x where x = [L101]$_0$ = 0.1–1 wt %, 170–210 °C.

sample	T_r [°C]	K [10^6]	$k_g/k_t^{1/2}$ [10^3]	E_a [kJ·mol^{-1}]
0.5-0.1		0.6057	5.98	-183.0
0.5-0.5	170	0.3555	3.51	-173.9
0.5-1		0.3283	3.24	-170.9
0.5-0.1		0.4316	1.69	-201.0
0.5-0.5	190	0.3506	1.37	-189.0
0.5-1		0.3003	1.18	-186.5
0.5-0.1		0.3402	0.57	-218.4
0.5-0.5	210	0.2385	0.40	-207.1
0.5-1		0.2317	0.39	-203.4

Rate constant K expressed by Equation 22 contains rate constants of individual reactions including decomposition of initiator (k_d), grafting (k_g) and termination (k_t). Using known values of K and k_d, it was able to express k_g^2/k_t (Table 12) whereas relation between its logarithmic form $\ln (k_g^2/k_t)$ and 1/T is reflected in Figure 20c. Linear regression provides slope which is relevant to E_a/R giving value of E_a. Plot in Figure 20c suggests its activation energy to be negative, interpreting that the addition reaction is faster or the termination reaction is slower at lower temperature in the elementary reactions. It implies that mobility of macroradicals would be limited at lower temperature and termination reactions among them hardly occur.

5.4.3.2 Kinetic parameters expressed from initial reaction rate

According to kinetic model proposed by Fukuoka [99], kinetic parameters of PLA grafting were determined using sytem of linear regressions derived from experimental data in

Figure 20a–c. Different method used for determination of kinetic parameters was presented by Cha and White [100] who focused on maleic anhydride grafting in an internal mixer. Except of reactions expressed by Equations 16a–e, the other different reactions were considered. Especially, different types of termination reactions and reactions between readical species and impurities were used in mathematical model. Accordingly:

$$PLA^{\bullet} + X \xrightarrow{\;k_{x1}\;} PLA - X \tag{25a}$$

$$PLA - g - IAH^{\bullet} + X \xrightarrow{\;k_{x2}\;} PLA - g - IAH - X \tag{25b}$$

$$PLA - g - IAH^{\bullet} + PLA^{\bullet} \xrightarrow{\;k_t\;} PLA - g - IAH + PLA \tag{25c}$$

$$PLA - g - IAH^{\bullet} + PLA - g - IAH^{\bullet} \xrightarrow{\;k_t\;} PLA - g - IAH + PLA - g - IAH \tag{25d}$$
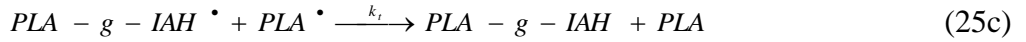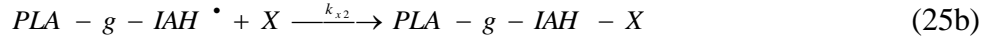
Euqations 25a–b present reactions between impurities (X) and macroradicals or grafted polymer radicals, respectively. Equations 25c–d express interactions between grafted polymer radicals and macroradicals or interactions between grafted polymer radicals each other.

Kinetic model presented by Cha and White [100] calculates $k_g/k_t^{1/2}$ from initial grafting rate R_{gi} which is derived from short reaction period. Finally, $k_g/k_t^{1/2}$ is determined according to Equation 26 which gives relation between concentration of reaction compounds, rate constants (k_d, k_g, k_t) and grafting rate:

$$-\frac{d[IAH]}{dt} = \frac{k_g}{1+f} \cdot \sqrt{\frac{2 \cdot k_d}{k_t}} \cdot [L101]^{1/2} \cdot [IAH] \tag{26}$$

Plots in Figure 20a were fitted with simple exponencial function to obtain initial grafting rate R_g which can be derived from linear part of conversion curve. Thus created function is demonstrated by solid line for all kinetic experiments in Figure 20a.

From initial rates R_g summarized in Table 13 it can be assumed that higher initial graftine rate R_g was observed at higher reaction temperature as a result of high concentration of L101$^{\bullet}$ due to low $\tau_{1/2}$ of L101 at 210 °C.

With respect to initial concentration of initiator, at temperatures of 170 and 190 °C R_g increases with increasing concentration of initiator. On the other hand at highest temperature R_g exhibits highest R_g at 0.1 wt % of L101 instead of reaction proceeded in the presence of both 0.5 and 1 wt % of L101. In this case lower viscosity of melt allows higher extent of termination of polymer macroradicals which is expected as the most important termination reaction in proposed kinetic model.

Kinetic parameter $k_g/k_t^{1/2}$ was calculated from Equation 26 for each reaction composition and reaction temperature. As both reaction temperature and $[L101]_0$ increases, $k_g/k_t^{1/2}$ decreases. With regard to obtained results it can be concluded that increase of both reaction temperature and $[L101]_0$ leads to increase of stationary concentration of L101$^{\bullet}$.

Table 13. Values of $k_g/k_t^{1/2}$ depending on reaction composition and initiator efficiency.

sample	T_r [°C]	R_g [10^8 mol.s^{-1}]	$f = 0$ $k_g/k_t^{1/2}$ [10^2]	$f = 1$ $k_g/k_t^{1/2}$ [10^2]
0.5-0.1		3.98	2.89	5.79
0.5-0.5	170	6.04	1.96	3.92
0.5-1		6.76	1.55	3.11
0.5-0.1		8.63	2.48	4.97
0.5-0.5	190	10.23	1.32	2.63
0.5-1		11.28	1.03	2.05
0.5-0.1		13.68	1.69	3.37
0.5-0.5	210	10.70	0.59	1.18
0.5-1		11.62	0.45	0.91

Figure 21 compares $k_g/k_t^{1/2}$ ratios obtained by two proposed kinetic models. Experimental results of both methods exhibit similar trend. As reaction temperature and $[L101]_0$ increase, $k_g/k_t^{1/2}$ decreases due to higher amount of L101$^\bullet$ resulting in increasing extent of termination reactions. Reaction rate constants calculated according to mathematical model suggested by Cha and White [100] reached lower values compared to those which were obtained from conversion curves proposed by Fukuoka [99]. This can be attributed to more kinds of termination reactions which are expected in mathematical model proposed by Cha and White [100]. Moreover, kinetic parameters calculated from R_g are affected by higher extent of termination reactions occurring during initial stage due to high content of L101$^\bullet$.
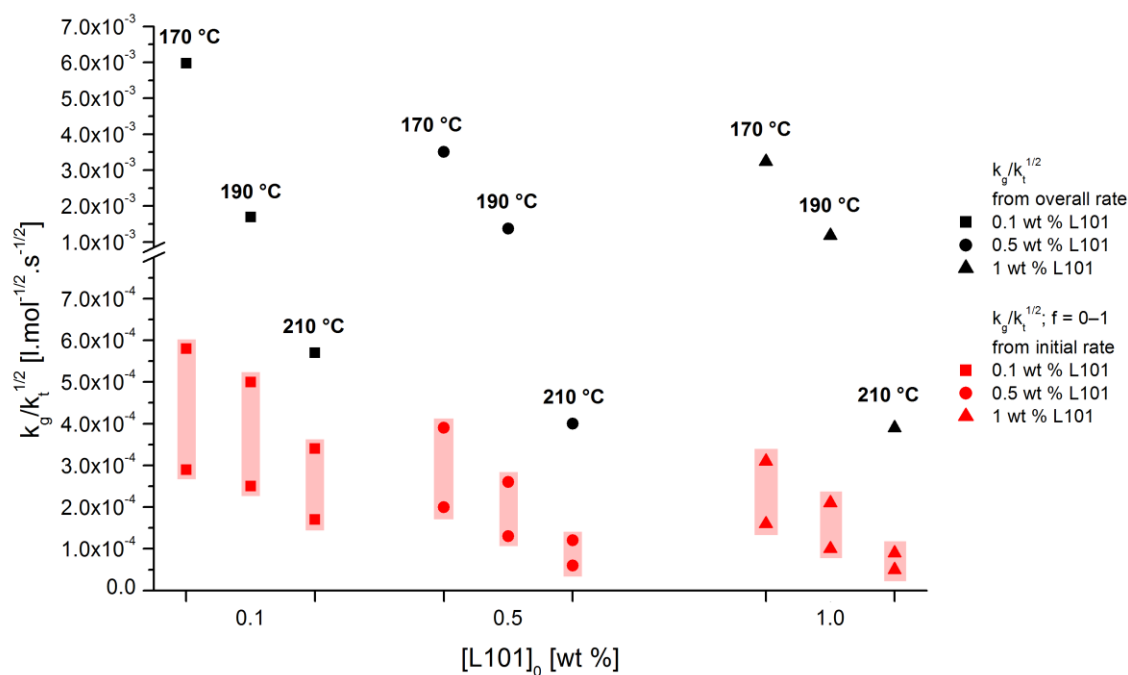
Figure 21. Comparison of $k_g/k_t^{1/2}$ ratio determined by mathematical model proposed by Fukuoka [99] and Cha and White [100]; samples 0.5-x where x = $[L101]_0$ = 0.1–1 wt %, T_r = 170–210 °C.

5.5 Side reactions during radical grafting

5.5.1 IAH homopolymerization

5.5.1.1 Extent of IAH-L101 interactions affected by concentration of reactants

As shown in Figure 22, color of PLA-g-IAH changes from clear to yellow as results of side reactions occurring simultaneously with grafting reaction. Observed coloration relates to the $[IAH]_0$ and $[L101]_0$ in reaction system whereas the same camera's setting was used to avoid the effect of lens optics on captured image. PLA-g-IAH samples functionalized with lowest $[L101]_0$ exhibit pale yellow color for 1, 5 and 10 wt % of IAH (Figure 22a, d, g). Increase of $[L101]_0$ enhances the yellowness of PLA-g-IAH which can be assigned to both β-scission and IAH-L101$^{\bullet}$ interactions. High $[L101]_0$ advantages chain scission while high $[IAH]_0$ and $[L101]_0$ could lead to higher content of p(IAH) and other reaction products formed via IAH-L101$^{\bullet}$ interactions. PLA-g-IAH prepared at high $[IAH]_0$ (5 and 10 wt %) exhibits lower transparency and enhanced yellowness when the highest $[L101]_0$ was applied. This phenomenon can reflect high content of low molecular fractions formed via reaction between IAH and L101$^{\bullet}$. Thus formed products are expected to be more crystalline due to short chains which can be organized in crystalline structure. PLA-g-IAH prepared by reaction with the highest $[IAH]_0$ and $[L101]_0$ exhibited enhanced brittleness which can be attributed to high content of low molecular fractions.
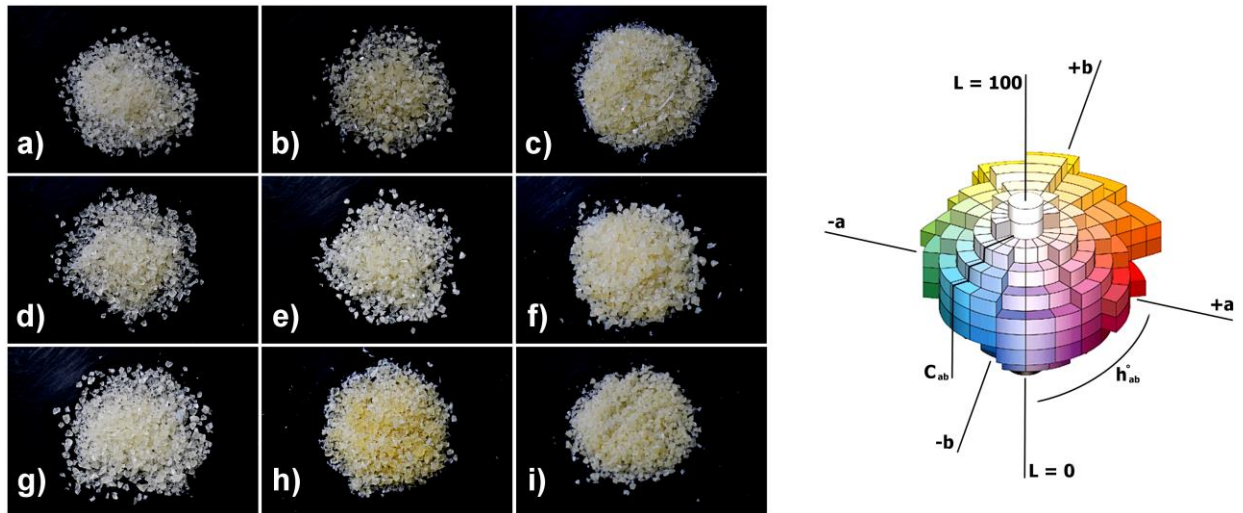
Figure 22. PLA-g-IAH samples: a) 1-0.1; b) 5-0.1; c) 10-0.1; d) 1-1; e) 5-1; f) 10-1; g) 1-2; h) 5-2; i) 10-2; 3-D CEI L-a-b color model consisting of trichromatic parameters L-a-b.

Fundamentals of colorimetry define obtained colorimetric parameters *L-a-b* as lightness and position on red-green scale and yellow-blue scale, respectively. Values of chroma C_{ab} and hue h°_{ab} were calculated according to Equation 27 and 28 using parameters *a* and *b* [101]–[102]:

$$C_{ab} = \sqrt{(a)^2 + (b)^2} \tag{27}$$

$$h°_{ab} = arctg\left(\frac{b}{a}\right) \tag{28}$$

Thus obtained parameters represent possition of PLA-g-IAH's color in 3-D spherical model in Figure 22. Numerical values obtained and calculated from experimental data are summarized in Table 14.

Trichromatic parameters *L-a-b* were used for calculation of x-y abscissa which allows transformation 3-D *L-a-b* system into 2-D x-y system. First, *X-Y-Z* parameters were derived from Equations 29a-c using known X_n, Y_n and Z_n. Finally, x-y parameteres were calculated according to Equations 30a-b.

$$L = 116 \cdot \left(\frac{Y}{Y_n}\right)^{1/3} - 16 \tag{29a}$$

$$a = 500 \cdot \left[\left(\frac{X}{X_n}\right)^{1/3} - \left(\frac{Y}{Y_n}\right)^{1/3}\right] \tag{29b}$$

$$b = 200 \cdot \left[\left(\frac{Y}{Y_n}\right)^{1/3} - \left(\frac{Z}{Z_n}\right)^{1/3}\right] \tag{29c}$$

$$x = \frac{X}{X + Y + Z} \tag{30a}$$

$$y = \frac{Y}{X + Y + Z} \tag{30b}$$

Table 14. Obtained trichromatic parameters L-a-b for PLA-g-IAH, PLA/L101 and PLA/IAH blends prepared by reaction/blending at different $[IAH]_0$ and $[L101]_0$; calculated chroma C_{ab} and hue $h^{°}_{ab}$.

Sample	L	a	b	C_{ab}	$h^{°}_{ab}$
neat	86.772	-0.074	2.576	2.577	-1.542
PLA-g-IAH					
0.5-0.1	86.036	-0.118	4.714	4.715	-1.546
0.5-0.5	87.574	-0.228	4.294	4.300	-1.518
0.5-1	87.298	-0.224	5.046	5.051	-1.526
1-0.1	87.036	-0.234	5.006	5.011	-1.524
1-0.5	87.768	-0.346	5.500	5.511	-1,508
1-1	86.500	-0.264	5.864	5.870	-1.526
5-0.1	86.876	-1.326	10.860	10.941	-1.449
5-0.5	86.160	-1.857	13.927	14.050	-1.438
5-1	86.110	-1.795	14.950	15.057	-1.451
PLA + L101					
0-0.1	84.040	0.034	2.726	2.726	1.558
0-0.5	84.514	-0.024	2.937	2.937	-1.563
0-1	83.704	-0.034	3.923	3.923	-1.562
PLA + IAH					
0.5-0	84.362	0.124	3.747	3.749	1.549
1-0	86.022	-0.010	3.605	3.605	-1.569
5-0	84.668	-0.340	7.674	7.666	-1.542

Most important parameter b and C_{ab} indicates that increasing $[IAH]_0$ enhances saturation of PLA-g-IAH color. This change of coloration relates to higher extent of side reactions between electron donor compounds and IAH. Electron donor compounds can be represented for example by secondary methyl radicals with preferable bonding to IAH instead of primary tert-butoxy radicals which prefer hydrogen abstraction from PLA backbone.

Resulting x-y values are given in Figure 23a which represents color of PLA-g-IAH prepared at different $[IAH]_0$ and $[L101]_0$ expressed by x-y values while equivalent color scale is schemed by red rectangle in 2-D x-y diagram (Figure 23b). Obtained results prove previous assumption that increasing concentration of reaction compounds enhances color change due to higher extent of reaction between IAH and L101˙.

Figure 23a also contains x-y values of reference samples prepared by reaction PLA with L101 and PLA with IAH. It can be concluded that increase of $[L101]_0$ slightly changes color of modified PLA due to chain scission. On the other hand, reactions of IAH (e.g. degradation, isomerization, homopolymerization) with absence of L101 enhance change of color more extensively.
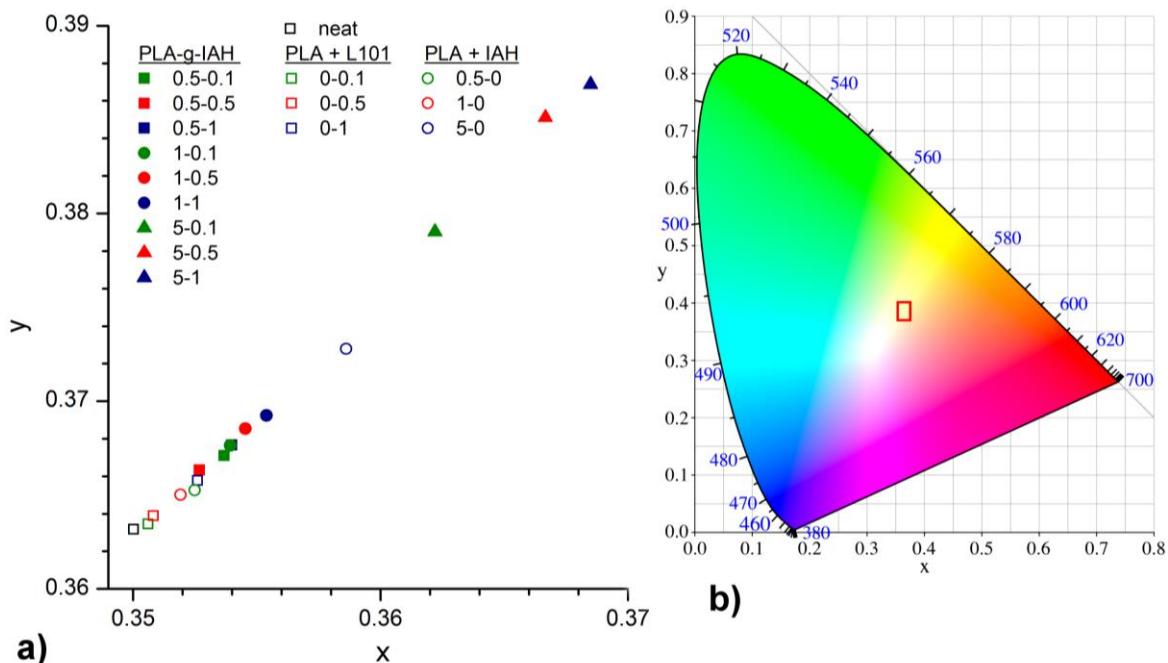
Figure 23. Calculated x-y parameters of PLA-g-IAH prepared at different $[IAH]_0$ and $[L101]_0$ (a); location of calculated x-y parameters in 2-D x-y diagram (b).

5.5.1.2 Simulation of IAH radical polymerization in melt

Supposed structure of PLA-g-IAH was evaluated using FTIR with respect to reaction mechanism in Scheme 1. Except of undesired reaction discussed in this work, homopolymerization of IAH occurs under certain conditions and is theoretically predicted in Scheme 1, reaction 1aa. Many researches neglect homopolymerization of cyclic anhydrides (e.g. maleic anhydride, citraconic anhydride, etc.)during functionalization of polymers. These assumptions are based on the value of ceiling polymerization temperature (T_c) determined for IAH solution polymerization [103]–[104]. Nevertheless, this prediction is not usually experimentally proved in the literature. Therefore, reaction between IAH and L101 at different IAH/L101 molar ratio was achieved in the glass tube heated at 190 °C for 6 min. Reaction products were analyzed by FTIR analysis and measured FTIR spectra are presented in Figure 24. Samples 2.59–259.11 represent IAH/L101 molar ratios used for radical grafting according to reaction conditions summarized in Table 9. FTIR spectrum of IAH exhibits absorption bands at 1850, 1760, 1665 and 930 cm^{-1} which are assigned to C=O (stretching vibration), C=O (stretching vibration), CH$_2$=C< (stretching vibration) and CH$_2$=C< (out plane deformation), respectively [105]. On the other hand, FTIR spectrum of p(IAH) prepared by low-temperature solution polymerization exhibits slight shifting of C=O absorption bands from 1850 and 1760 cm^{-1} to 1860 and 1775 cm^{-1}, respectively. Low intensity of shifted bands may reflect low reaction conversion which was reported by Otsu and Yang [93] who discussed results of radical IAH polymerization at different reaction temperatures and initiators. In consistence with results

presented by Otsu and Yang, relatively low polymerization degree can be expected due to low reactivity of secondary radicals generated from thermal decomposition of L101.

In the case of p(IAH), absorption bands typical for $CH_2=C<$ fragment (1665 and 930 cm^{-1}) disappeared due to consumption of double bonds during IAH polymerization. Integral intensity of absorption band at 930 cm^{-1} decreases as IAH/L101 molar ratio decreases. It corresponds to the higher extent of IAH-L101$^\bullet$ interactions and decreasing concentration of $CH_2=C$ bonds due to formation of p(IAH) macromolecules. It can be expected that at high concentration of L101, reaction between L101$^\bullet$ and IAH occur with higher probability. Consequently, absorption band at 1665 cm^{-1} disappeared due to mentioned preferable reactions. However, weak peak at 1665 cm^{-1} was observed for for samples 129.56 and 259.11 due to low extent of IAH-L101$^\bullet$ interactions as well as low polymerization yield.

Further difference in FTIR spectra was observed in wavenumber range 1850–1860 cm^{-1} which is typical for C=O stretching vibrations of IAH and p(IAH) detected at lower and higher wavenumber, respectively. FTIR spectra of samples 2.59, 5.18, 25.91 and 51.28 contain absorption band at 1860 cm^{-1} which suggests presence of p(IAH). On the other hand, only weak shoulder of mentioned absorption band was observed for samples with high IAH/L101 molar ratio (129.56 and 259.11). Consequently, IAH homopolymerization seems to be supressed at high IAH/L101 ratio due to low concentration of L101$^\bullet$ and high degree of termination reactions.

FTIR spectra in Figure 24a were deconvoluted in order to detect overlapped absorption bands characteristic for C=O groups (detail in Figure 24b) in wavenumber range 1900–1800 cm^{-1}. Thus obtained FTIR spectra are depicted in Figure 24c. Absorption band centered at 1840 cm^{-1} was split into three and four individual peaks for samples 2.59–259.11 and p(IAH), respectively. Absorption band at 1845 cm^{-1} was detected for all samples. With regard to previous text, this absorption band was attributed to C=O stretching vibrations of anhydride ring as a single molecule. On the other hand, samples 2.59, 5.18, 25.91, 51.28 and p(IAH) exhibit absorption band shifted to higher frequency of C=O stretching with maximum at 1870 cm^{-1}. This fact is consistent with formation of p(IAH). C=O stretch vibrations of samples 129.56 and 259.11 are shifted to 1875 cm^{-1} which may indicate polymeric chains with higher amount of IAH units incorporated in p(IAH) chain. Unfortunately, relatively low intensity of this absorption band predicts low concentration of p(IAH) chains with high polymerization degree. This is in agreement with position of absorption band at around 1810 cm^{-1} which is characteristic for C–H vibrations of vinyl hydrocarbon compounds. Samples 129.56 and 259.11 contain peak centered at 1816 and 1815 cm^{-1}, respectively. On the other hand, samples with lower IAH/L101 molar ratio exhibit peak maximum at 1810 cm^{-1} which is closer to p(IAH). Consequently, lower frequency of C=C stretch could reflect C–C single bonds presented in p(IAH).

FTIR spectra presented in Figure 24 proved possibility of radical polymerization of IAH at low IAH/L101 molar ratio under reaction conditions used for PLA grafting. Polymerization of IAH is expected with regard to the thermal stability of products of reaction between IAH and L101. In consistence with structure analysis, IAH and p(IAH) were used as reference samples.
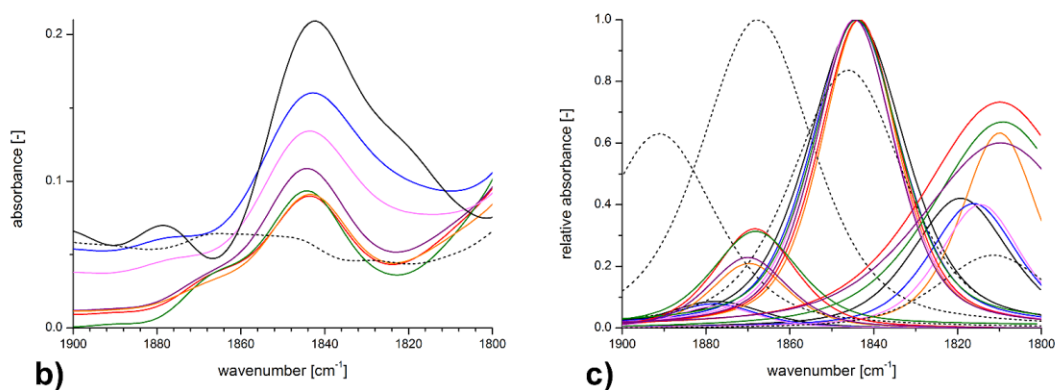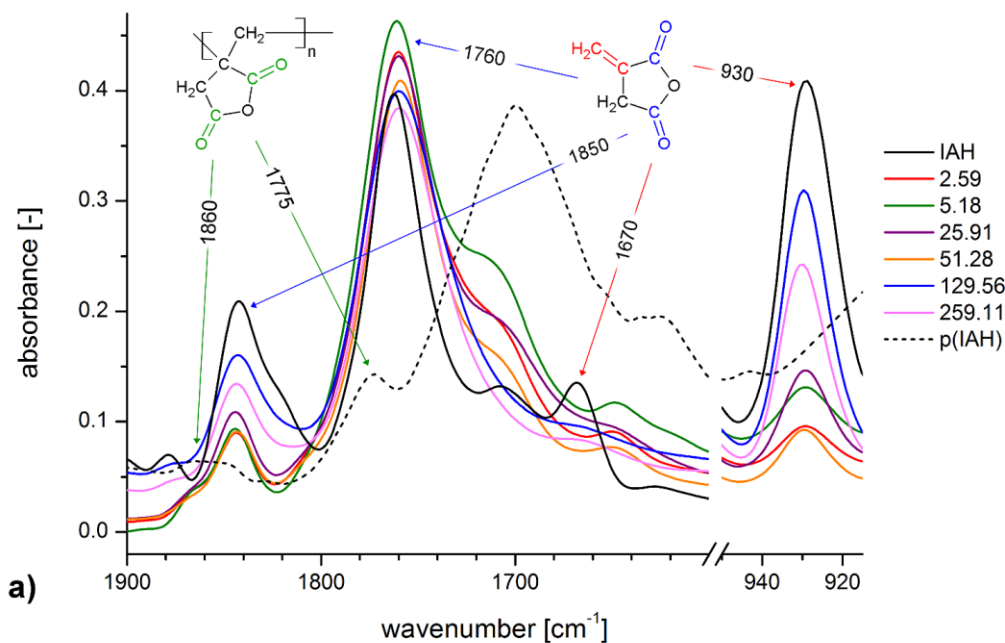
Figure 24. FTIR spectra of IAH, p(IAH) prepared by solution polymerization of IAH and products of radical reaction in melt between IAH and L101at different IAH/L101 molar ratio and 190 °C; FTIR spectra normalized to intensity of C=O absorption band centered at 1760 cm^{-1} (a); detailed FTIR spectra in wavenumber range 1900–1800 cm^{-1} (b) and their deconvoluted form (c).

Figure 25a represents TGA experimental data given by plot between weight loss and temperature whereas Figure 25b shows its first derivation which allows determining T_{max}. IAH is decomposed in two steps. First decomposition step is situated in the temperature range 60–180 °C with T_{max} 150 °C and can be assigned to the release of water from hydrated IAH and its subsequent decomposition. Second decomposition step observed in the range 180–220 °C could reflect self-induced polymerization of IAH. This prediction is inspired by results of Katime, Madoz and Velada [106] who proved self-induced polymerization of itaconate esters without using AIBN. In the case of IAH, approximately 2 wt % of carbonaceous char residue remained at 600 °C. On the other hand, TGA curve of p(IAH) consists of five distinct decomposition steps with T_{max} ~70, 160, 190, 290 and 400 °C. At 600 °C ~27.6 wt % of carbonaceous char residue remained which is typical for p(IAH) and will be also discussed in chapter 5.5.1.3.

68
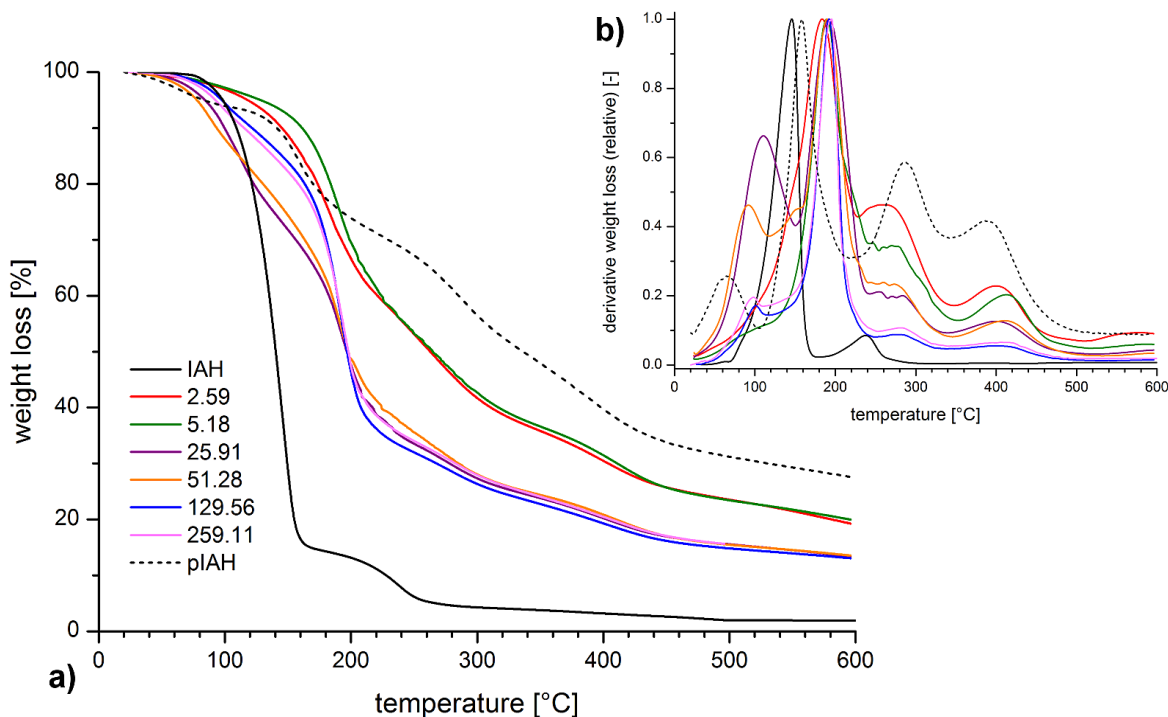
Figure 25. TGA curves of samples prepared by reaction between IAH and L101 at 190 °C and different IAH/L101 molar ratio; plot weight loss vs. temperature (a) and its derivative form (b).

Samples 2.59–259.11 exhibit similar shape of TGA curves which consist of four decomposition steps. Weight losses of individual decomposed fractions are summarized in Table 15. It was expected that conversion of IAH polymerization will be low and this assumption was proved for samples 25.91–259.11. These samples contained ~13 wt % of char residue which is lower than for both p(IAH) and samples 2.59 and 5.18. As discussed previously, IAH homopolymerization under proposed reaction conditions is complicated due to several factors, such as low thermal stability of IAH, isomerization into more stable CAH or favoured coupling of radical species. Therefore, it can be predicted that solution polymerization reaches higher conversion due no IAH isomerization, low concentration of free radicals and limited degradation. This was proved by higher amount of char residue of p(IAH) prepared by solution polymerization compared to samples 2.59–259.11 prepared via reaction in melt. High $[L101]_0$ applied for sample 2.59 leads to higher extent of IAH-L101· interactions and formation of p(IAH) with higher polydispersity. Increasing IAH/L101 molar ratio could increase molecular weight of p(IAH). However, for example thermal stability of sample 259.11 is similar to the thermal stability of sample 5.18. This fact is probably caused by allylic hydrogen situated in IAH that can act as a chain transfer agent in radical polymerization which limits molecular weight of p(IAH [107] In addition, chain transfer is energetically demanding process which is favoured at elevated temperatures.

Table 15. Individual decomposition steps and their T_{max} derived from TGA curves in Figure 25.

| Sample | decomp. step #1 | | decomp. step #2 | | decomp. step #3 | | decomp. step #4 | | decomp. step #5 | |
	T_{max} [°C]	Δw [%]	T_{max} [°C]	Δw [%]	T_{max} [°C]	Δw [%]	T_{max} [°C]	Δw [%]	T_{max} [°C]	Δw [%]
IAH			146	85.7	238	10.1	-	-	-	-
2.59	100	4.7	-	-	190	24.7	260	22.5	400	12.7
5.18	110	4.4	-	-	190	37.6	270	21.7	410	13.8
25.91	110	26.6	-	-	190	36.4	270	12.8	400	9.3
51.28	90	16.9	-	-	190	43.9	270	14.5	410	9.8
129.56	100	9.1	-	-	190	59.3	280	8.6	410	8.9
259.11	100	9.0	-	-	190	57.4	280	9.6	410	8.4
p(IAH)	70	6.3	160	16.1	190	6.7	290	22.0	400	18.1

5.5.1.3 IAH polymerization during grafting reaction

As discussed above, concentration of reaction compounds influences many reaction markers, such as grafting degree or extent of side reactions. Byproducts can be detected according to different thermal stability compared to PLA matrix. Due to low concentration of byproducts generated during grafting process, extraction of these fractions was necessary. As discussed in previous chapter, the yield of IAH polymerization increases with increasing $[L101]_0$ due to more preferable reaction between $L101^{\cdot}$ and PLA backbone. Therefore, extraction was achieved for samples prepared by grafting reaction with different $[IAH]_0$ (0.5, 1, 5 and 10 wt %) and constant $[L101]_0$ (2 wt %).

Thermal stability of prepared extracts is shown in Figure 26a. Extract of neat PLA exhibits two decomposition steps with T_{max} ~120 and ~350 °C. First decomposition step is assigned to release of residual moisture and residual monomer (lactide) whereas the second major decomposition step reflects decomposition of PLA matrix. Sample 0.5-2 and 1-2 exhibits two distinct degradation steps with T_{max} ~200 and ~340 °C. Degradation step at lower temperature can be assigned to combination of release of water from anhydride ring and beginning degradation of IAH and p(IAH). With respect to TGA curve of neat PLA, upper degradation temperature can be assigned to degradation of PLA. No char residue remained at 500 °C. On the other hand, TGA curve of sample 5-2 and 10-2 consists of three decomposition steps with T_{max} ~180, ~260 and ~350 °C. In addition, 4.6 and 8.3 wt % of carbonaceous char residue remained at 500 °C for sample ex 5-2 and ex 10-2, respectively. The carbonaceous char is expected to be condensed crosslinked structure formed by decarboxylation and decarbonylation of the anhydride ring [108].
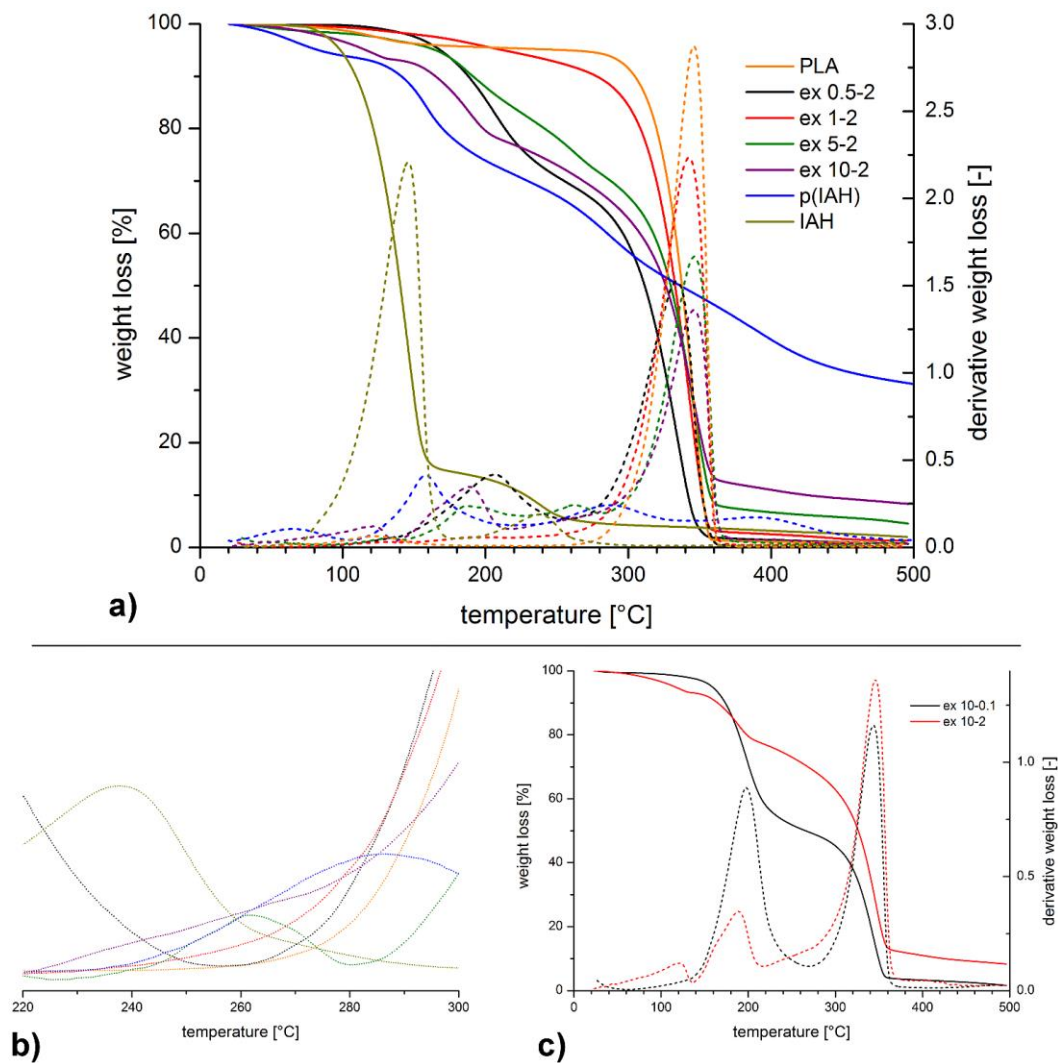
Figure 26. Thermal stability of neat PLA, IAH, p(IAH) and samples prepared by extraction of PLA-g-IAH in acetone (a); detail of derivative weight loss in the temperature range 220–300 °C (b); thermal stability of samples extracted from samples 10-0.1 and 10-2 (c).

Thermal stability of extracted samples were compared to those obtained for p(IAH) prepared according to method described in chapter 4.2.3.1. Four decomposition steps were observed at ~60, ~160, ~290 and ~390 °C and the amount of char remaining was 27.6 wt % which is in agreement with TGA data described by Shang et al. [91] who synthesized and characterized itaconic anhydride and stearyl methacrylate copolymers.

Detail of TGA derivative plot is given by Figure 26b. TGA curves of samples ex 5-2 and ex 10-2 are similar to p(IAH) in the temperature range 220–300 °C. Third decomposition step of p(IAH) begins at ~240 °C which is similar to sample ex 5-2 and ex 10-2. Sample ex 5-2 exhibits third decomposition step which is clerly separated from the decomposition of PLA matrix centered at ~350 °C. On the other hand, sample ex 10-2 exhibits continuous degradation from ~220 °C up to ~280 °C where above this temperature PLA begins degrading. Broad range of

decomposition temperature reflects gradual weight loss suggesting higher polydispersity of p(IAH) extracted from the sample ex 10-2 compared to the sample ex 5-2.

Theoretically, general polymerization requires high IAH/L101 ratio in order to prepare polymer with high molecular weight. Therefore, thermal stability of extracted samples ex 10-0.1 and ex 10-2 was compared in order to prove this theory. As shown in Figure 26c, both samples are decomposed in two major decomposition steps. First decomposition step is centered at ~200 °C, second one is centered at ~350 °C. Furthermore, sample 10-2 exhibit significant weight loss above 220 °C which was desribed above as a result of p(IAH) decomposition. Obtained results prove assumption that most of L101$^\bullet$ are consumed via reaction with PLA or via their recombination. Similar δ of IAH and L101 allow IAH homopolymerization at $[IAH]_0$ and $[L101]_0$.

5.5.1.4 *Reaction conditions supporting self-induced reactions of IAH*

High reactivity of IAH allows its application for reactive modification of polymers due to several factors. First, reactivity of –CO–O–CO– anhydride group allows subsequent reactions with different compounds such as amines. These amines can be derived from natural sources (e.g. proteins) or can be synthetically prepared. This fact enlarges applicability of PLA modified with IAH. Second, higher reactivity of IAH can be predicted due to different possition of C=C double bond of IAH compared to MAH. This may positively affect grafting process. On the other hand, IAH polymerization could become more favourable during functionalization.

Some studies propose that IAH isomerizes to citraconic anhydride (CAH) at the temperature above 100 °C [109]. Therefore, most of functionalization procedures are achieved in solution at low temperature to avoid IAH isomerization. Since exact temperature of IAH-CAH isomerization was not found in the literature, structure analysis was achieved for IAH which was treated under different temperature (80–180 °C) for 6 min. Reaction temperature was chosen with respect to the melting temperature of IAH (66–68 °C) and residence time was the same as used for grafting reaction.

Figure 27 represents FTIR spectra of analyzed samples in the range of 950–750 cm^{-1} as well as structure of both IAH and CAH. Samples prepared at the temperature above 120 °C exhibit weak absorption band at around 870 cm^{-1} which can be attributed to –C=CH– functional group included in the CAH structure. Peaks at around 910 cm^{-1} and 780 cm^{-1} can be assigned to vibrations of –C=CH$_2$ functional group characteristic for IAH structure [110].
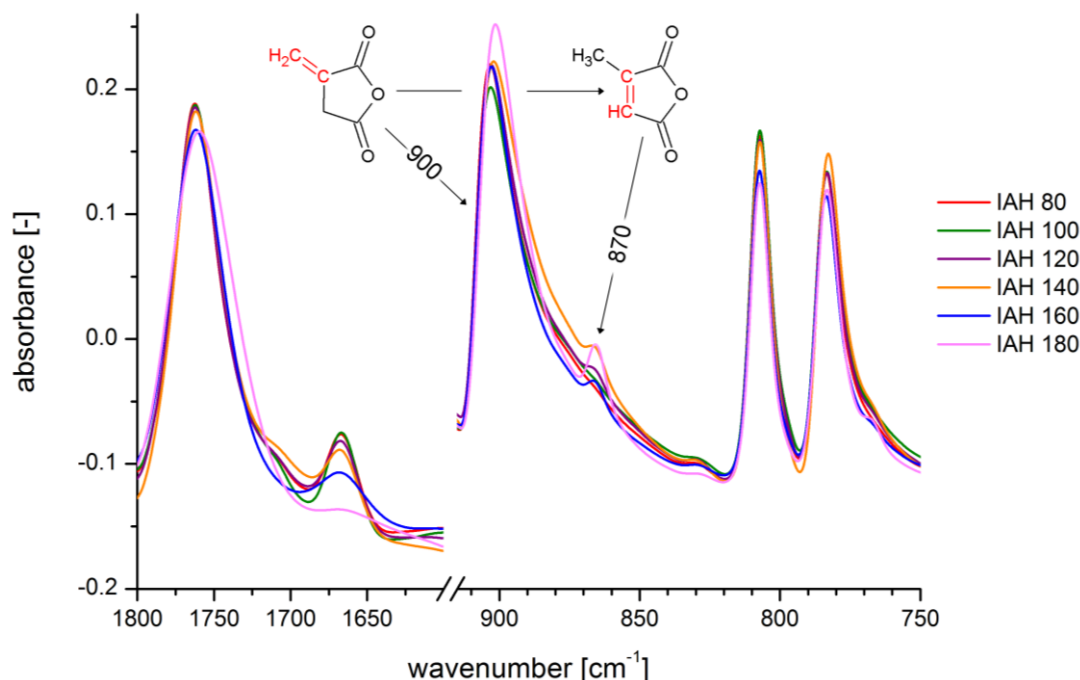
Figure 27. FTIR spectrum for IAH heated at different temperature.

IAH isomerization was also observed on both DSC and DTA thermograms shown in Figure 28a. DSC curve exhibits sharp endothermic peak at around 70 °C which relates to the melting of IAH. Except of melting, exothermic peak with maximum at ~130 °C was detected. It can be attributed to the isomerization from IAH to citranonic anhydride (CAH) [109] which was proved by FTIR analysis. Exothermic peak located at ~170 °C could be assigned to self induced polymerization. This hypothesis is based on the results presented by Katime, Madoz and Velada [104] who described self induced polymerization of itaconate derivates. In this research, polymerization temperature range was evaluated for different itaconate esters with and without using AIBN. Unlike diphenyl itaconate, both dibenzyl itaconate and di-2-phenylethyl itaconate polymerized without AIBN. It was explained by the sterric effect of side groups and loss of conjugation which corresponds to monomer-polymer transformation. Polymerization of unsaturated bonds consists of the opening of one double bond and formation of two single bonds. Accordingly, reaction heat was calculated as a difference between reaction heat of disruption of C=C double bond (608.8 kJ.mol^{-1}) and formation of C-C bond (702.9 kJ.mol^{-1}) equals to 94.1 kJ.mol^{-1} [106]. From the heat of reaction derived from DSC curve in Figure 28a (22.5 J.g^{-1} ≈ 2.5 kJ/mol) it can be assumed that self-induced polymerization of IAH becomes very difficult. This fact is also supported by isomerization IAH-CAH whereas less reactive CAH limits polymerization yield. Degradation of IAH was detected on DTA thermogram as an endothermic peak (red curve, T_{max} ~150 °C) and degradation products were detected in FTIR spectra. Therefore, it can be concluded that IAH degradation and self-induced polymerization proceed simultaneously.

TGA thermograms in Figure 28b proved self-induced IAH polymerization. Decomposition profile of samples IAH 80–140 is similar to the decomposition profile of neat IAH. Main decomposition step was detected at ~140–160 °C. Second minor decomposition step was

73

observed at ~230–240 °C. Approximately 1–2 wt % of char residue remained at 500 °C for those samples. On the other hand, samples IAH 160 and IAH 180 decompose differently whereas second minor decomposition step was not so clear and char residue increased up to 4 wt %. Change of thermal stability and higher content of char residue can be attributed to higher content of polymerized IAH.
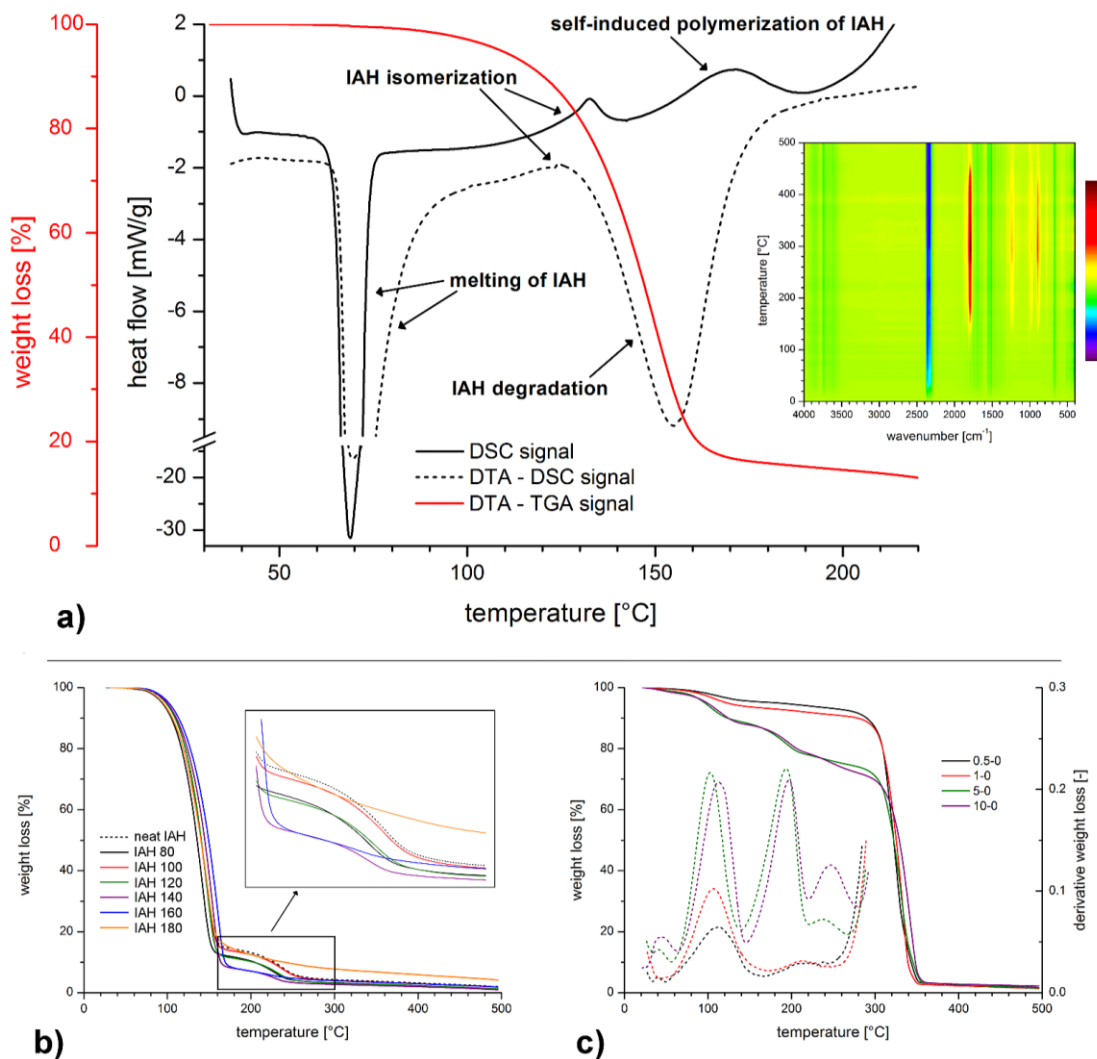
Figure 28. Self-induced polymerization of IAH investigated "in situ" by DSC and DTA (a); decomposition of IAH treated at different temperatures (b); thermal stability of fractions extracted from PLA/IAH blends (c).

Only a few authors deal with thermal stability of IAH and IAH based polymers for last few decades. For example, Rice and Murphy [105] briefly described isothermal decomposition of IAH where methylacetylene, allene, carbon monooxide and carbon dioxide were detected as decomposition products. Compared to this, proposed thesis illustrates IAH decomposition upon temeprature ramp. As mentioned previously, IAH isomerizes at temperature above 120 °C. Major decomposition step can be assigned to decomposition of IAH whereas IAH probably isomerizes

while it was being evaporated. Second decomposition step begins at ~170 °C probably as a result of formation of more stable dimer and/or oligomer form of IAH. It can be assumed that both self-induced and L101-initiated IAH polymerization can occur under reaction conditions used for radical grafting of PLA.

Self-induced IAH polymerization was considered to be possible at temperature above 160 °C. Previous experiments were achieved without presence of any other compounds such as polymer matrix. Therefore, PLA/IAH blends were prepared at 190 °C and thermal stability of acetone soluble fractions was evaluated using TGA analysis. Decomposition profile of thus prepared samples is given in Figure 28c. Fractions extracted from PLA/IAH blends with low $[IAH]_0$ (samples 0.5-0 and 1-0) contain low amount of low-molecular fractions composed of IAH oligomers. It is probably caused by combination of several factors. First, high reaction temperature and low $[IAH]_0$ enhance IAH degradation and limit IAH-IAH interactions. Second, low concentration and high melt viscosity limit IAH-IAH interactions due to intensive homogenization during processing. On the other hand, samples ex 5-0 and ex 10-0 contain significantly higher amount of IAH oligomers. At high $[IAH]_0$, IAH molecules can partially agregate although intensive homogenization was applied. In this case, IAH polymerization can reach higher yield.

As mentioned above, Shang et al. [91] observed thermal decomposition of p(IAH) beginning at ~170 °C. However, authors did not describe individual fractions decomposed during heat ramp. Therefore, thermal decomposition of IAH was studied using TGA achieved at different heating rate (2–50 °C/min.) and obtained data are shown in Figure 29a. Two distinct decomposition steps were detected which is in consistence with previous results. Major decomposition step is assigned to decomposition of IAH or its isomeric form CAH which can be generated simultaneously with decomposition of IAH. Further decomposition continues at temperature above 150 °C while onset temperature depends on the haeting rate. Shang et al. [91] reflect this decomposition step as a consequence of radical polymerization of IAH. However, experimental data in Figure 29a were obtained for IAH without initiator. Therefore, second decomposition step may reflect decomposition of IAH dimers or oligomers.

Increase of T_{max} of both decomposed fractions relates to slower response of TGA signal due to higher heating rate. Figure 29 includes values of weight losses of both decomposed fractions. It can be concluded that higher heating rate results in lower amount of decomposed IAH while amount of IAH dimers/oligomers increases. Low heating rate gives greater yield of IAH degradation whereas high heating rate (i.e. 20 °C/min.) inhibits IAH degradation and higher amount of IAH is available for coupling reactions at higher temperature.
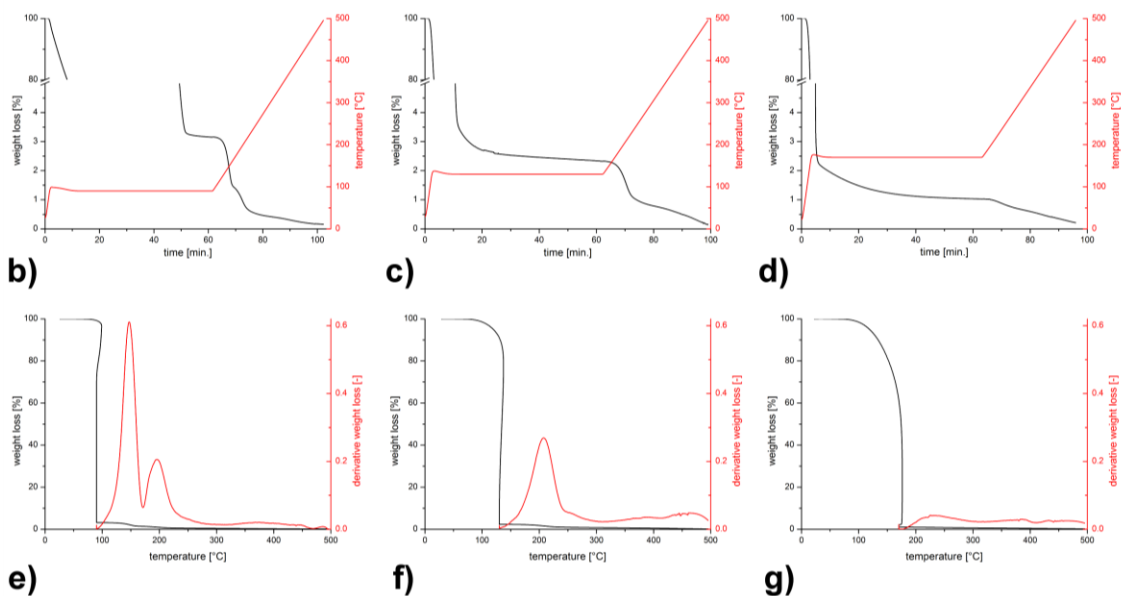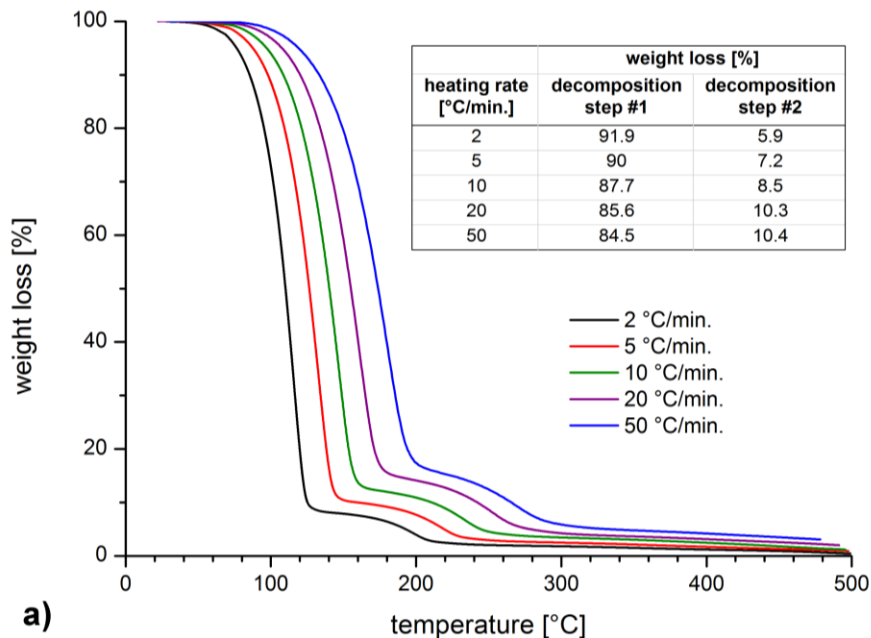
Figure 29. TGA thermogram of IAH decomposed at different heating rate (a); plot between weight loss and decomposition time derived from isothermal decomposition of IAH at 90 °C (b), 130 °C (c) and 170 °C (d); decomposition temperatures of products of coupling reactions occured at 90 °C (e), 130 °C (f) and 170 °C (g).

As mentioned previously, content of recombination products and their decomposition temperature are affected by reaction parameters chosen for TGA analysis. With respect to this fact, isothermal experiments were achieved for three different isothermal temperatures (90, 130 and 170 °C). IAH was heated to desired isothermal temperature at heating rate of 50 °C/min in order to minimize degradation during temperature ramp. Figure 29b represents TGA data for IAH

heated isothermally at 90 °C. IAH is decomposed n after 50 min of isothermal segment whereas approximately 3 wt % of thermaly stable fraction was decomposed during further heating (10 °C/min up to 500 °C). As shown in Figure 29e, two decomposition steps can be distinguished with T_{max} at 150 and 200 °C which could be assigned to two fractions with different thermal stability. Lower decomposition temperature could reflect IAH dimer complexes while high decomposition temperature could be attributed to IAH oligomers. Higher amount of IAH oligomers was observed for isothermal heating at 130 °C (Figure 29c). Approximately 2.5 wt % of residue was decomposed after isothermal heating in one step with T_{max} at 210 °C (Figure 29f). Compared to IAH decomposed at 90 °C, higher content of oligomer fraction was observed which is in consistence with DSC thermogram in Figure 28a which contains exothermic peak of coupling reactions beginning at 140 °C. When temperature of 170 °C was used, high extent of degradation during isothermal segment (Figure 29d) caused low amount of IAH oligomers compared to lower temperatures (Figure 29g). It is in good agreement with TGA thermograms in Figure 28c. Low amount of IAH melted in PLA matrix resulted in low amount of IAH oligomers. High concentration of IAH resulted in increase of concentration of IAH oligomers although concentration of mentioned products was low due to predomination of IAH degradation.

5.5.2   Chain scission

As mentioned above, reaction parameters such as $[IAH]_0$, $[L101]_0$ and reaction temperature strongly affect character of reaction, its rate and properties of prepared material. Side reactions occur during grafting process and affect molecular weight of reaction products which may have effect on its rheological, mechanical and thermal properties.

Molecular weight of all tested PLA-g-IAH sample was lower compared to neat PLA due to degradation reactions. Non-radical degradation caused by PLA nature was limited by optimized reaction temperature, time and shear stress. However, interactions between PLA and radical species lead to chain scission represented by reaction 2c included in Scheme 1. This reaction was proved by GPC analysis of representative series of PLA-g-IAH. As mentioned above, grafting yield reached maximum for the reaction system with low $[IAH]_0$. With regard to quantitative analysis, molecular weight of PLA-g-IAH decreases while $[IAH]_{PLA}$ increases. Based on these results it can be expected that grafting of IAH proceeds via both side and end chain grafting mechanism according to reaction 3 and 2ca in Scheme 1.

Increase of $[IAH]_0$ up to 5 wt % enhances PLA degradation which was detected by decrease of molecular weight of PLA-g-IAH (Figure 30a). At 5 wt % IAH termination between PLA macroradicals and IAH limit PLA degradation due to hydrogen abstraction from IAH. In that case, PLA macroradicals are abolished while low reactive IAH$^\bullet$ are formed.

Side reactions of radical species complicate description of grafting mechanism and four possible reactions may occur depending on $[L101]_0$: grafting, β-scission, chain branching and crosslinking. As discussed previously, grafting in the presence of IAH and L101 leads to decrease of molecular weight of PLA-g-IAH. Regarding GPC results presented in Figure 30b, it can be assumed that β-scission predominates at low $[L101]_0$ (0.1 wt %). Low concentration of PLA$^\bullet$ inhibits the probability of their interactions leading to crosslinked structure characterized by

greater molecular weight. As [L101]$_0$ increases, concentration of PLA macroradicals increases and both β-scission and chain branching can be observed. This was observed for PLA-g-IAH prepared at 0.5 and 1 wt % L101 where decrease of molecular weight is not so significant. Though molecular weight of sample 1-2 is lowest, high [L101]$_0$ increases content of crosslinked PLA due to higher amount of generated macroradicals which undergo a coupling reaction. This was proved by change of melt behavior of raw PLA-g-IAH and will be discussed below (see chapter 5.5.4). From proposed results it can be assumed that ballance between β-scission and crosslinking is most signifficant at high [L101]$_0$. Molecular weight of sample 1-2 is low because of non-crosslinked soluble fractions contained in purified PLA-g-IAH.
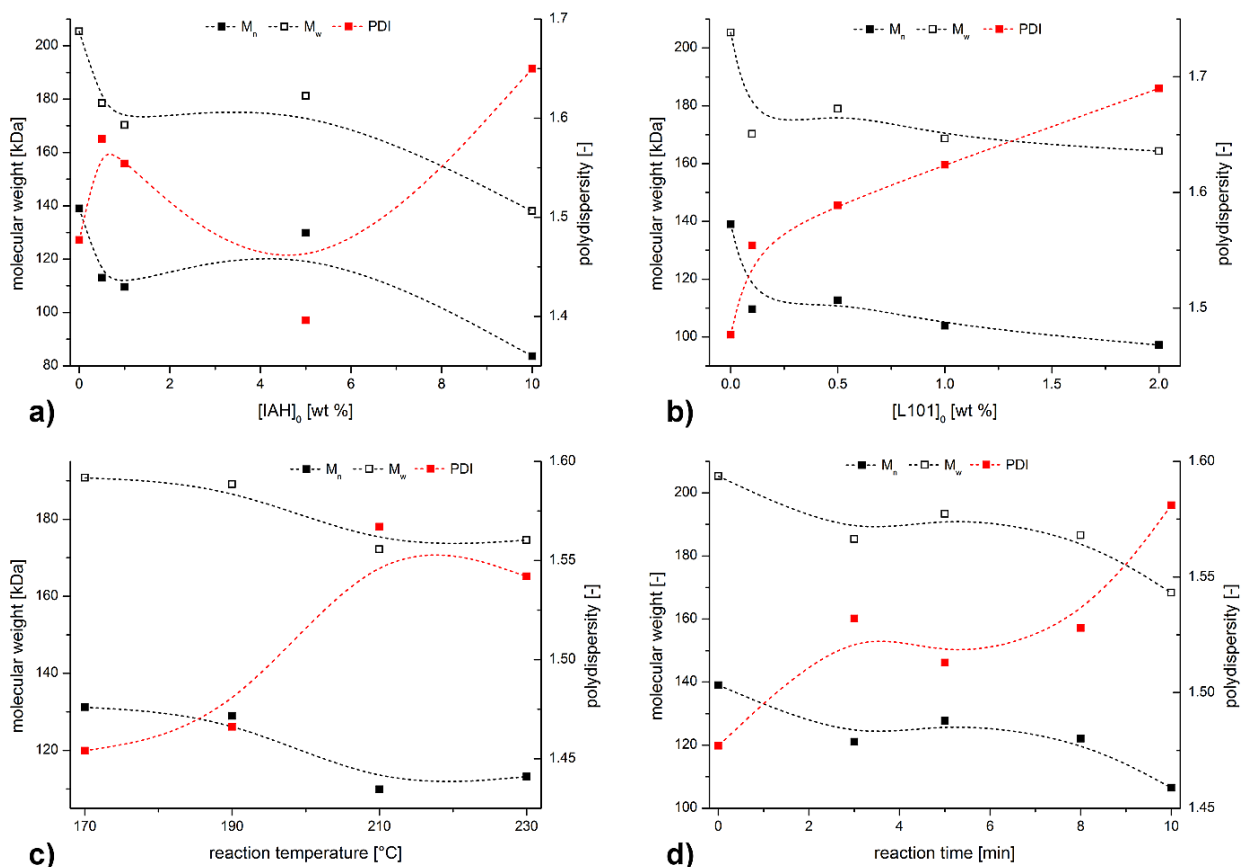
Figure 30. Experimental data obtained by SEC; influence of a) different [IAH]$_0$, at [L101]$_0$ = 0.5 wt %, b) different [L101]$_0$ at [IAH]$_0$ = 1 wt %, c) reaction temperature 170–230 °C (1-0.5) and d) reaction time 1–10 min. (1-0.5) on molecular weight of PLA-g-IAH.

Molecular weight of PLA-g-IAH decreases as reaction temperature increases. Grafting at low temperature (170 °C) doe not lead to signifficant decrease of molecular weight of prepared PLA-g-IAH (Figure 30c). At this temperature, non-radical degradation (i.e. thermohydrolysis) has negligible effect on PLA degradation. Moreover, concentration of radical species is relatively low to affect molecular weight of PLA-g-IAH via β-scission, chain branching or crosslinking. As the reaction temperature increases the importance of β-scission raises which results in more signifficant decrease of molecular weight of PLA-g-IAH. When the reaction temperature rises

above 200 °C, non-radical mechanisms participate on PLA degradation. Molecular weight of PLA-g-IAH prepared at reaction temperature 230 °C is slightly higher than molecular weight of PLA-g-IAH modified at 210 °C. High concentration of L101$^{\bullet}$ at 230 °C leads to higher extent of their coupling reactions compared to the reaction temperature 210 °C. According to obtained results, radical mechanism of PLA degradation can be considered to more important than non-radical mechanisms.

Change of molecular weight of PLA-g-IAH was also determined for samples prepared at different reaction periods. Reaction composition 1 wt % of IAH and 0.5 wt % of L101 was used for demonstration the influence of reaction time on molecular weight of PLA-g-IAH. As shown in Figure 30d molecular weight decreases up to 3 min of reaction period. During this reaction period concentration of L101$^{\bullet}$ is relatively high and most of L101 is decomposed which relates to higher extent of β-scission. After 5 min, initiator is completely consumed and molecular weight of PLA-g-IAH reached maximum which can be attributed to higher extent of coupling reaction between macroradicals and other radical species. Further increase of reaction time leads to decrease of molecular weight which is caused by non-radical degradation.

The extent of β-scission was distinguished by a change of intrinsic viscosity of PLA-g-IAH solution while PLA's intrinsic viscosity was 0.183 dL/g. Presence of peroxide initiator resulted in chain scission and reduction in intrinsic viscosity which equals to molecular weight. This is in good agreement with SEC results presented in text above. Intrinsic viscosity of PLA-g-IAH prepared at low $[L101]_0$ exhibit high values which predicts low extent of chain scission due to low concentration of PLA$^{\bullet}$ (Figure 31). As $[L101]_0$ is low, intrinsic viscosity increases with increasing $[IAH]_0$. In this case, increasing $[IAH]_{PLA}$ leads to altering chain mobility due to bulky functional groups of IAH.
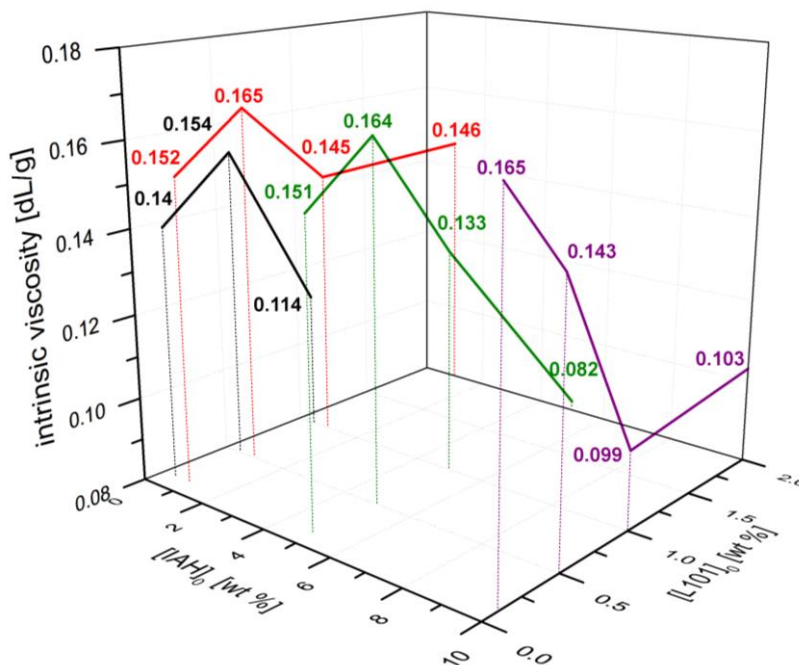
Figure 31. Intrinsic viscosity of grafted PLA at different $[IAH]_0$ and $[L101]_0$.

5.5.3 Radical branching

Except of reactions decreasing molecular weight, opposite reactions may occur simultaneously with chain scission which cause increase of molecular weight. Especially at low $[IAH]_0$, crosslinking and branching was expected due to change of melt properties detected by MFR analysis (chapter 5.5.4). Since crosslinking can be determined for raw samples, branching was observed for purified PLA-g-IAH. From these reasons, PLA-g-IAH samples with 0.5 wt % of IAH and different $[L101]_0$ (0.1, 0.5 and 1 wt %) were tested.

Regarding previous experiments it was predicted that radical branching can occur at low $[IAH]_0$ where interactions between IAH and L101 are not prefered. Branched structure was considered to be dependent on $[L101]_0$ using SEC chromatography equipped with light scattering detector. Chromatograms of selected purified PLA-g-IAH samples are shown in Figure 32a. It is clear that molecular weight of 0.5-1 is greater due to radical branching. Polydispersity of 0.5-1 sample is higher whereas polymer fractions with lower molecular weight were not observed instead of samples 0.5-0.1, 0.5-0.5 and neat PLA.
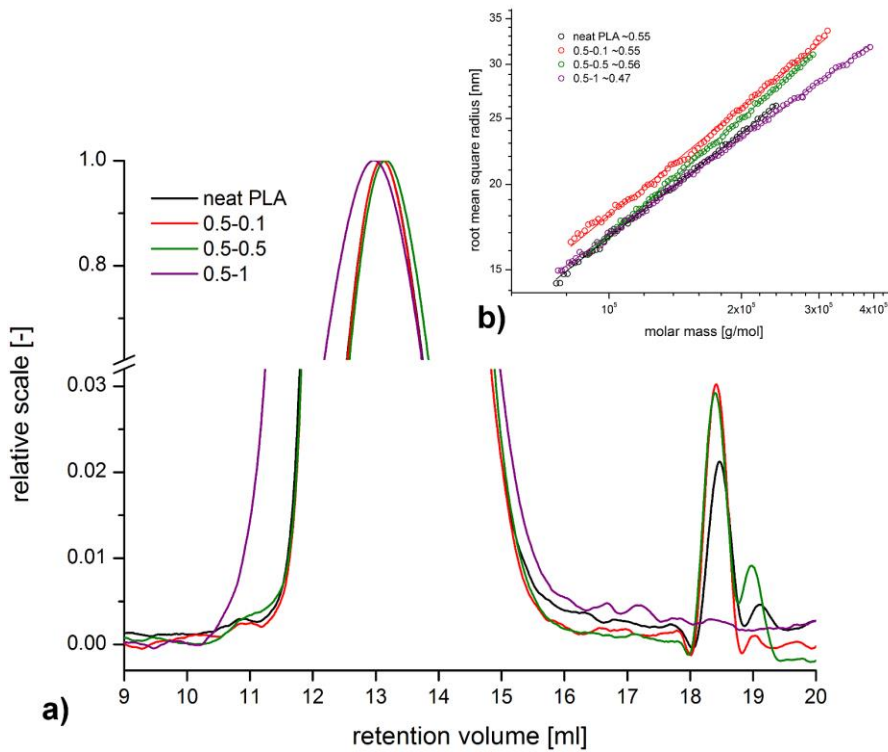
Figure 32. SEC data from radical branching analysis: a) SEC chromatogram of neat PLA and PLA-g-IAH samples; b) conformation plot root mean square radius vs. molar mass obtained from experimental data.

Figure 32b demonstrates conformation plot representing relation between root mean square radius (RMS) and molar mass for neat PLA and PLA-g-IAH. Branching can be identified from linear regression of proposed conformation plot. Slope of conformation plot in Figure 32b for spheres would be ~0.33. However, polymers in good solvent are shaped like expanded coils. It

means that slope for all linear polymers in thermodynamically good solvents are ~0.58 whereas lower values indicate branched structure. With respect to presented results, branched structure was observed for sample 0.5-1 (slope ~0.46) while neat PLA and PLA-g-IAH samples prepared at lower $[L101]_0$ exhibit slope values typical for linear polymers (0.55–0.56). Obtained results are in good agreement with study Carlson et al. [76] focused on branching of PLA. Authors concluded that reaction between PLA and 0.1–0.25 wt % of initiator caused branched structure and highly branched structure was formed at initiator concentration of 0.5 wt %. In the case of radical grafting with IAH, branched structure was observed for initiator concentration of 1 wt %. It can be attributed to simultaneous grafting reaction and side reactions which also consume substantial amount of generated $L101^{\bullet}$. From this reason, $[L101]_0$ responsible for branched PLA is higher compared to that determined by Carlson et al.

5.5.4 Crosslinking

As discussed in previous text, undesired reactions occur during reactive modification depending on reaction conditions. It is expected that these reactions strongly affect reaction process and properties of reaction product.

Experimental data in Figure 33 illustrate the influence of reactants concentration on MFR of PLA-g-IAH. PLA-g-IAH prepared at low $[L101]_0$ (up to 0.5 wt %) exhibits approximately linear increase of MFR with increasing $[IAH]_0$. This phenomenon is partially caused by increasing content of unreacted IAH which was observed for PLA/IAH blends (MFR increased from 2.9 to 8.4 g/10 min). With further increase of both $[IAH]_0$ and $[L101]_0$, MFR increases more rapidly. As discussed in chapter 5.5.1.1, high concentration of both IAH and L101 supports their interactions while formation of IAH oligomers can be expected. Both unreacted IAH and low molecular IAH oligomers can act as a plasticizer which enhances MFR value. On the other hand, PLA modified by addition of 10 wt % IAH and 2 wt % L101 exhibits lower MFR than PLA modified with 5 wt % of IAH and 2 wt % of L101. With regard to previous results, crosslinking occur even at high $[IAH]_0$ where reactions between IAH and radical species are prefered. In addition, the highest $[L101]_0$ is responsible for the highes content of p(IAH) (see chapter 5.5.1.3) which exhibits improved thermal stability compared to low molecular byproducts.

Influence of $[L101]_0$ on MFR was evaluated for samples without addition of IAH. As shown in Figure 33b, MFR increases up to 0.5 wt % of L101 due to favoured chain scission. As $[L101]_0$ increases above 0.5 wt %, MFR slightly decreases due to balance between chain scission and radical branchin/crosslinking as a result of coupling reactions between $PLA^{\bullet}$.

Although crosslinking was expected for the samples with the lowest $[IAH]_0$ and highest $[L101]_0$, MFR values do not prove this hypothesis exactly. To compare, MFR value of sample 0.5-0.1 equals to 16.6 g/10 min while MFR of sample 0.5-2 reaches 23.1 g/10 min. It is in contrast with proposed theory. On the other hand, experimental data show different run time of analysis for both samples. When the same amount of both samples was loaded into the measurement capillary, different run times were detected. For example, total run time for sample 0.5-0.1 was 561 s while total run time for sample 0.5-2 was 916 s. This period was much longer compared to samples prepared at lower $[L101]_0$. After that period, MFR was probably affected by

non-radical degradation (hydrolytic and thermal degradation) as a result of long residence time in heated capillary. Accordingly, it can be expected that MFR of sample 0.5-2 is in fact lower than 23.1 g/10 min. Although C–O bonds were expected to be cleaved, new bonds formed via crosslinking reaction kept the MFR approximately constant for the whole run time. This explanation is illustrated by plot between total run time and melt viscosity in Figure 33c completely derived from experimental data.
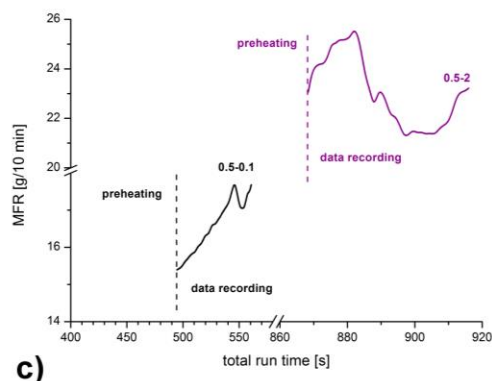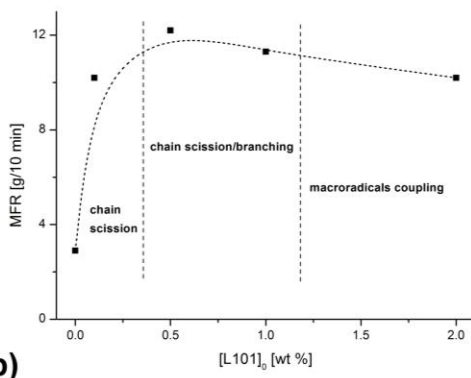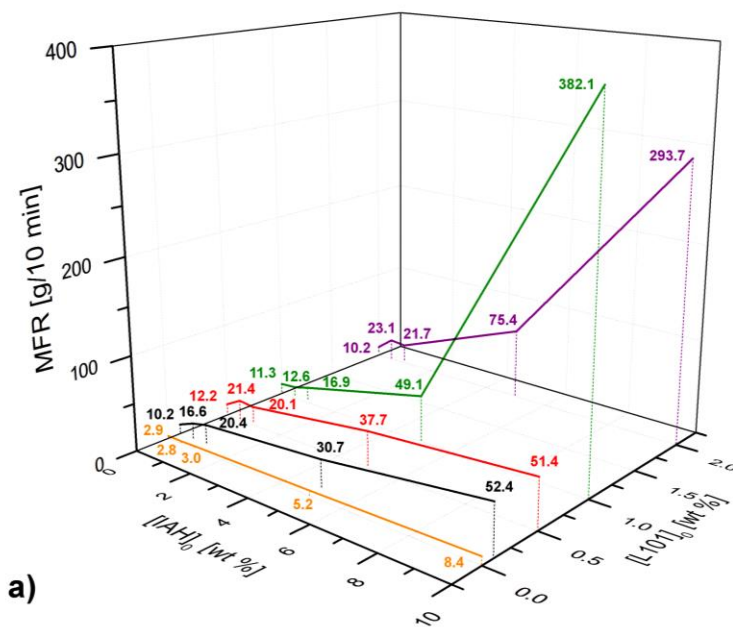
Figure 33. Melt behavior of PLA-g-IAH - relationship $[IAH]_0$-$[L101]_0$-MFR (a); balance between chain scission and macroradicals coupling depending on $[L101]_0$ (b); experimental data obtained during melt flow test for sample 0.5-0.1 and 0.5-2 (c).

5.6   Effect of reactive modification on PLA biodegradability

The influence of reaction conditions on PLA-g-IAH structure and relating degradation rate was investigated during long-term biodegradation test for 12 weeks. The effect of accumulated degradation products on pH values and degradation profile of PLA-g-IAH prepared at various $[IAH]_0$ (0.5, 1 and 5 wt %) and $[L101]_0$ (0.1, 0.5 and 1 wt %) was investigated. Neat PLA was used as a reference sample to evaluate the effect of grafted IAH on biodegradation.

Figure 34 represents degradation profile of PLA-g-IAH samples. As PLA-g-IAH was incubated in distilled water, pH of medium decreased with increasing time. Generally, decrease of pH can be assigned to higher concentration of degradation products. The degradation of PLA and PLA-g-IAH consist of four consecutive steps: hydration, initial degradation, further degradation and solubilization [111].

Three degradation steps can be observed in Figure 34. First part of degradation process is characterized by decrease of pH from 5.1 to 5.0 for neat PLA and from 5.7 to 3.7 for PLA-g-IAH. During this degradation medium penetrates into the polymer matrix without chain cleavage. It is clear, that hydration of neat PLA occured for two weeks while first degradation phase of PLA-g-IAH occured within one week. Furthermore, first degradation phase is characterized by slight decline of pH value which was observed for neat PLA while PLA-g-IAH exhibited strong decline of pH value within first week. This can be attributed to PLA-g-IAH's higher content of amorphous phase which enhances faster penetration of aqueous medium into PLA. In addition, first phase can be overlapped by second phase in the case of PLA-g-IAH. With respect to the concentration of reaction compounds, increase of both $[IAH]_0$ and $[L101]_0$ results in more intensive first hydration stage due to higher content of amorphous phase, higher grafting degree and reduced chain mobility. This is mostly evident for samples 5-1 which exhibits pH value drop from 5.5 to 3.8 within one week.

Second phase of PLA degradation exhibits increasing rate of degradation which is observed by significant decline of pH value. During this phase, ester bond are hydrolyzed and increasing concentration of carboxyl groups accelerates hydrolysis. This phase was observed from second to fourth week for neat PLA and from first to fourth week for PLA-g-IAH. In this degradation period, pH value dropped from 5.0 to 4.0 and from 5.2 to 3.5 for neat PLA and PLA-g-IAH, respectively. In the case of PLA-g-IAH, presence of grafted IAH supports hydrolysis of ester bond. Anhydride groups in PLA-g-IAH hydrolyze to form carboxyl groups which drop pH values of aqueous medium. This effect could be desired in certain medical applications which require fast and controlled degradation of applied material with intensive drug release.

In the third phase, pH decreases gradually from 4.0 to 3.0 and from 3.5 to 2.7 for neat PLA and PLA-g-IAH, respectively. In this phase, the rate of degradation declines and after eleven weeks the pH values reach plateau due to the slowdown of polymer degradation [112].
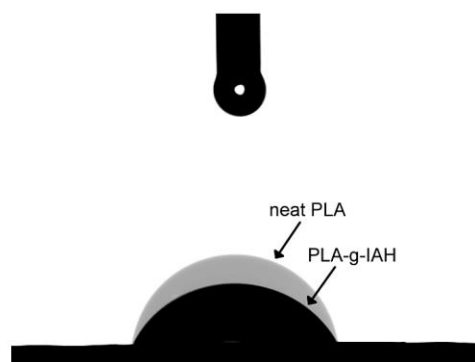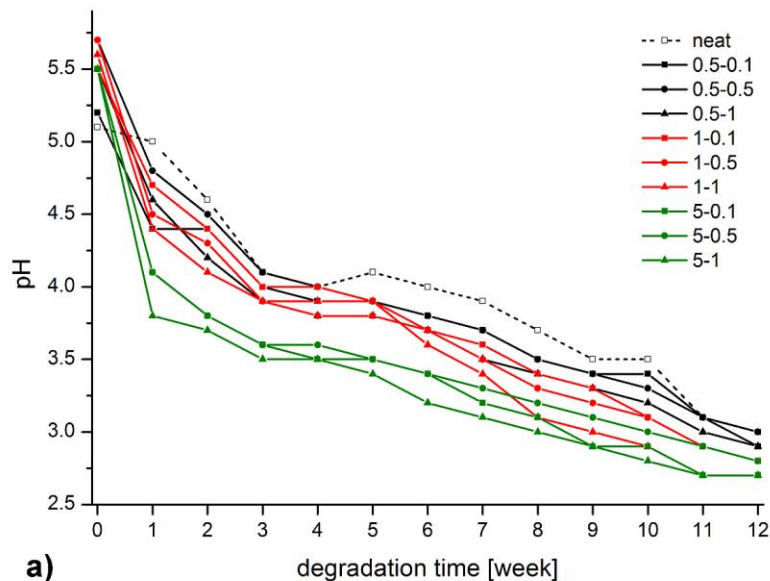
Figure 34. Time dependence of pH of aqueous media during the biodegradation of PLA and PLA-g-IAH at 37±0.1 °C; [IAH]$_0$ = 0.5, 1 and 5 wt %, [L101]$_0$ = 0.1, 0.5 and 1 wt % (a); PLA-g-IAH sample before (A) and after (B) biodegradation test (b).contact angle of neat PLA and PLA-g-IAH (c).

As discussed previously, grafted IAH enhances biodegradability of modified PLA. Contact angle measurement proved enhanced hydrophilicity of PLA-g-IAH detected by decrease of contact angle compared to neat PLA. Improved hydrophilicity supports degradation of PLA-g-IAH as well as lower crystallinity.

5.7 Change of thermal properties due to radical grafting

5.7.1 PLA-g-IAH structure detected by change of thermal properties

Relation between structure of modified PLA and thermal properties was interpreted using DSC analysis. DSC thermograms were obtained for purified PLA-g-IAH prepared at different $[IAH]_0$ and $[L101]_0$. Data obtained from the second heating cycle are presented in order to avoid the effect of thermal history. Absence of exothermic peak located above melting of PLA and endothermic peak of IAH melting (m.p. 60–70 °C) suggests complete grafting reaction with no reactants residue and succesful removing IAH from raw samples, respectively.

DSC curves obtained for x-0.1 samples (x = $[IAH]_0$ = 0.5–10 wt %) are given in Figure 35. The influence of PLA-g-IAH structure on characteristic phase transitions was observed. For all samples glass transition temperature T_g, cold crystallization temperature T_{cc} and melting temperature T_m were observed at around 50, 100 and 150 °C, respectively. For all PLA-g-IAH samples, lower T_g was observed as a result of change of segmental mobility of polymer chains compared to unprocessed PLA ($T_g = 52.7$ °C). As shown in Figure 35, relationship between $[IAH]_0$ and T_g of PLA-g-IAH is not clear. However, enhanced chain mobility resulted in decrease of T_g due to grafting of bulky anhydride ring. Similar results were discussed by Hwang et al. [82] who studied physical and mechanical properties of PLA grafted with maleic anhydride MAH (PLA-g-MAH). In this study T_g of PLA-g-MAH decreased as MAH content increased.

Side reactions (e.g. β-scission, chain branching) affects chain irregularity leading to change of T_g. It is well known from the literature that molecular weight of polymer has effect on T_g. Generally, expression relating the T_g to the molecular weight is accepted to be the following:

$$T_g = T_{g\infty} - \frac{K}{M_n} \tag{31}$$

in which $T_{g\infty}$ is the glass transition temperature when the polymer molecular weight goes to infinity. According to Equation 40, lower molecular weight is relevant to lower T_g.

DCS curve recorded for neat PLA contains exothermic peak attributed to cold crystallization at 100.9 °C which reflects organization of PLA structure upon heating cycle. PLA-g-IAH exhibits lower T_{cc} compared to neat PLA whereas T_{cc} increases with increasing $[IAH]_0$. Lower T_{cc} of PLA-g-IAH may suggest decrease of molecular weight which was discussed in previous chapters. According to this hypothesis, PLA-g-IAH chains with lower molar mass can be oriented at lower temperature compared to PLA chains with greater molar mass which require higher temperature to be oriented. Two endothermic peaks at around 150 °C can be attributed to the melting of two different phase structures. Peak at lower temperature relates to α' phase and the second peak corresponds with α phase [113]. These two crystal modifications have a similar chain packing with 10_3 helix conformation and orthorhombic unit cell [114].

Degree of crystallinity of PLA-g-IAH was calculated according to Equation 7 in chapter 4.3.5. Degree of crystallinity of PLA-g-IAH was found to be lower compared to neat PLA as a result of

irregular PLA-g-IAH due to both IAH grafted on PLA backbone and side reactions such as branching or β-scission.
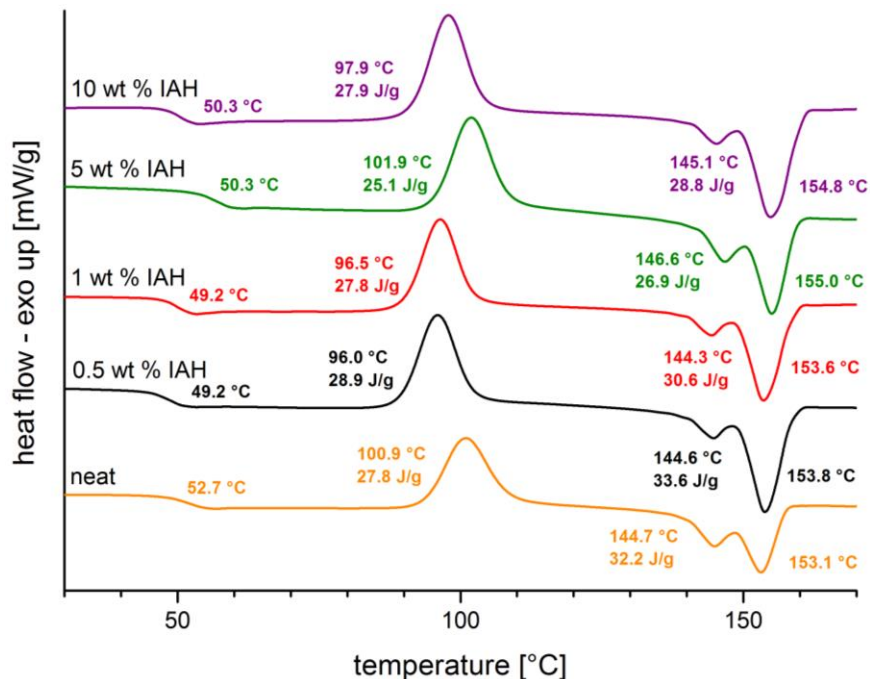
Figure 35. DSC thermograms of neat PLA and purified PLA-g-IAH with constant $[L101]_0$ (0.5 wt %) and different $[IAH]_0$; 2nd heating cycle.

Thermal properties of PLA-g-IAH prepared at different $[L101]_0$ were evaluated from DSC thermograms illustrated in Figure 36. As mentioned previously, radical reaction between PLA and IAH causes change of T_g and T_{cc} as a result of change of chain mobility and chain scission. Similar results were determined in proposed experiments where T_g of modified PLA was significantly lower in whole range of $[L101]_0$ compared to neat PLA. On the other hand, increase of $[L101]_0$ has no significant effect on the T_g value. Decrease of T_g can be also caused by higher amount of free volume due to grafted IAH and increasing content of amorphous phase [115]. These explanations are in cosistence with lower X_c of PLA-g-IAH compared to neat PLA. It can be expected that at low $[L101]_0$ low amount of macroradicals is available for branching which is reflected by higher T_{cc}. In addition, branched structure reduces crystallinity due to longer side chains. At high $[L101]_0$, greater content of branched structure can be expected detected by lower T_{cc} and higher crystal nucleating potential [116].

Experiments described in chapter 4.2.3.2 were focused on reaction between PLA and L101 in order to observe the influence of $[L101]_0$ on PLA structure using DSC response. DSC thermograms of thus modified PLA are represented by dashed curves in Figure 36a with detailed description in Figure 36b–d suggesting the influence of branching/crosslinking on T_g value. With regard to DSC data it can be assumed that radical modification of PLA results in increase of both T_g and T_{cc} of thus modified PLA. It can be assigned to retarded chain mobility of branched and crosslinked chains as well as higher molecular weight which was predicted with regard to results in chapter 5.5.4. Moreover, branched and crosslinked structure exhibit retarded chain segments

packing into crystalline structure which is in good agreement with low X_c determined for 0-x samples.
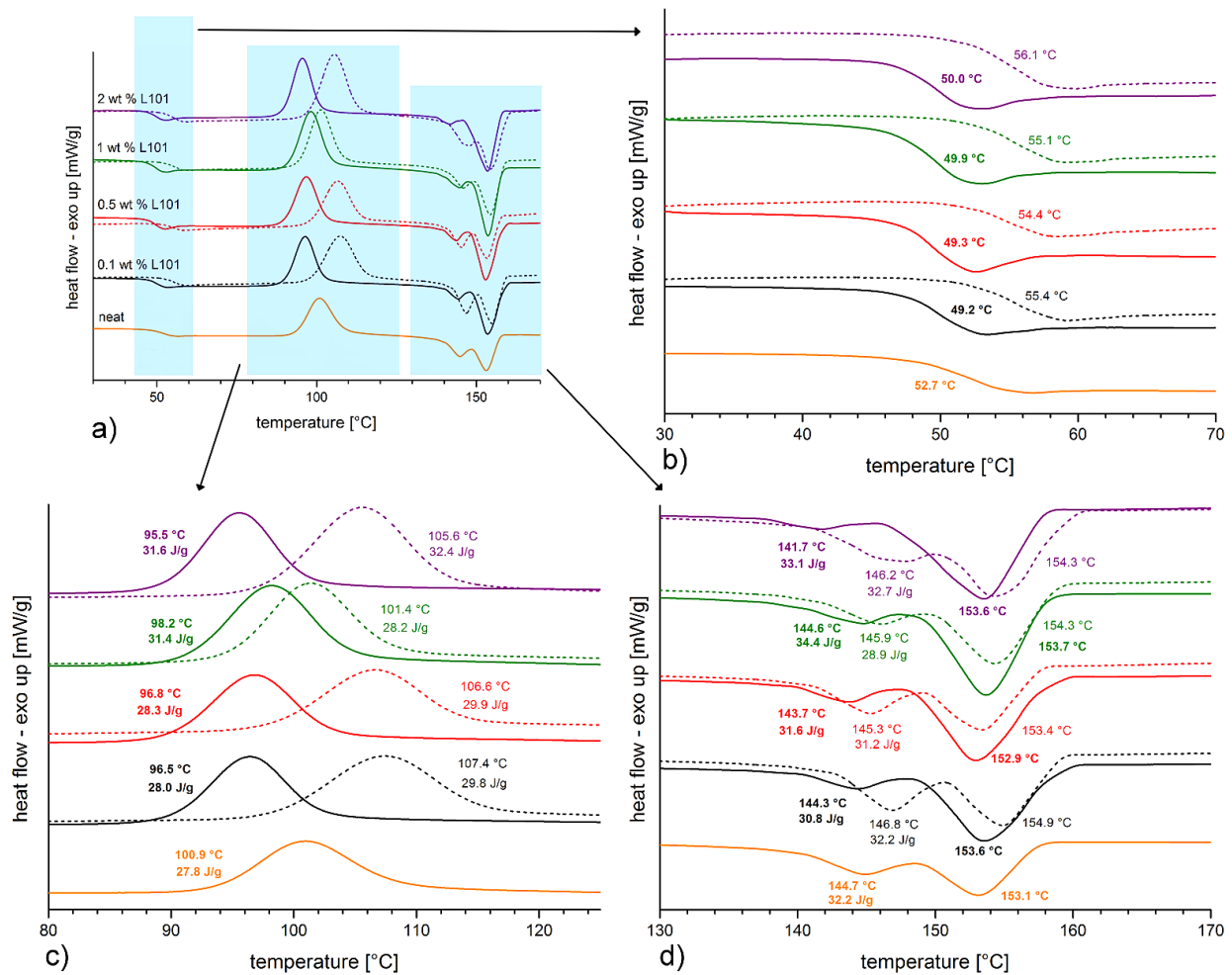
Figure 36. DSC curve of neat PLA and 1-x samples where x = [L101]₀ = 0.1–2 wt %; DSC thermograms (a) with detail of T_g (b), T_{cc} (c) and T_m (d); 2nd heating cycle; curves shifted vertically for clarity.

Yang et al. [117] studied thermal and mechanical properties of chemical crosslinked PLA using crosslinking agent triallyl isocyanurate (TAl) and dicumyl peroxide (DCP). Double-exothermic peak of chemical crosslinked samples was observed due to two kinds of chain structure - crosslinked and non-crosslinked PLA chains. These two exothermic peaks were observed for samples with low concentration of TAl as a result of coexistence of crosslinked and non-crosslinked phase. In this study, single exothermic peak was observed due to not significant difference between crosslinking and non-crosslinking structure.

As discussed in chapter 5.5.3, ends of branched chains act as nucleation centers which may lead to increase of crystallinity. However, samples presented in Figure 36 exhibit lower X_c compared to neat PLA. Low [L101]₀ probably causes low extent of branching where the

influence of low oriented structure predominates over the amount of PLA chain ends. On the other hand, PLA reacted with 2 wt % L101 forms highly crosslinked structure with low X_c.

Finally, change of phase transitions can be considered as indirect proof of IAH grafted on PLA. In this thesis, IAH homopolymerization was observed at high both $[IAH]_0$ and $[L101]_0$ even though it is not expected by many authors due to thermodynamic criteria. Regarding results of DSC analysis it can be assumed that grafting of single IAH is the most probable grafting mechanism. This assumption was proved due to absence of new T_g at ~120 °C which could be attributed to the glass transition of p(IAH) predicted by Shang et al. [91].

5.7.2   Change of thermal stability

Experiments investigated radical grafting of PLA "in situ" proved existence and degradation of byproducts generated simultaneously with main reaction. These byproducts were also detectede in PLA-g-IAH prepared in internal mixer due to different thermal stability. Figure 37a illustrates thermal stability of selected PLA-g-IAH samples prepared with 0.5 and 5 wt % IAH and 0.1–2 wt % L101. All tested grafted PLA had a lower thermal stability compared to neat PLA. The slight decrease in thermal stability supports earlier observations regarding a decrease in crystallinity. With regard to the results discussed in chapter 5.5.2, decrease of thermal stability can be relevant to decrease of molecular mass of functionalized PLA as a result of chain scission during radical grafting.

Compared to raw PLA-g-IAH, purified PLA-g-IAH contained only one decomposition step reflecting decomposition of PLA matrix. Regarding TGA thermograms in Figure 37b it is clear that both unreacted IAH and p(IAH) were succesfully removed by one-step purification.

Raw samples of PLA-g-IAH contain different byproducts detected according their different thermal stability. It is clear for PLA-g-IAH prepared with 0.5 and 5 wt % IAH. For samples 0.5-x weight loss due to water release and decomposition of unreacted IAH and residual lactide was observed whereas thermal stability of possible residues is shown in Figure 37c. On the other hand, TGA curves of samples 5-x contain derivative maxima assigned to decomposition of unreacted IAH, residual lactide and IAH oligomers. As discussed in chapter 5.5.1.2, thermal decomposition consists of two distinct decomposition steps attributed to degradation of IAH and its dimers or oligomers which can be formed even without initiator (Figure 25a, black curve).
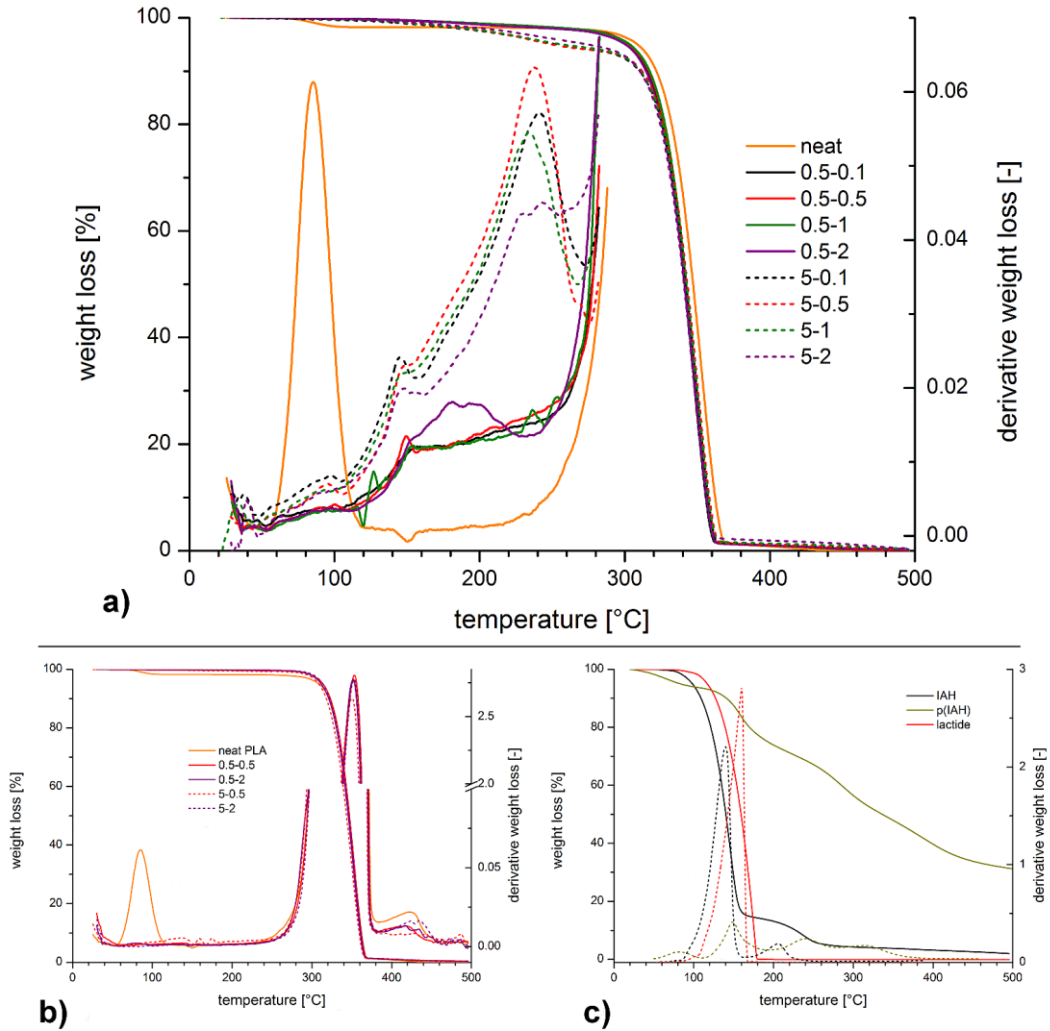
Figure 37. Selected TGA thermograms of raw PLA-g-IAH prepared at different $[IAH]_0$ and $[L101]_0$ (a); thermal stability of purified PLA-g-IAH prepared at different $[IAH]_0$ and $[L101]_0$ (b); thermal stability of possible byproducts (IAH, p(IAH), lactide) contained in raw PLA-g-IAH (c).

5.8 Suppression of non-radical degradation of PLA during reactive modification

5.8.1 Evidence of non-radical degradation of PLA

Presented results proved that degradation reactions affect properties of modified PLA, e.g. thermal properties, molecular weight, structure, etc. These reactions occur simultaneously with main grafting reaction and can be sorted on radical and non-radical based processes. Radical degradation can be limited by convenient reaction conditions such as concentration and type of initiator or reaction temperature. On the other hand, PLA degradation also occurs following non-radical mechanism. These degradation mechanisms include trans-esterification, cis-elimination, thermooxidation, hydrolysis, thermal degradation and chain end groups degradation (back-biting). Trans-esterification, cis-elimination, thermooxidation and back biting can be neglected due to low significance at reaction temperature 190 °C. Therefore, hydrolysis and thermal degradation can participate on overall degradation. These degradation mechanisms are depicted in Scheme 2.
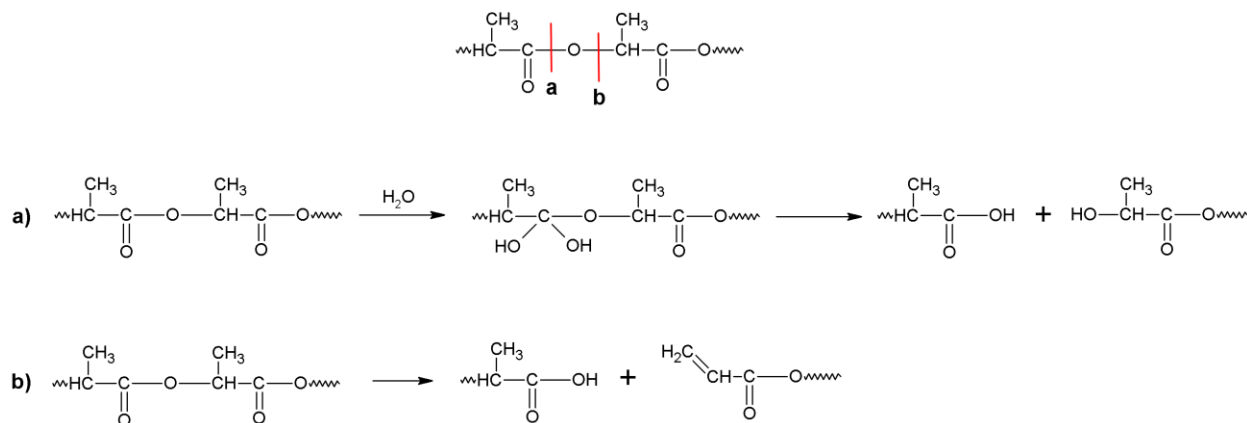
Scheme 2. Expected degradation mechanisms occuring during grafting reaction achieved at 190 °C; hydrolytic scission (a) and thermal degradation (β-H-C hydrogen transfer) (b).

As shown in Scheme 2 (reaction a), hydrolytic degradation requires presence of water, e.g. as a moisture residue. In this case, carbonyl carbon-oxygen linkages are randomly cleaved. Reaction b in Scheme 2 represents thermal degradation (β-H-C hydrogen transfer) leading to vinyl ester and acid end groups.

PLA degradation was observed by change of flow properties measured by MFR. Dried PLA was prepared by removing water residue in vacuum oven at 60 °C for 12 h. MFR of untreated PLA was measured in order to demonstrate hydrolytic degradation and was signed as "wet PLA". Results of MFR analysis are given in Figure 38. MFR of dried PLA was 5.1 g/10 min which is close to the value given by supplier. Absence of moisture causes lower MFR compared to wet PLA (10.7 g/10 min). For dried PLA, thermal degradation seems to be favoured while wet PLA is cleaved either by hydrolytic scission. Combination of both degradation mechanisms correponds

with increase of MFR during measuring for wet PLA where MFR raises from 9.3 to 12.0 g/10 min. Compared to this, MFR of dried PLA raises from 4.7 to 5.4 g/10 min even during longer measuring period.
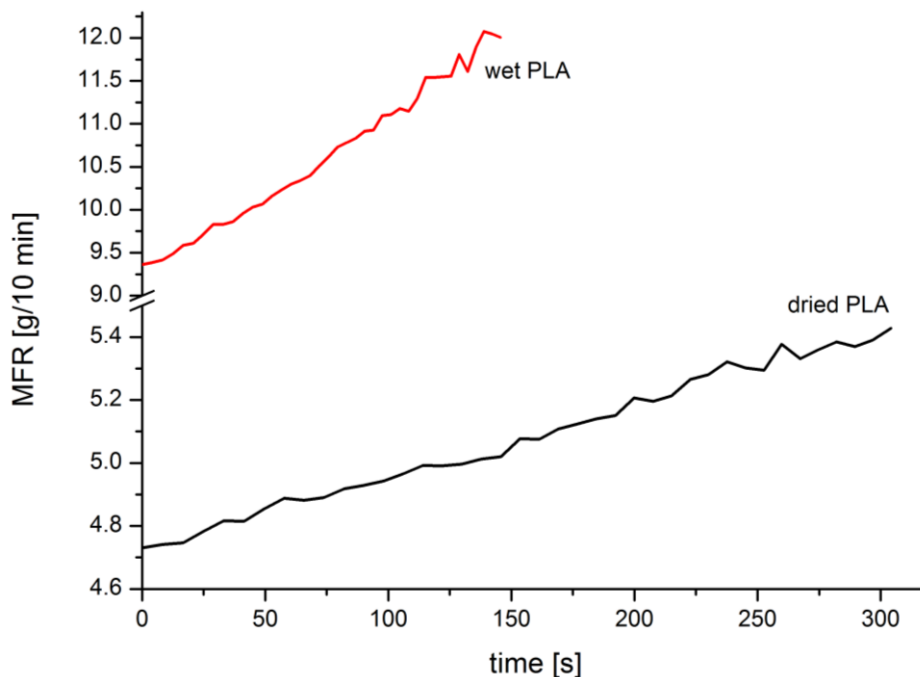
Figure 38. Experimental data obtained during melt flow test; time-dependent melt behavior of wet and dried PLA.

5.8.2 Function of chain extender during grafting reaction

Chain extender Joncryl ADR-4368 C (CHE) was used for reactive modification to supress PLA degradation following Scheme 2. Function of CHE and mechanism of its reaction with neat PLA has been already described by Al-Itry, Lamnawar and Maazouz [88]. This proposal is illustrated in Scheme 3 and describes reaction between epoxide group of CHE and carboxylic/hydroxyl end group of PLA (reaction a1 and a2 in Scheme 3) or carboxylic group of hydrolyzed PLA (reaction b, Scheme 3), respectively. Due to relatively high reactivity of epoxide group, reaction between CHE and carboxylic group of IAH can be expected as a side reaction occuring simultaneously with radical grafting (reaction c, Scheme 3).

Regarding to kind of functional group of reactant, some reactions can be preferable against to the others. Although the epoxide groups of CHE can react with both hydroxyl and carboxyl groups of PLA or IAH. Japon et al. [118] proved that glycidyl esterification of carboxylic group precedes hydroxyl end etherification. Reaction rate of the reaction between epoxide group and carboxylic group is approximately fifteen times greater than between epoxide group and hydroxyl group. Therefore, reaction between CHE and unreacted IAH can significantly affect properties of modified PLA.
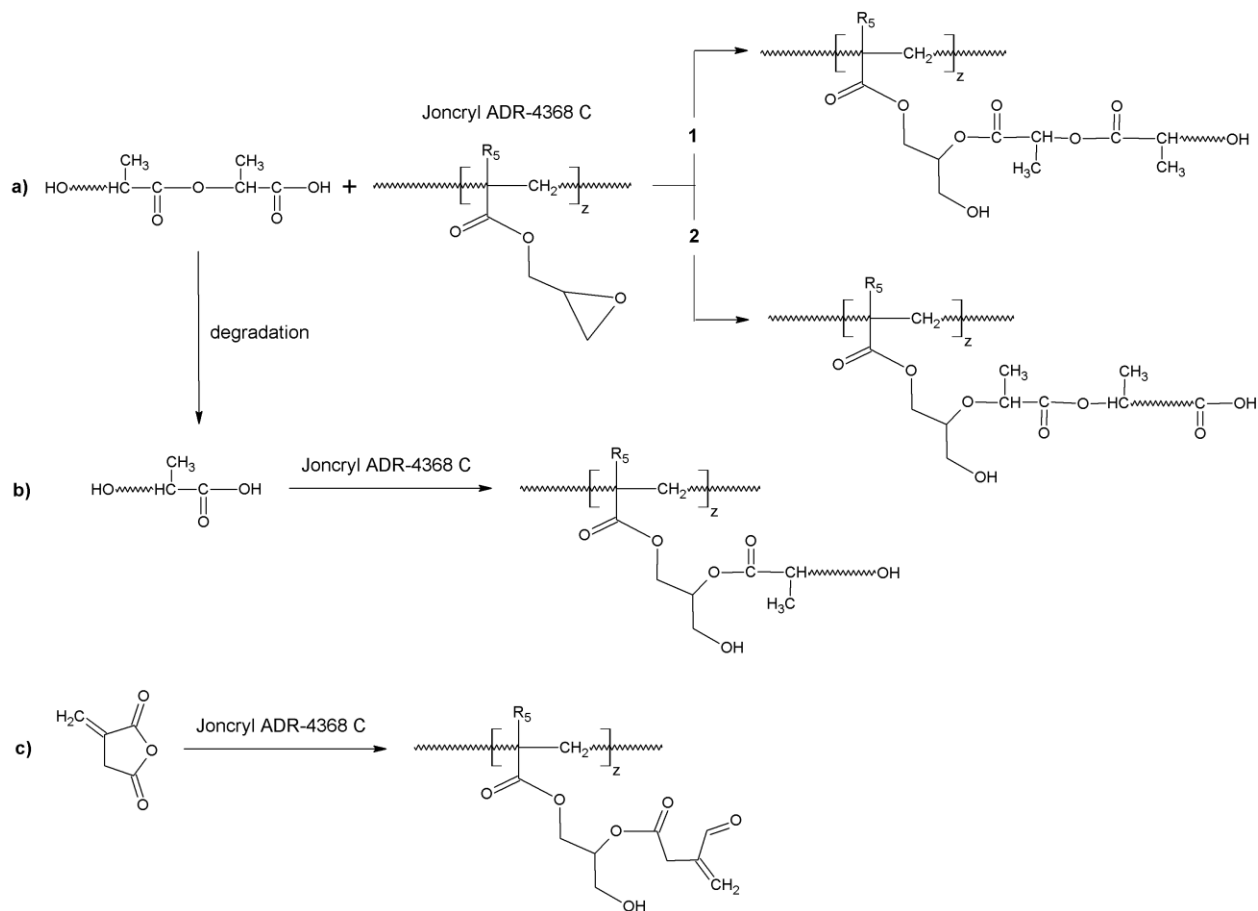
Scheme 3. Mechanism of the reaction between Joncryl ADR-4368 C and: carboxylic acid end group of PLA (a1); hydroxyl end group of PLA (a2); carboxylic acid group of degradation product of PLA (b); IAH (c).

First, function of chain extender was study for processed neat PLA whereas both dried and moist PLA was processed with/without chain extender under the same reaction conditions which were used for grafting reaction (190 °C, 6 min). MFR of dried PLA and dried PLA + CHE was 3.9 and 0.5 g/10 min., respectively. Hydrolytic degradation of moist PLA was observed due to increase of MFR to 5.4 and 0.9 g/10 min for neat and extended PLA, respectively.

Figure 39a represents FTIR spectra of neat PLA, PLA-g-IAH and PLA-g-IAH with addition of CHE. FTIR spectra are in accordance with results presented by Ibrahim et al. [119]. Broad absorption band was observed in the range 3600–3100 cm^{-1} due to stretching vibrations of –OH groups. Neat PLA exhibits intensive peak centered at 3300 cm^{-1} which can be assigned to –OH associated with carboxylic group. This peak was not observed for sample "PLA-g-IAH + CHE" which can be attributed to the reaction between caboxylic group of PLA and epoxide group of CHE forming new –CO–O– bonds according to reaction a and b in Scheme 3. Peak at around 3000 and 2850 cm^{-1} corresponds with the symmetric stretching vibration of the axial –CH groups in PLA backbone. The strong peak originating from C=O stretching vibrations is located at around 1720 and 1750 cm^{-1} (Figure 39b). The peak at around 1630 cm^{-1} may correspond to H–O–H bending vibrations. Intensity of this peak for neat PLA is much higher compared to

PLA-g-IAH with/without CHE. This fact could explain the occurrence of thermal chain scission at C–O bond. This hypothesis is supported by occurence of peak at 1550 cm^{-1} which may reflect C=C stretching vibrations formed during β-H-C hydrogen transfer. There is no hint of this peak in FTIR spectrum of "PLA-g-IAH + CHE". Peaks detected in the range 1300–1050 cm^{-1} are assigned to C–O from carboxyl groups and C–O–C stretching vibrations (Figure 39c). Moreover, peak located at 1210 cm^{-1} can be assigned to C–O–C group incorporated in fragment R–COO–R$_1$ where R represents vinyl group. Intensity of this peak is highr for neat PLA which could indicate higher extent of β-H-C hydrogen transfer for neat PLA. FTIR spectrum of unprocessed PLA (black line) exhibits absorption band at 920 cm^{-1} which can be assigned to –CH–O– bond situated in the PLA backbone. Absorption band at 900 cm^{-1} can be assigned to –CH$_2$=CH– of both IAH and PLA cleaved via β-H-C hydrogen transfer.
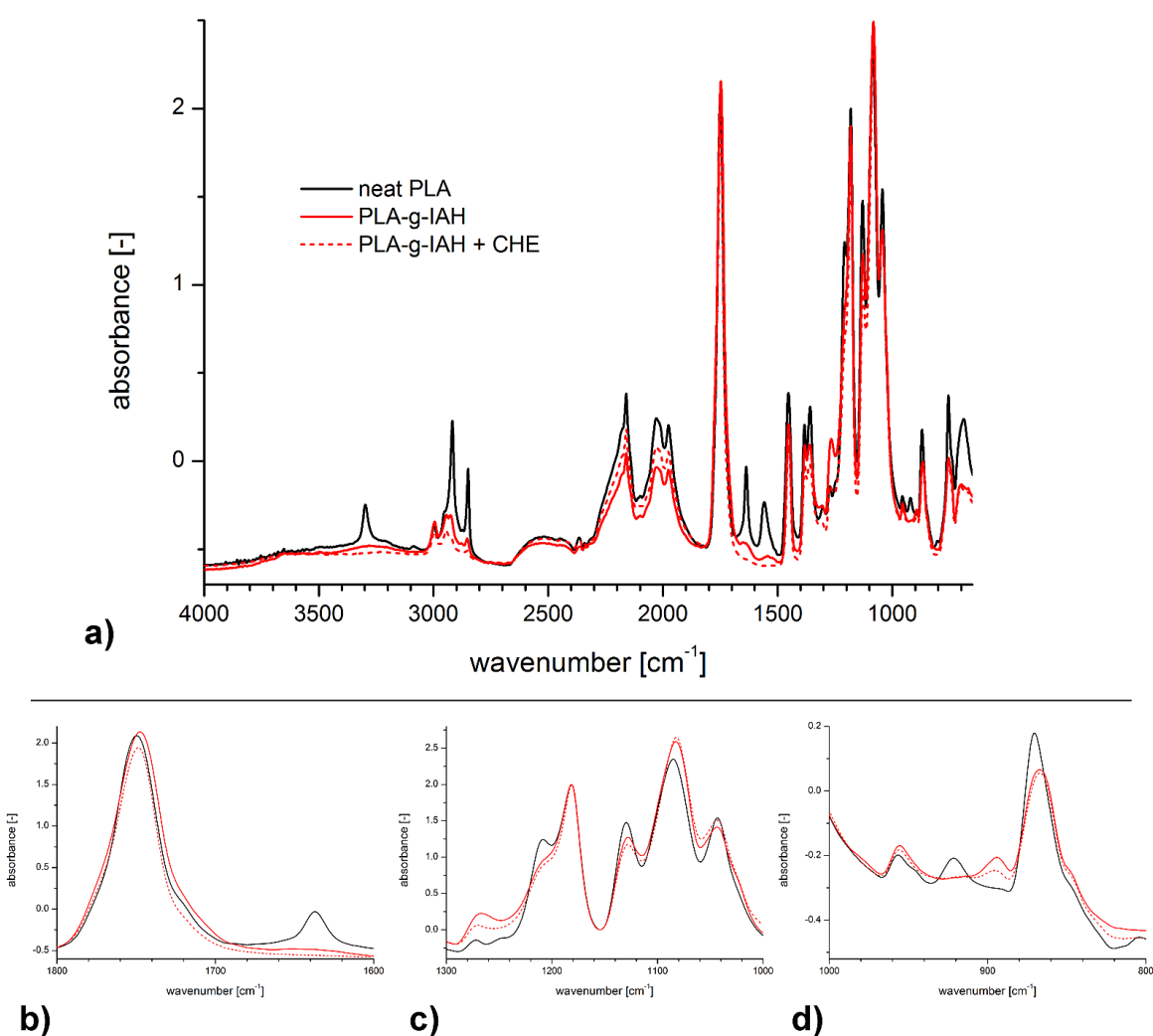
Figure 39. FTIR spectra of neat PLA, PLA-g-IAH and PLA-g-IAH with CHE (a); detail in the wavenumber range 1800–1600 cm^{-1} (b), 1300–1000 cm^{-1} (c) and 1000–800 cm^{-1} (d).

93

With respect to mentioned reaction rates, epoxide groups of Joncryl can also interact with carboxylic groups of IAH which can be formed via ring-opening mechanism by interaction with moisture at high temperature. Proposed reaction between IAH and Joncryl (Scheme 3, reaction c) can limit the undesired effect of unreacted IAH on rheological and mechanical properties. This assumption was partially proved by results derived from acid-base titration. Grafting yield was determined for purified PLA-g-IAH prepared by grafting reaction with 0.5/5 wt % of IAH, different $[L101]_0$ (0.1–2 wt %) and with/without 0.5 wt % of chain extender. Higher grafting degree was observed for PLA-g-IAH with addition of chain extender for both $[IAH]_0$ (Figure 40). This effect was observed especially for PLA-g-IAH grafted with low $[IAH]_0$. As 5 wt % IAH and 0.5 wt % of CHE was applied, $[IAH]_{PLA}$ was higher up to 0.5 wt % L101 compared to samples without CHE. Interactions between IAH and $L101^{\bullet}$ are favoured at high $[IAH]_0$ and $[L101]_0$ which disadvantages reaction between IAH and CHE.
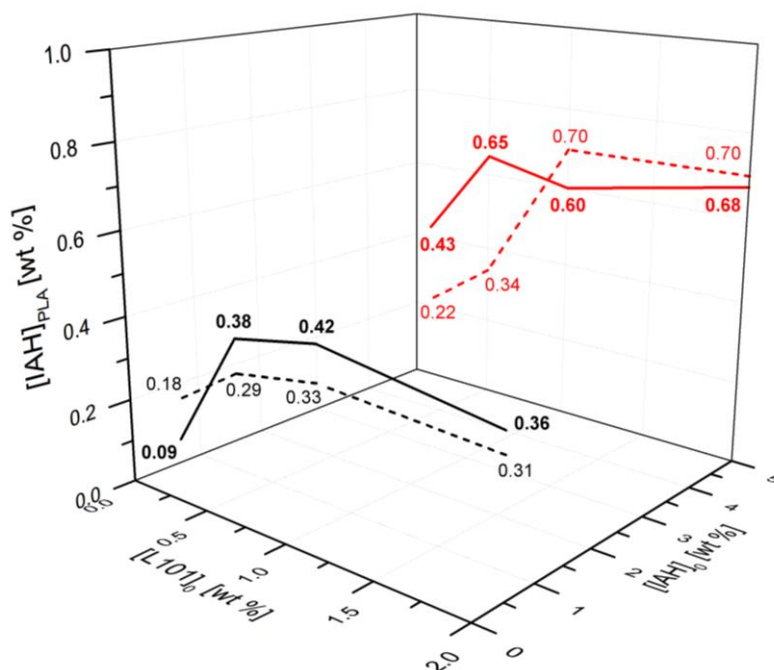
Figure 40. Relationship between $[IAH]_{PLA}$ and $[L101]_0$ for PLA-g-IAH; 0.5 wt % IAH (black curves), 5 wt % IAH (red curves), with CHE (solid curves), without CHE (dashed curves).

The effect of CHE during reactive modification was studied for reaction system PLA/IAH/L101 with $[IAH]_0 = 0.5$ and 5 wt %. $[L101]_0$ was in the range 0.1–2 wt %. Results of MFR test are shown in Figure 41. Generally, MFR values of samples with CHE are significantly lower compared to PLA-g-IAH without CHE. MFR of sample with 5 wt % of IAH reaches plateu at 1 wt % of added L101. Above this concentration MFR slightly decreases due to favoured crosslinking. PLA-g-IAH which was prepared by addition of 0.5 wt % of IAH exhibits slight increase of MFR with increasing $[L101]_0$. The reason of this phenomenon is the same as was shown in Figure 33c, (see chapter 5.5.4) for sample 0.5-2. It is clear for sample 0.5-2 with CHE where the run time was 3418 s compared to run time of 916 s for sample 0.5-2 without chain

extender. It can be assumed that both decrease of MFR and increase of run time (especially for 0.5-2) relates to increase of molecular weight and improved thermal stability.
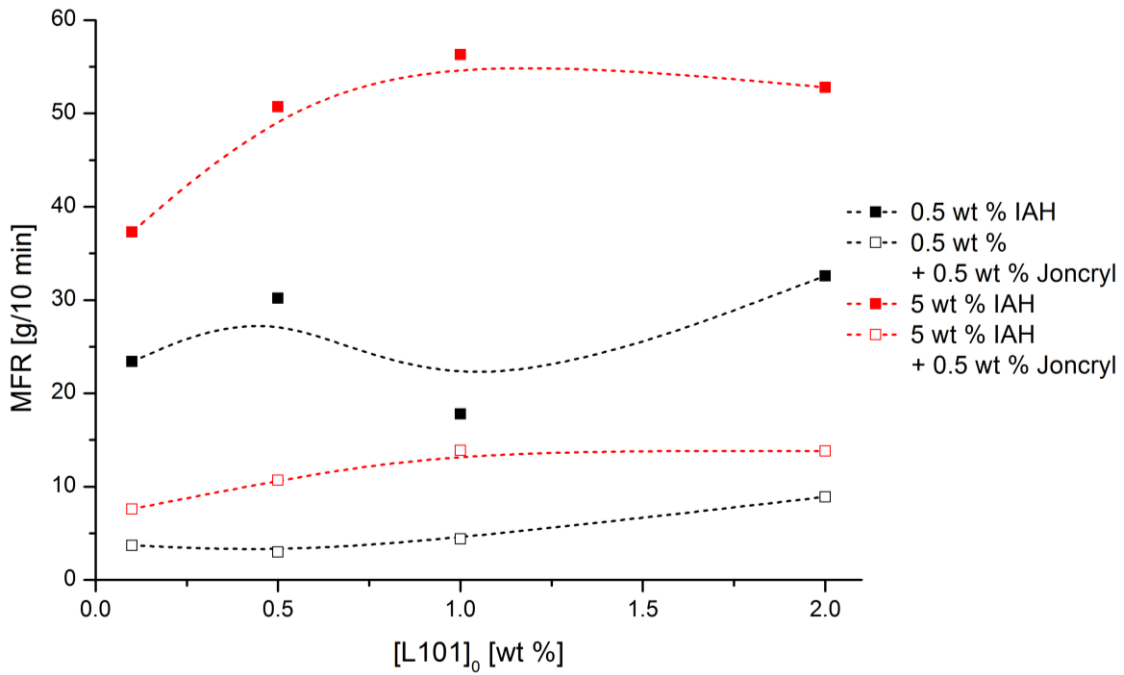
Figure 41. Influence of chain extending mechanism on MFR values for the PLA-g-IAH with constant [IAH]₀ (0.5 and 5 wt %) and various [L101]₀ (0.1–2 wt %).

5.8.3 Effect of chain extender on melt behavior

Capillary rheological test can be performed at different operation temperatures and different weight of load. Experimental data obtained by capillary rheometer provide flow curves suggesting the effect of reaction conditions on rheological behavior. Rheological behavior was study for PLA-g-IAH with 0.5 and 5 wt % of added IAH and 0.1–2 wt % of added L101. The effect of chain extender was also examined for samples prepared at the same reaction conditions.

Flow curve represents the relation between shear rate D and shear stress τ for given parameters of measurement. In this study, flow curves were derived from experimental data generated by capillary rheometer Ceast at constant temperature 190 °C and three different loads – 2.16, 3.8 and 5 kg.

If thermoplastics obey power-law behavior, then the relation between D and τ can be written as follows [120]:

$$\frac{4 \cdot Q}{\pi \cdot R^3} = \frac{4 \cdot \phi}{m + 3} \cdot \left(\frac{\Delta p \cdot R}{2 \cdot L} \right)^m \tag{32a}$$

$$\frac{\Delta p \cdot R}{2 \cdot L} = k \cdot \left(\frac{4 \cdot Q}{\pi \cdot R^3} \right)^n \tag{32b}$$

where Q is flow rate (m^3.s^{-1}), R is inner diameter of the capillary (m), ϕ represents flow coefficient (s^{-1}), m is index of flow behavior (-), k is consistency index, n equals to flow index, Δp is pressure gradient (Pa) and L is the length of capillary. Logarithmic form of Equation 32a gives rheological constants ϕ and m:

$$\log\left(\frac{4 \cdot Q}{\pi \cdot R^3} \right) = \log\left(\frac{4 \cdot \phi}{m + 3} \right) + m \cdot \log\left(\frac{\Delta p \cdot R}{2 \cdot L} \right) \tag{32c}$$

$$\log \frac{\Delta p \cdot R}{2 \cdot L} = \log k + n \cdot \left(\frac{4 \cdot Q}{\pi \cdot R^3} \right) \tag{32d}$$

Values of Q and Δp can be calculated from Equation 32c and 32d using parameters of capillary rheometer and output of measurement:

$$Q = \frac{V}{t} \tag{32e}$$

$$\Delta p = \frac{F}{S} \tag{32f}$$

where V (m^3) is the volume of extruded melt, t (s) is time of the melt extrusion, F (N) is the load of piston and S (m^2) is the surface of piston.

Flow curves of sample with 0.5 wt % of IAH is represented by plot between log D and log t in Figure 42. According to linear fitting rheological constants m and ϕ were determined. When log τ = 0 (τ = 1) then constant ϕ can be calculated from the increment of every single curve in Figure 42. As plot in Figure 42 was generated according to Equation 32c, reverse plot can be generated from Equation 32d giving constant k and n. Constants derived from Figure 42 and Figure 43 are summarized in Table 16. Finally, apparent viscosity and corrected viscosity were calculated from rheological constants by Equation 32g and 32h.

$$\eta_{apparent} = \frac{\tau}{D} = \frac{\Delta p \cdot \pi \cdot R^4}{8 \cdot L \cdot Q} \tag{32g}$$

$$\eta_{corrected} = \frac{1}{\phi} = \frac{\pi \cdot R^{m+3}}{(m + 3) \cdot 2^m \cdot L^m} \cdot \frac{\Delta p^m}{Q} \tag{32h}$$
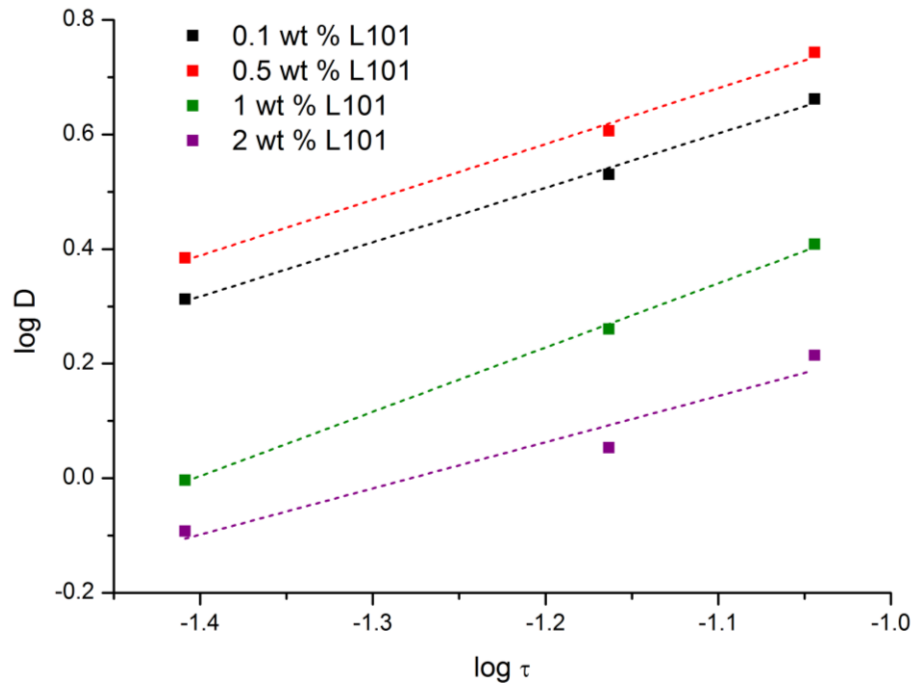
Figure 42. Flow curve as a relationship between log D and log τ for PLA-g-IAH prepared by the reaction with 0.5 wt % of IAH and various [L101]$_0$ – constants m and ϕ.
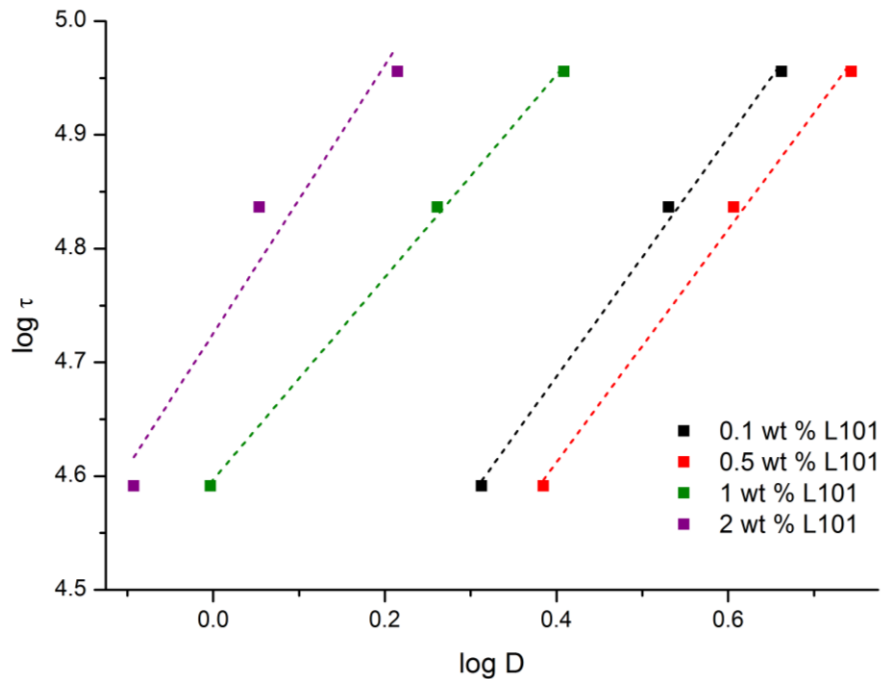
Figure 43. Flow curve as a relationship between log τ and log D for PLA-g-IAH prepared by the reaction with 0.5 wt % of IAH and various [L101]$_0$ – constants n and k.

Table 16. Rheological constants derived from flow curves.

Sample	m [-]	ϕ [s^{-1}]	$\phi_{0.1}$ [s^{-1}]	n [-]	k [10^{-4} Pa.s^n]	$\eta_{corrected}$ [10^{-4} Pa.s]
0.5-0.1	0.95	43.6	4.9	1.05	1.85	2.29
0.5-0.5	0.97	56.0	6.0	1.02	1.59	1.79
0.5-1	1.12	38.7	2.9	0.89	3.95	2.58
0.5-2	0.81	10.2	1.6	1.18	5.32	9.80
5-0.1	0.94	379.2	44.0	1.06	0.18	0.26
5-0.5	0.99	930.2	96.1	0.99	0.10	0.11
5-1	1.04	2060.5	187.7	0.95	0.07	0.05
5-2	1.08	1762.0	146.6	0.92	0.10	0.06
0.5-0.1-0.5J	1.54	118.8	3.4	0.64	4.88	0.84
0.5-0.5-0.5J	1.49	80.0	2.6	0.66	5.69	1.25
0.5-1-0.5J	0.93	16.6	2.0	1.08	4.74	6.02
0.5-2-0.5J	0.01	1.3	1.3	6.31	1.57	76.92
5-0.1-0.5J	1.81	598.8	9.4	0.55	3.21	0.17
5-0.5-0.5J	1.49	295.6	9.4	0.66	2.45	0.34
5-1-0.5J	1.81	1096.4	17.2	0.55	2.29	0.09
5-2-0.5J	1.56	458.1	12.7	0.64	2.12	0.22

Proposed theoretical introduction gives the relationship between index of flow behavior m and structure of tested material. The most intensive response of material on shear stress is detected for samples with high [IAH]$_0$ and low [L101]$_0$. At these conditions high extent of grafting reaction is expected in contrast with low probability of crosslinking. On the other hand high [L101]$_0$ at low [IAH]$_0$ leads to decrease of m. In the case of PLA-g-IAH without chain extender this phenomenon is caused by appearance of crosslinked chains, while the effect of chain entanglements can be expected for samples with chain extender.

Flow coefficient ϕ was calculated from Equation 41c where the last item (shear stress) equals to 1 (log $\tau = 0$). From experimental data and known constant m relation between material structure and ϕ was observed. Increase of [L101]$_0$ at any [IAH]$_0$ (except of 0.5 wt % of IAH with chain extender) leads to the increase of ϕ up to the limit value of [L101]$_0$ depending on [IAH]$_0$. For samples without chain extender this limit [L101] is 0.5 and 1 wt % for 0.5 and 5 wt % of IAH, respectively. It can be concluded that above 1 wt % of L101 crosslinking precedes undesired reactions leading to chain scission.

Flow index n represents the deviation from Newtonian behavior (n = 1) which is relevant for low shear stresses applied during MFR analysis. If n is below 1 then that rheological behavior is called as pseudoplastic (shear thinning). Material with this kind of behavior exhibits increasing viscosity with increasing stress. On the other hand, dilatant (shear thickening) behavior is characteristic by n above 1. This behavior is characteristic by decreasing viscosity with increasing stress. Table 16 introduces values of n PLA-g-IAH melt with respect to different reaction conditions. Generaly, it can be concluded that addition of chain extender leads to decrease of n and therefore more intensive pseudoplastic behavior of material can be predicted at shear stress applied within testing conditions. This kind of behavior is typical for the most of

polymer melts. Moreover, it is usually desired because of low energetic heftiness within processing by blending, extrusion, etc. Especially for samples with highest $[L101]_0$ (sample 0.5-2 and 0.5-2-0.5J), constant n reaches high value for lowest content of IAH. These values can be assigned to dilatant behavior. These experimental results can be explained by existence of long branched and crosslinked macromolecules with limited content of low molecular fractions. At higher shear stress there is enhanced friction between polymer chains which tends to change of rheological behavior as well as change of corrected viscosity. Corrected viscosity was calculated by Equation 41h using index of flow behavior m. In fact it means that thus corrected viscosity does not depend on the shear stress. Its highest value was reached for sample 0.5-2-0.5J where the effect of chain extender and side reactions are combined resulting in high corrected viscosity.

6. CONCLUSION

Functionalization of PLA with IAH was achieved by post-polymerization grafting technique performed in the melt by using discontinuous mixer. This method is generally considered as one of the most practical solvent-free method which can be applied for large-scale polymers including PLA.

Reaction temperature 190 °C was calculated according to Arrhenius equation for the reaction time 6 min. This temperature is convenient for radical grafting since: a) L101 was consumed in 5 min which was proved by calculation; b) melting temperature of PLA is at least 30 °C below proposed reaction temperature which allows complete melting; c) non-radical degradation of PLA is limited at temperature below 200 °C. Under these conditions, IAH was successfuly grafted onto PLA backbone which was proved by FTIR analysis. Since C=O groups of PLA exhibit strong absorption band which overlaps C=O vibrations of grafted moieties, peak normalization method proved increased integral area of absorption band centered at 1760 cm^{-1}. In addition, C=O vibrations characteristic for IAH (1780 and 1850 cm^{-1}) were distinguished in PLA/IAH blends with amount of IAH above 1 wt % which is higher than maximum grafting degree obtained. Grafted IAH was also detected by ^{1}H-NMR spectroscopy whereas chemical shift typical for IAH oligomers was not observed.

With regard to quantitative analysis, relationship between concentration of reactants and grafting yield was determined. Low $[IAH]_0$ and $[L101]_0$ resulted in relatively high reaction conversion and low extent of undesired reactions. On the other hand, high concentration of reactants increased both grafting degree and probability of side reactions while reaction conversion was too low. After 6 min of reaction period, reaction conversion did not increase when optimized reaction conditions were applied. At low reaction temperature, low concentration of primary radicals results in higher $k_g/k_t^{1/2}$ and low both initial grafting rate and reaction conversion. At high reaction temperature, recombination of primary radicals is favoured which causes lower $k_g/k_t^{1/2}$, higher initial grafting rate and termination of grafting within short reaction period.

Despite of presumption of many researchers, polymerization of IAH was observed under conditions used for grafting. Radical polymerization of IAH in the presence of L101 was simulated whereas p(IAH) was formed at different polymerization yield depending on IAH/L101 molar ratio. It was found that low IAH/L101 molar ratio relates to higher polymerization yield because of inhibition effect of allylic hydrogen located in IAH structure. IAH polymerization was also detected in the presence of PLA during grafting reaction. High $[IAH]_0$ and $[L101]_0$ allows higher extent of IAH-L101 interactions resulting in formation of p(IAH). Possibility of IAH polymerization was considered regarding enhanced thermal stability of acetone-soluble fractions and enhanced yellowness of PLA-g-IAH samples. Except of radical polymerization of IAH, self-induced polymerization was observed using DSC and DTA. The extent of self-induced polymerization was determined to be low due to simultaneous degradation and isomerization of IAH.

Modification of PLA with IAH influenced structure of prepared PLA-g-IAH. Decrease of T_g suggests higher mobility of PLA-g-IAH chains and higher content of free volume compared to neat PLA due to bulky anhydride ring. Decrease of T_{cc} reflects decrease of molecular weight

which in consistence with results obtained from SEC. Decrease of crystallinity and grafted IAH relates to enhanced biodegradability of PLA-g-IAH compared to neat PLA.

Except of radical chain scission, non-radical degradation of PLA was evidenced. Hydrolytic degradation was suppressed by addition of chain extender Joncryl ADR-4368 C. It was predicted that reactive functional groups of chain extender reacted with both end –COOH groups of PLA and –COOH groups of IAH. Function of chain extender was identified by change of melt behavior reflecting increase of molecular weight.

PLA modified with IAH can be used for seubsequent reactions with compounds reactive towards anhydride group. PLA-g-IAH with reactive anhydride group may act as polymer substrate for "grafting through" or undergo coupling during compatibilization of polymer blends or composite materials (see Figure 1, chapter 2.1). Potential of IAH polymerization in melt could be also interesting topic for further investigation of preparation rigid p(IAH) with enhanced thermal stability and high reactivity.

7. REFERENCES

[1] Fink, J. K.: *Reactive polymers: Fundamentals and applications – A concise guide to industrial polymers*. New York: William Andrew, Inc., 2005. 770 s. ISBN 0-8155-1515-4.

[2] Moad, G.: *The synthesis of polyolefin graft copolymers by reactive extrusion*. Progress in polymer science. 1999, vol. 24, no. 1, pp. 81–142. doi:10.1016/S0079-6700(98)00017-3.

[3] Bhattacharya, A.; Misra, B. N.: *Grafting: a versatile means to modify polymers. Techniques, factors and applications*. Prog. Polym. Sci. 2004, vol. 29, no. 8, pp. 767–814. doi:10.1016/j.progpolymsci.2004.05.002.

[4] Cobo, I., Li, M., Sumerlin, B.S., Perrier, S.: *Smart hybrid materials by conjugation of responsive polymers to biomacromolecules*. Nature Materials. 2015, vol. 14, no. 2, pp. 143–159. DOI: 10.1038/nmat4106.

[5] Bhattacharya, A., Ray, P.: *Polymer grafting and crosslinking*. New Jersey: John Wiley & Sons, Inc., 2009. 341 s. ISBN 978-0-470-40465-2.

[6] Xanthos, M.: *Reactive extrusion: Principles and practice*. Hanser, Mnichov, 1992, 1st edition.

[7] Lambla, M.: *Reractive extrusion: A new tool for the diversification of polymeric materials*. Macromolecular Symposia. 1994, vol. 83, no. 1, pp. 37–48. doi: 10.1002/masy.19940830107

[8] Antonovskii, V. L.: *Initiating and cross-linking ability of organic peroxides: Chemical kinetic methods for the determination. Kinetics and catalysis*. 2003, vol. 44, no. 1, pp. 54–73. doi: 10.1023/A:1022568601041

[9] Al-Malaika, S.: *Reactive modifiers for polymers*. London: Blackie Academic & Professional, 1997. 400 s. ISBN 0-7514-0265-6.

[10] Denisov, E. T., Denisova, T. G., Pokidova, T. S.: *Handbook of free radical initiators*. New Jersey: John Wiley & Sons, Inc., 2003, 879 s. ISBN 0-471-20753-5.

[11] Berzin, F., Vergnes, B.: *Modeling of peroxide initiated controlled degradation of polypropylene in twin screw extruder*. Polymer engineering and science. 2000, vol. 40, no. 2. pp. 344–356. doi: 10.1002/pen.11168.

[12] Akbar, S., Beyou, E., Cassagnau, P., Chaumont, P., Farzi, G.: *Radical grafting of polyethylene onto MWCNTs: A model compound approach*. Polymer. 2009, vol. 50, no. 12, pp. 2535–2543. doi: 10.1016/j.polymer.2009.03.056.

[13] Lamb, D., Anstey, J.F., Fellows, C.M., Monteiro, J.M., Gilbert, R.G.: *Modification of natural and artificial polymer colloids by "topology-controlled" emulsion polymerization*. Biomacromolecules. 2001, vol. 2, no. 2, pp. 518–525. DOI: 10.1021/bm005654e.

[14] Seakins, P.W., Pilling, M.J., Niiranen, J.T., Gutman, D., Krasnoperov, L.N.: Kinetics and thermochemlstry of $R + HBr \leftrightarrow RH + Br$ reactions: determinations of the heat of formation of C_2H_5, i-C_3H_7, sec-C_4H_9, and t-C_4H_9. Journal of polymer chemistry. 1992. vol. 96, no. 24. pp. 9847–9855. doi: 10.1021/j100203a050

[15]   Bhattacharyya, S. N., Maltas, D.: *Graft copolymerization onto cellulosis*. Progress in polymer science. 1984, vol. 10, issues 2–3, pp. 171–270. doi:10.1016/0079-6700(84)90002-9.

[16]   Russell, G.T., Gilbert, R.G. and Napper, D.H.: *Chain-length-dependent termination rate processes in free-radical polymerizations. 1. Theory*. Macromolecules. 1992, vol. 25, no. 9, pp. 2459–2469. DOI: 10.1021/ma00035a026.

[17]   Heuts, J.P.A., Russell, G.T., Smith, G.B., Herk, A.M.: *The Importance of Chain-Length Dependent Kinetics in Free-Radical Polymerization: A Preliminary Guide*. Macromolecular Symposia. 2007, vol. 248, no. 1, pp. 12–22. DOI: 10.1002/masy.200750202.

[18]   Gilbert, R.G.: *Emulsion polymerization: A mechanistic approach*. Polymer. 1997, vol. 38, no. 10, pp. 2577–2578. doi:10.1016/S0032-3861(96)01078-6.

[19]   Ng, L.-T., Garnett, J.L., Zilic, E., Nguyen, D.: *Effect of monomer structure on radiation grafting of charge transfer complexes to synthetic and naturally occurring polymers*. Radiation Physics and Chemistry. 2001, vol. 62, no. 1, pp. 89–98. doi:10.1016/S0969-806X(01)00425-X.

[20]   Cardona, F., George, G.A., Hill, D.J.T., Rasoul, F., Maeji, J.:*Copolymers obtained by the radiation-induced grafting of styrene onto poly (tetrafluoroethylen-co-perfluoropropylvinyl ether) substrates. 1. Preparation and structural investigation*. Macromolecules. 2002, vol. 35, no. 2, pp. 355–364. DOI: 10.1021/ma0022295.

[21]   Sakurai, H., Shiotani, M., Yahiro, H.: *Graft copolymerization of methylmethacrylate onto poly (tetrafluoroethylene): an ESR and XPS study on crystallinity dependence*. Radiation physics and chemistry. 1999, vol. 56, no. 3, pp. 309–313. doi:10.1016/S0969-806X(99)00292-3.

[22]   Ibrahem, A. A., Nada, A. M. A.: *Grafting of acrylamide onto partially acetylated and carboxymethylated cellulos*e. Acta polymerica. 1986, vol. 37, no. 5, pp. 320–322. DOI: 10.1002/actp.1986.010370516.

[23]   Okieimen, F. E., Idehen, K. I.: *Note graft copolymerization of methyl methacrylate on thiolated holocellulose*. Journal of macromolecular science: Part A – Chemistry. 1987, vol. 24, no. 11, pp. 1381–1384. DOI:10.1080/00222338708076953.

[24]   Nakanuta, S., Yoshikawa, E., Matsuzuki, K.: *Graft copolymerization of styrene onto cellulose acetate p-nitrobenzoate by chain transfer reaction*. Journal of applied polymer science. 1980, vol. 25, no. 9, pp. 1833–1837. DOI: 10.1002/app.1980.070250903.

[25]   Bremner, T., Rudin, A.: *Modification of high density polyethylene by reaction with dicumyl peroxide*. Plastics and rubber processing and applications. 1990, vol. 13, no. 1, pp. 61–66.

[26]   Bremner, T., Rudin, A., Haridoss, S.: *Effects of polyethylene molecular structure on peroxide crosslinking of low density polyethylene*. Polymer engineering and science. 1992, vol. 32, no. 14, pp. 939–943. DOI: 10.1002/pen.760321405.

[27]   Lachtermacher, M. G., Rudin, A.: *Reactive processing of LLDPES in corotating intermeshing twin-screw extruder. II. Effect of peroxide treatment on processability*.

Journal of applied polymer science. 1995, vol. 58, no. 13, pp. 2433–2449. DOI: 10.1002/app.1995.070581311.

[28] Suwanda, D., Balke, S. T.: *The reactive modification of polyethylene. II: Mathematical modeling*. Polymer engineering science. 1993, vol. 33, no. 24, pp. 1585–1591. DOI: 10.1002/pen.760332403.

[29] Smedberg, A., Hjertberg, T., Gustaffson, B.: *Crosslinking reactions in an unsaturated low density polyethylene*. Polymer. 1997, vol. 38, no. 16, pp. 4127–4138. doi:10.1016/S0032-3861(96)00994-9.

[30] Clark, D.C., Baker, W.E., Whitney, R.A.: *Peroxide-initiated comonomer grafting of styrene and maleic anhydride onto polyethylene: Effect of polyethylene microstructure*. Journal of Applied Polymer Science. 2001, vol. 79, no. 1, pp. 96–107. DOI: 10.1002/1097-4628(20010103)79:1<96::AID-APP120>3.0.CO;2-X.

[31] Tyuganova, M.A., Galbraikh, L.S., Ulmasove, A.A., Tsarevskaya, I.Y., Khidoyator, A.A.: *Use of rice straw as cellulosic raw material for ion exchanger production*. Cellulose Chemistry and Technology. 1985, vol. 19, no. 5, pp. 557–568.

[32] Roover, B. D., Sclavons, M., Carlier, V., Devaux, J., Legras, R., Momtaz, A.: *Molecular characterization of maleic anhydride-functionalized polypropylene*. Journal of polymer science: Part A: Polymer chemistry. 1995, vol. 33, no. 5, pp. 829–842. DOI: 10.1002/pola.1995.080330509.

[33] De Roover, B., Devaux, J., Legras, R.: *Maleic anhydride homopolymerization during melt functionalization of isotactic polypropylene*. Journal of polymer science: Part A: Polymer chemistry. 1996, vol. 34, no. 7, pp. 1195–1202. DOI: 10.1002/(SICI)1099-0518(199605)34:7<1195::AID-POLA5>3.0.CO;2-2.

[34] Bettini, S. H. P., Agnelli, J. A. M.: *Grafting of maleic anhydride onto polypropylene by reactive processing. I. Effect of maleic anhydride and peroxide concentrations on the reaction*. Journal of applied polymer science. 1999, vol. 74, no. 2, pp. 247–255. DOI: 10.1002/(SICI)1097-4628(19991010)74:2<247::AID-APP2>3.0.CO;2-A.

[35] García-Martínez, J. M., Laguna, O., Collar, E. P.: *Chemical modification of polypropylenes by maleic anhydride: Influence of stereospecificity and process conditions*. Journal of applied polymer science. 1998, vol. 68, no. 3, pp. 483–495. DOI: 10.1002/(SICI)1097-4628(19980418)68:3<483::AID-APP14>3.0.CO;2-W.

[36] Romero, M. A., Domard, A.: *Physicochemical characterization of polypropylene films grafted by poly(acrylic acid): 2*. Polymer. 1994, vol. 35, no. 24, pp. 5342–5348. doi:10.1016/0032-3861(94)90488-X.

[37] Dogué, L. J., Mermilliod, N., Gandini, A.: *Modification of industrial polypropylene film by grafting of poly(acrylic acid)*. Journal of applied polymer science. 1995, vol. 56, no. 1, pp. 33–40. DOI: 10.1002/app.1995.070560105.

[38] Vainio, T., Hu, G-H., Lambla, M., Seppala, J.V.: *Functionalized polypropylene prepared by melt free radical grafting of low volatile oxazoline and its potential in compatibilization of PP/PBT blends*. Journal of applied polymer science. 1996, vol. 61, no. 5, pp. 843–852. DOI: 10.1002/(SICI)1097-4628(19960801)61:5<843::AID-APP17>3.0.CO;2-Y.

[39]   Vainio, T., Hu, G-H., Lambla, M., Seppala, J.V.: *Functionalization of polypropylene with oxazoline and reactive blending of PP with PBT in a corotating twin-screw extruder.* Journal of applied polymer science. 1997, vol. 63, no. 7, pp. 883–894. DOI: 10.1002/(SICI)1097-4628(19970214)63:7<883::AID-APP8>3.0.CO;2-M.

[40]   Antilla, U., Vocke, C., Seppälä, J.: *Functionalization of polyolefins and elastomers with an oxazoline compound.* 1999, vol. 72, no. 7, pp. 877–885. DOI: 10.1002/(SICI)1097-4628(19990516)72:7<877::AID-APP3>3.0.CO;2-6.

[41]   Pesetskii, S.S., Jurowski, B., Krivoguy, Y.M., Kelar, K.: *Free-radical grafting of itaconic acid onto LDPE by reactive extrusion: I. Effect of initiator solubility.* Polymer. 2001, vol. 42, no. 2, s. 469–475. doi:10.1016/S0032-3861(00)00356-6

[42]   Rätzsch, M., Bucka, H., Ivanchev, S.S., Mesh, A.M., Khaikine: *Some peculiar features of radiation grafting of monomers of various structures and reactivities onto polyolefines.* Journal of applied polymer science. 2000, vol. 77, no. 4, pp. 711–718. DOI: 10.1002/(SICI)1097-4628(20000725)77:4<711::AID-APP1>3.0.CO;2-Y.

[43]   Naguib, H.F., Aly, R.O., Sabaa, M.W., Mokhtar, S.M.: *Gamma radiation induced graft copolymerization of vinylimidazole-acrylic acid onto polypropylene films.* Polymer Testing. 2003, vol. 22, no. 7, pp. 825–830. DOI: 10.1016/S0142-9418(03)00018-7.

[44]   Misra, B.N., Sharma, R.K., Mehta, I.K.: *Grafting onto wool. XV. Graft copolymerization of MA and MMA by use of Mn(acac)₃ as initiator.* Journal of Macromolecular Science. Chemistry A. 1982, vol. 17, no. 3, pp. 489–500. DOI: 10.1080/00222338208056486.

[45]   Bhattacharya, A., Das, A., De, A.: *Structural influence on grafting of acrylamide based monomers on cellulose acetate.* Indian journal of chemical technology. 1998, vol. 5, no. 3, pp. 135–138.

[46]   Varma, D.S., Narashinan, V.: *Thermal behavior of graft copolymers of cotton cellulose and acrylate monomers.* Journal of Applied Polymer Science. 1972, vol. 16, no. 12, pp. 3325–3339. DOI: 10.1002/app.1972.070161222.

[47]   Huang, N. J., Sundberg, D. C.: *Fundamental studies of grafting reactions in free radical copolymerization. I. A detailed kinetic model for solution polymerization.* Journal of polymer science Part A: Polymer chemistry. 1995, vol. 33, no. 15, pp. 2533–2549. DOI: 10.1002/pola.1995.080331502.

[48]   Tsavalas, J. G., Luo, Y., Schork, F. J.: *Grafting mechansims in hybrid miniemulsion polymerization.* Journal of applied polymer science. 2003, vol. 87, no. 11, pp. 1825–1836. DOI: 10.1002/app.11916.

[49]   Spencer, M., Parent, J.S., Whitney, R.A.: *Composition distribution in poly(ethylene-graft-vinyltrimethoxysilane).* Polymer. 2003, vol. 44, no. 7, pp. 2015–2023. DOI:10.1016/S0032-3861(03)00085-5.

[50]   Gaylord, N.G., Mehta, M.: *Role of homopolymerization in the peroxide-catalyzed reaction of maleic anhydride and polyethylene in the absence of solvent.* Journal of Polymer Science: Polymer Letters Edition. 1982, vol. 20, no. 9, pp. 481–486. DOI: 10.1002/pol.1982.130200903.

[51]   Kaur, I., Misra, B.N., Gupta, A., Chauhan, G.S.: *Graft copolymerization of 4-vinyl pyridine and methyl acrylate onto polyethylene film by radiochemical method*. Journal of Applied Polymer Science. 1998, vol. 69, no. 3, pp. 599–610. DOI: 10.1002/(SICI)1097-4628(19980718)69:3<599::AID-APP20>3.0.CO;2-N.

[52]   Sun, T., Xu, P., Liu, Q., Xue, J., Xie, W.: *Graft copolymerization of methacrylic acid onto carboxymethyl chitosan*. European Polymer Journal. 2003, vol. 39, no. 1, pp. 189–192. DOI:10.1016/S0014-3057(02)00174-X.

[53]   Moad, G., Solomon, D.H.: *The Chemistry of Radical Polymerization*. Elsevier. 2005, 665 pages, ISBN 0080454798.

[54]   Bray, T., Damiris, S., Grace, A., Moad, G., O'Shea, M., Rizzardo, E., Van Diepen, G.: Developments in the synthesis of maleated polyolefins by reactive extrusion. Macromolecular Symposia. 1998, vol. 129, no. 1, pp. 109–118. DOI: 10.1002/masy.19981290110.

[55]   Tang, F., Huyser, E. S.: Thermal decomposition of bifunctional peroxides. Journal of Organic Chemistry. 1977, vol. 42, no. 12, 2160–2163. DOI: 10.1021/jo00432a031.

[56]   Misra, B. N., Jassal, J. K., Pande, C. S.: *Grafting onto cellulose. Part II. AIBN and BPO initiated grafting of poly(vinyl acetate)*. Journal of Polymer Science. 1978, vol. 16, no. 1. pp. 295–297. doi: 10.1002/pol.1978.170160127.

[57]   Prasoetsopha, N., Chumsamrong, P., Suppakarn, N.: *Effects of type and concentration of initiator on grafting of acrylic monomer onto depolymerized natural rubber*. Advanced Materials Research. 2011, vol. 264–265, pp. 565–570.

[58]   Zytowski, T., Fischer, H.: *Absolute Rate Constants and Arrhenius Parameters for the Addition of the Methyl Radical to Unsaturated Compounds: The Methyl Affinities Revisited*. Journal of the American Chemical Society. 1997, vol. 119, no. 52,, pp. 12869–12878. DOI: 10.1021/ja973128y.

[59]   Hu, G.H., Sun, Y.J., Lambla, M.: Devolatilization: *A critical sequential operation for in situ compatibilization of immiscible polymer blends by one-step reactive extrusion*. Polymer Engineering Science. 1996, vol. 36, no. 5, pp. 676–684. DOI: 10.1002/pen.10455.

[60]   Samay, G., Nagy, T., White, J. L.: *Grafting maleic-anhydride and comonomers onto polyethylene*. Journal of applied polymer science. 1995, vol. 56, no. 11, pp. 1423–1433. DOI: 10.1002/app.1995.070561105.

[61]   Li, Y., Xie, X. M., Guo, B. H.: *Study on styrene-assisted melt free-radical grafting of maleic anhydride onto polypropylene*. Polymer. 2001, vol. 42, no. 8, pp. 3419–3425. doi:10.1016/S0032-3861(00)00767-9.

[62]   Cartier, H., Hu, G. H.: *Styrene-assisted melt free radical grafting of glycidyl methacrylate onto polypropylene*. Journal of polymer science Part A: Polymer chemistry. 1998, vol. 36, no. 7, pp. 1053–1063. DOI: 10.1002/(SICI)1099-0518(199805)36:7<1053::AID-POLA3>3.0.CO;2-3.

[63]   Augier, S., Coiai, S., Gragnoli, T., Passaglia, E., Pradel, J.L., Flat, J.J.: *Coagent assisted polypropylene radical functionalization: monomer grafting modulation and molecular*

weight conservation. Polymer. 2006, vol. 47, no. 15, pp. 5243–5252. doi:10.1016/j.polymer.2006.05.049.

[64] Chaudhary, B.I., Chopin, L., Klier, J.: *Nitroxyls for scorch suppression, cure control, and functionalization in free-radical crosslinking of polyethylene*. Polymer Engineering Science. 2007, vol. 47, no. 1, pp. 50–61. DOI: 10.1002/pen.20664.

[65] Anbarasan, R., Babout, O., Degueil, M., Maillard, B.: *Munctionalization and cross-linking of high-density polyethylene in the presence of dicumyl peroxide - An FTIR study*. Journal of Applied Polymer Science. 2005, vol. 97, no. 3, pp. 766–774. DOI: 10.1002/app.21343.

[66] Gaylord, N.G., Mehta, R.: *Peroxide-catalyzed grafting of maleic anhydride onto molten polyethylene in the presence of polar organic compounds*. Journal of Polymer Science Part A: Polymer Chemistry. 1988 vol. 26, no. 4, pp. 1189–1198. DOI: 10.1002/pola.1988.080260419.

[67] Gaylord, N.H., Mehta, R., Kumar, V., Tazi, M.: *High density polyethylene-g-maleic anhydride preparation in presence of electron donors*. Journal of Applied Polymer Science. 1989, vol. 38, no. 2, pp. 359–371. DOI: 10.1002/app.1989.070380217.

[68] Dilli, S., Garnett, J.L.: *Radiation induced reactions with cellulose. III. Kinetics of styrene copolymerisation in methanol*. Journal of Applied Polymer Science. 1967, vol. 11, no. 6, pp. 859–870. DOI: 10.1002/app.1967.070110608.

[69] Samal, S., Sahu, G., Lenka, S., Nayak, P.L.: Photoinduced graft copolymerization. XI. Graft copolymerization of methyl methacrylate onto silk using isoquinoline-sulphur dioxide charge transfer complex as the initiator. Journal of Applied Polymer Science. 1987, vol. 33, no. 5, pp. 1853–1858. DOI: 10.1002/app.1987.070330538.

[70] Sun, T., Xu, P., Liu, Q., Xue, J., Xie, W.: *Graft copolymerization of methacrylic acid onto carboxymethyl chitosan*. European Polymer Journal. 2003, vol. 39, no. 1, pp. 189–192. DOI: 10.1016/S0014-3057(02)00174-X.

[71] Sacak, M., Pulat, E.: *Benzoyl peroxide initiated graft copolymerization of poly(ethylene terephthalate) fibers with acrylamide*. Journal of Applied Polymer Science. 1989, vol. 38, no. 3, pp. 539–546. DOI: 10.1002/app.1989.070380313.

[72] Sanli, O., Pulat, E.: *Solvent assisted graft copolymerization of acrylamide on poly(ethylene terephthalate)films using benzoyl peroxide initiator*. Journal of Applied Polymer Science. 1993, vol. 47, no. 1, pp. 1–6. DOI: 10.1002/app.1993.070470101.

[73] Schamberg, E., Hoigne, J.: *Radical and radiation-induced grafting of some synthetic high polymers within the temperature range of their glass transition*. Journal of Polymer Science Part A: Polymer Chemistry. 1970, vol. 8, no. 3, pp. 693–698. DOI: 10.1002/pol.1970.150080312.

[74] Garlotta, D.: *A literature review of poly(lactic acid)*. Journal of polymers and the environment. 2002, vol. 9, no. 2, pp. 63–84. DOI: 10.1023/A:1020200822435.

[75] Mani, R., Bhattacharya, M., Tang, J.: *Functionalization of polyesters with maleic anhydride by reactive extrusion*. Journal of polymer science: Part A: Polymer chemistry.

1999, vol. 37, no. 11, pp. 1693–1702. DOI: 10.1002/(SICI)1099-0518(19990601)37:11<1693::AID-POLA15>3.0.CO;2-Y.

[76] Carlson, D., Dubois, P., Nie, L.,Narayan, R.: *Free radical branching of polylactide by reactive extrusion*. Polymer engineering and science. 1998, vol. 38, no. 2, pp. 311–321. DOI: 10.1002/pen.10192.

[77] Ramkumar, D.H.S., Bhattacharya, M., Vaidya, U.R.: *Properties of injection moulded starch/synthetic polymer blends - II. Evaluation of mechanical properties*. European Polymer Journal. 1997, vol. 33, no. 5, pp. 729–742. doi:10.1016/S0014-3057(96)00216-9.

[78] John, J., Tang, J., Yang, Z., Bhattacharya, M.: *Synthesis and characterization of anhydride-functional polycaprolactone*. Journal of Polymer Science Part A: Polymer Chemistry. 1997, vol. 35, no. 6, pp. 1139–1148. DOI: 10.1002/(SICI)1099-0518(19970430)35:6<1139::AID-POLA17>3.0.CO;2-7.

[79] Mani, R., Bhattacharya, M.: *Properties of injection moulded blends of starch and modified biodegradable polyesters*. European Polymer Journal. 2001, vol. 37, no. 3, pp. 515–526. doi:10.1016/S0014-3057(00)00155-5.

[80] Pan, J.; Wang, Y., Qin, S., Zhang, B., Luo, Y.: *Grafting reaction of poly($_{D,L}$)lactic acid with maleic anhydride and hexanediamine to introdukce more reactive groupy in its bulk*. Applied biomaterials. 2005, vol. 74, no. 1, pp. 476–480. DOI: 10.1002/jbm.b.30208.

[81] Carlson, D., Nie, L., Narayan, R., Dubois, P.: *Maleation of polylactide (PLA) by reactive extrusion*. Journal of applied polymer science. 1999, vol. 72, no. 4, pp. 477–485. DOI: 10.1002/(SICI)1097-4628(19990425)72:4<477::AID-APP3>3.0.CO;2-Q.

[82] Hwang, S. W., Lee, S.B., Lee, Ch.K., Lee, J.Y., Shim, J.K., Selke, S.E.M., Soto-Valdez, H., Matuana, L., Rubino, M., Auras, R.: *Grafting of Maleic Anhydride on Poly(L-lactic acid): Effects on Physical and Mechanical Properties*. Polymer Testing. 2012, vol. 31, no. 2, pp. 333–344. doi:10.1016/j.polymertesting.2011.12.005.

[83] Plackett, D.: *Maleated polylactide as an interfacial compatibilizer in biocomposites*. Journal of polymers and the environment. 2004, vol. 12, no. 3, pp. 131–138. DOI: 10.1023/B:JOOE.0000038544.75554.0e.

[84] Zhang, J. F., Sun, X.: *Mechanical properties of poly(lactic acid)/starch composites compatibilized by maleic anhydride*. Biomacomolecules. 2004, vol. 5, no. 4, pp. 1446–1451. DOI: 10.1021/bm0400022.

[85] Rezgui, F., G'Sell, C., Dahoun, A., Hiver, J.M., Sadoun, T.: *Plastic deformation of low-density polyethylene reinforced with biodegradable , part 1: Microstructural analysis and tensile behavior at konstant true strain-rate*. Polymer engineering and science. 2011, vol. 51, no. 1, pp. 117–125. DOI: 10.1002/pen.21797.

[86] Reddy, N., Nama, D., Yang, Y.: *Polylactic acid/polypropylene polyblend fibres for better resistence to degradation*. Polymer Degradation and Stability. 2008, vol. 93, no. 1, pp. 233–241. doi:10.1016/j.polymdegradstab.2007.09.005.

[87] Singh, G., Bhunia, H., Rajor, A., Jana, R.N., Choudhary, V.: *Mechanical properties and morfology of polylactide, linear low-density polyetylene and their blends*. Journal of applied polymer science. 2010, vol. 118, no. 1, pp. 496–502. DOI: 10.1002/app.32305.

[88]   Al-Itry, R., Lamnawar, K., Maazouz, A.: *Improvement of thermal stability, rheological and mechanical properties of PLA, PBAT and their blends by reactive extrusion with functionalized epoxy*. Polymer degradation and stability. 2012, vol. 97, no. 10, pp. 1898–1914. DOI 10.1016/j.polymdegradstab.2012.06.028.

[89]   Signori, F., Coltelli, M.B., Bronco, S.: *Thermal degradation of poly(lactic acid) (PLA) and poly(butylene adipate-co-terephthalate) (PBAT) and their blends upon melt processing*. Polymer Degradation and Stability. 2009, vol. 94, no. 1, pp. 74–82. doi:10.1016/j.polymdegradstab.2008.10.004.

[90]   Cao, M., Durant, Y.: *Polymerization of poly (itaconic acid)*. Polymer preprints. 2007, vol. 48, no. 2, 886–887.

[91]   Shang, S., Huang, S.J., Weiss, R.A.: *Synthesis and characterization of itaconic anhydride and stearyl methacrylate copolymers*. Polymer. 2009, vol. 50, no. 14, pp. 3119–3127. doi:10.1016/j.polymer.2009.05.012.

[92]   Yokota, K., Hirabayashi, T., Takashima, T.: *Preparation of poly(itaconic acid)*. Die Makromolekulare Chemie. 1975, vol. 176, no. 5, pp. 1197–1205. doi: 10.1002/macp.1975.021760501.

[93]   Otsu, T., Yang, J-Z.: *Radical polymerization of itaconic anhydride and reactions of the resulting polymers with amines and alcohols*. Polymer international. 1991, vol. 25, no. 4, pp. 245–251. DOI: 10.1002/pi.4990250408.

[94]   Domenichelli, I., Coiai, S., Cicogna, F., Pinzino, C., Passaglia, E.: *Towards a better control of the radical functionalization of poly(lactic acid)*. Polymer International. 2015, vol. 64, no. 5, pp. 631–640. DOI: 10.1002/pi.4799.

[95]   Karst, D., Yang, Y.: *Using the solubility parameter to explain disperse dye sorption on polylactide*. Journal of Applied Polymer Science. 2000, vol. 96, no. 2, pp. 416–422. DOI: 10.1002/app.21456.

[96]   Fischer, E. W., Sterzel, H. J., Wenger, G.: *Investigation of the structure of solution grown crystals of lactide copolymers by means of chemical reactions*. Kolloid-Zeitschrift und Zeitschrift für Polymere. 1973. vol. 251, no. 11, pp. 980–990. DOI: 10.1007/BF01498927.

[97]   Passaglia, E, Siciliano, P., Ciardelli, F., Maschio, G.: *Kinetics of the free radical grafting of diethyl maleate onto linear polyethylene*. Polymer International. 2000, vol. 49, no. 9, pp. 949–952. DOI: 10.1002/1097-0126(200009)49:9<949::AID-PI403>3.0.CO;2-R.

[98]   Atofina Chemical Inc. Organic Peroxides. U.S.A: Technical Data. 2001.

[99]   Fukuoka, T.: *Numerical analysis of a reactive extrusion process. Part I: Kinetics study on grafting of vinylsilane to polyethylene*. Polymer Engineering and Science 2000, vol. 40, no. 12, pp. 2511–2523. DOI: 10.1002/pen.11382.

[100] Cha, J., White, J. L.: *Maleic anhydride modification of polyolefin in an internal mixer and a twin-screw extruder: Experiment and kinetic model*. Polymer Engineering and Science. 2001, vol. 41, no. 7, pp. 1227–1237. DOI: 10.1002/pen.10824.

[101] Zmeškal, O., Čeppan, M., Dzik, P.: *Barevné prostory a správa barev*. Published in Barevné prostory a správa barev (10/2002) [online]. Brno : Fakulta chemická, Vysoké

učení technické v Brně, 2002 [cit. 2011-05-14]. Available at: <http://www.fch.vutbr.cz/lectures/imagesci/download/stud06_rozn02.pdf>.

[102] Ohta, N., Robertson, A.: *Colorimetry: Fundamentals and applications*. Wiley; 1st edition 2005. 350 pages. ISBN: 978-0-470-09472-3.

[103] Heinen, W., Rosenmöller, C.H., Wenzel, C.B., de Groot, H.J.M., Lugtenburg, J., van Duin, M.: *^{13}C NMR Study of the Grafting of Maleic Anhydride onto Polyethene, Polypropene, and Ethene−Propene Copolymers*. Macromolecules. 1996, vol. 29, no. 4, pp. 1151–1157. DOI: 10.1021/ma951015y.

[104] Russell, K.E., Kelusky, E.C.: *Grafting of maleic anhydride to n-eicosane*. Journal of Polymer Science Part A: Polymer Chemistry. 1988, vol. 26, no. 8, pp. 2273–2280. DOI: 10.1002/pola.1988.080260821.

[105] Rice, F.O., Murphy, M.T.: The Thermal Decomposition of Five-Membered Rings. Journal of the american chemical society. 1942, vol. 64, no. 4, pp. 896–899. DOI: 10.1021/ja01256a046.

[106] Katime, I., Madoz, A., Velada, J. L.: *The kinetics of bulk polymerization of itaconate derivates. Part 2. Diphenyl, dibenzyl and di-2-phenylethyl itaconates*. Thermochim. Acta. 1993, vol. 220, pp. 91–101. DOI: 10.1016/0040-6031(93)80457-L.

[107] Milovanovic, M.B., Trifunovic, S., Katsikas, L., Popovic, I.G.: Preparation and modification of itaconic anhydride-methyl methacrylate copolymers. Journal of the Serbian chemical society. 2007, vol. 72, no. 12, pp. 1507–1514. doi:10.2298/JSC0712507M.

[108] Velada, J.L., Hernáez, E., Cesteros, L.C., Katime, I.: A study of the thermal degradation of several poly(monoalkylaryl itaconates). Polymer Degrdation and Stability. 1996, vol. 52, no. 3, pp. 273–282. doi:10.1016/0141-3910(96)00008-0.

[109] Ishida S, Saito S.: Polymerization of itaconic acid derivatives. Journal of Polymer Science, Part A-1: Polymer Chemistry. 1967, vol. 5, no. 4, pp. 689–705. DOI: 10.1002/pol.1967.150050401.

[110] Nagai, S.: The polymerization and polymer sof itaconic acid derivates. VI. The polymerization and copolymerization of itaconic anhydride. 1964, vol. 37, no. 3, pp. 369–373. DOI: 10.1246/bcsj.37.36.

[111] Luo, Y., Wang, Y., Niu, X., Fu, Ch., Wang, S.: *Synthesis, characterization and biodegradation of butanediamine-grafted poly($_{DL}$-lactic acid)*. European polymer journal. 2007, vol. 43, no. 9, pp. 3856–3864. doi:10.1016/j.eurpolymj.2007.06.022.

[112] Wu, X. S., Wang, N.: *Synthesis, characterization, biodegradation and drug delivery application of biodegradable lactic/glycolic acid polymers. Part II: Biodegradation.* Journal of biomaterial science polymer edition. 2001, vol. 12, no. 1, pp. 21–34. DOI:10.1163/156856201744425.

[113] Tábi, T., Sajó, I.E., Szabó, F., Luyt, A.S., Kovács, J.G.: *Crystalline structure of annealed polylactic acid and its relation to processing*. eXPRESS polymer letters. 2010, vol. 4, no. 10, pp. 659–668. DOI: 10.3144/expresspolymlett.2010.80.

[114] Fakirov, S.: *Biodegradable polyesters*. John Wiley & Sons, 2015. ISBN 3527330860.

[115] Solarski, S., Ferreira, M., Deavux, E.: *Characterization of thermal properties of PLA fibers by modulated differential scanning calorimetry*. Polymer. 2005, vol. 46, no. 25, pp. 11187–11192. doi:10.1016/j.polymer.2005.10.027.

[116] Wang, L., Jing, X., Cheng, H., Hu, X., Yang, L., Huang, Y.: *Blends of linear and long- chain branched poly(L-lactide)s with high melt strength and fast crystallization rate*. Industrial and Engineering chemistry research. 2012, vol. 51, no. 30, pp. 10088–10099. DOI: 10.1021/ie300526u.

[117] Yang, S., Wu, Z-H., Yang, W., Yang, M-B.: *Thermal and mechanical properties of chemical crosslinked polylactide (PLA)*. Polymer testing. 2008, vol. 27, no. 8, pp. 957–963. doi:10.1016/j.polymertesting.2008.08.009.

[118] Japon, S., Luciani, A., Nguyen, Q. T., Leterrier, Y., Mánson, J-A E.: *Molecular characterization andrheological properties of modified poly(ethylene terephthalate) obtained by reactive extrusion*. Journal of Polymer Science. 2001, vol. 41, no. 8, pp. 1299–1309. DOI: 10.1002/pen.10830.

[119] Ibrahim, N. A., Hadithon, K. A., Abdan, K.: *Effect of fiber treatment on mechanical properties of kenaf fiber-ecoflex composites*. Journal of reinforced plastics and composites. 2010, vol. 29, no. 14, pp. 2192–2198. doi: 10.1177/0731684409347592.

[120] Prentice, P.: *Rheology and Its Role in Plastics Processing*. iSmithers Rapra Publishing, 1995. ISBN 1859570534.

LIST OF ABBREVIATIONS

PLA	poly(lactic acid)
IAH	itaconic anhydride
L101	2,5-bis(tert-butylperoxy)-2,5-dimethylhexane
PLA-g-IAH	poly(lactic acid) grafted with itaconic anhydride
$[IAH]_{PLA}$	grafting degree
$[IAH]_0$	initial concentration of itaconic anhydride
$[L101]_0$	initial concentration of initiator 2,5-bis(tert-butylperoxy)-2,5-dimethylhexane
$PLA^{\bullet}$	PLA macroradical
$IAH^{\bullet}$	IAH radical
$L101^{\bullet}$	radical species generated via thermal decomposition of initiator
$\tau_{1/2}$	half-life time of peroxide initiator
T_g	glass transition temperature
T_{cc}	cold crystallization temperature
T_m	melting temperature
X_c	degree of crystallinity
T_{max}	maximum decomposition rate temperature
k_i	initiation rate constant
k_p	propagation rate constant
k_t	termination rate constant
E_a	activation energy
E_d	dissociation energy
δ	solubility parameter
T_c	ceiling polymerization temperature
ΔH_p	polymerization enthalpy
ΔS_p	polymerization entropy
ΔH_r	heat of reaction
FTIR	Fourier transform infrared spectroscopy
ATR	attenuated total reflection measurement mode
DSC	differential scanning calorimetry
TGA	thermogravimetric analysis
DTA	differential thermal analysis
SEC	size exclusion chromatography
^{1}H-NMR	proton nuclear magnetic resonance
MFR	melt flow rate
PE	polyethylene
PP	polypropylene
PFA	poly(tetrafluoroethylene-co-perfluoropropylvinyl ether)
PTFE	poly(tetrafluoroethylene)

PLA-g-MAH poly(lactic acid) grafted with maleic anhydride
p(IAH)   poly(itaconic anhydride)
MA   methacrylate
MMA   methyl methacrylate
EA   ethyl acrylate
BA   butyl acrylate
VAc   vinyl acetate
VTMS   vinyltrimethoxysilane
DBP   dibenzoyl peroxide
D-1   2,2-di(tert-butyl peroxy)-5,5,6-trimethyl bicyclo [2.2.1] heptane
D-2   2,2-di(3-methyl-1-butine-3-ylperoxy)-5,5,6-trimethyl bicyclo [2.2.1] heptane
TBP   tert-butyl peroxide
CDCl$_3$ deuterated chloroform
KOH   potassium hydroxide
THF   tetrahydrofuran

LIST OF FIGURES

LIST OF TABLES